NOT MEASUREMENT SENSITIVE

MIL-HDBK-530-1
1 JULY 2019

DEPARTMENT OF DEFENSE HANDBOOK

AIRCRAFT USAGE AND SERVICE LOADS STATISTICS, VOLUME 1, CRITERIA AND METHODOLOGY

AMSC N/A FSG 15GP

DISTRIBUTION STATEMENT A. Approved for public release, distribution is unlimited.

FOREWORD

1. This handbook is approved for use by all Departments and Agencies of the Department of Defense.

2. This handbook covers the results from work performed to develop aircraft usage and operational loading statistics from parameter data recorded during operational flight conditions. The Flight Systems Integrity Group of the Aerospace Mechanics Division at the University of Dayton Research Institute (UDRI) performed this work under the Navy Service Loads Handbook Program supported by Air Force Funding. Mr. Daniel Tipps was the principal investigator for the University of Dayton and provided coordination with the Navy and Air Force. Mr. Nam D. Phan of the Navy and Mr. William Buckey of the Air Force provided valuable direction in completion of this effort. Mr. John Rustenburg developed the separation methodology, performed the data analysis and prepared the report. Mr. Donald Skinn developed the data reduction algorithms, and performed the data reduction in support of the methodology development.

3. Comments, suggestions, or questions on this document should be addressed to AFLCMC/EZSS, 2145 Monahan Way, Bldg. 28, Wright-Patterson AFB OH, 45433-7017 or emailed to Engineering.Standards@us.af.mil. Since contact information can change, you may want to verify the currency of this address information using the ASSIST Online database at https://assist.dla.mil.

CONTENTS

PARAGRAPH **PAGE**

LIST OF FIGURES

FIGURE **PAGE**

LIST OF TABLES

TABLE **PAGE**

1. SCOPE

1.1 Scope.

The objective of the handbook is to serve as a practical reference guide to aircraft usage and operational statistics that can be used to establish rational repeated loads criteria for aircraft structure. The aircraft structure is understood to include the fuselage, wing, empennage, landing gear, control system and surfaces, engine mounts, and structural operating mechanisms. The handbook will consolidate available aircraft usage and operational statistics obtained from many in-service aircraft into a single document. It is intended to serve as a reference document for those individuals charged with developing aircraft usage and repeated load spectra. The information in the handbook will allow those individuals to make intelligent selection of the expected operating statistics where such information is not otherwise readily available. It will allow the determination of repeated loads for new designs or for use in the evaluation of previously designed aircraft. The handbook is divided into eight separate volumes. Volume 1 covers the criteria and methodology used in the derivation of usage and operational statistics from measured data. Successive volumes cover seven main aircraft categories consisting of refueling, cargo, bomber, fighter, attack, trainer, and special aircraft. For each aircraft within a category the specific volume of the handbook includes statistical data for four loading environments consisting of aircraft mission usage, ground operations, flight operations and system operations are shown. Also included, is a listing of the recorded parameters used to derive the loading statistics.

The aircraft operational usage will influence the repeated loading conditions to which the aircraft is subjected and ultimately determine the durability, damage tolerance, and maintenance requirements of the aircraft's structure. The operational usage consists of a definition of the different flight profiles and profile mix. These flight profiles are described in terms of flight duration or distance for the flight phases of departure, climb, cruise, descent, and approach with their attendant altitudes and speeds. Takeoff and landing weights also form part of the usage description. The mission mix will describe the distribution of different profiles that the aircraft encounters in services. Subsequently, the aircraft usage is used in conjunction with statistical ground and flight loads data to establish repeated loading/stress spectra for input to the analysis for durability and damage tolerance, definition of testing requirements, or establishment of inspection intervals. Figure 1 shows the information flow for determining the repeated loading spectra for input to the durability and damage tolerance analyses of the aircraft structure.

All the data presented in subsequent volumes of this handbook represent average data from a fleet of aircraft over a period of time and is presented herein for development of a repeated load spectrum necessary to perform a Damage Tolerance Analysis. Guidance from JSSG 2006, Section A.3.2.14.6 indicates that all Durability Analysis will be performed using a more severe spectra such that 90 percent of the fleet is expected to meet the aircraft service life. Appendix F of this handbook presents one approach based on a normal distribution approximation that could be used by the spectra developer to generate such a spectra. When using this approach or any other, the 90 percentile spectra should produce a given severity damage related to a mean spectra to ensure 90 percent of the fleet meets the service life for that particular weapon system. The target severity or usage severity factor (USF) needs to be approved by the government agency. As an example, actual usage variation of legacy data has determined that a USF of ~1.6 is appropriate for a fighter aircraft and will vary for other types of aircrafts.

This volume of the handbook describes the criteria and data editing methodology used in the derivation of operational usage and load statistics from measured data. This volume also contains appendices that describe methodologies which can be used to derive aircraft design usage and load parameter spectra from the load parameter statistical data presented in subsequent volumes. This handbook is for guidance only. Do not cite this document as a requirement.

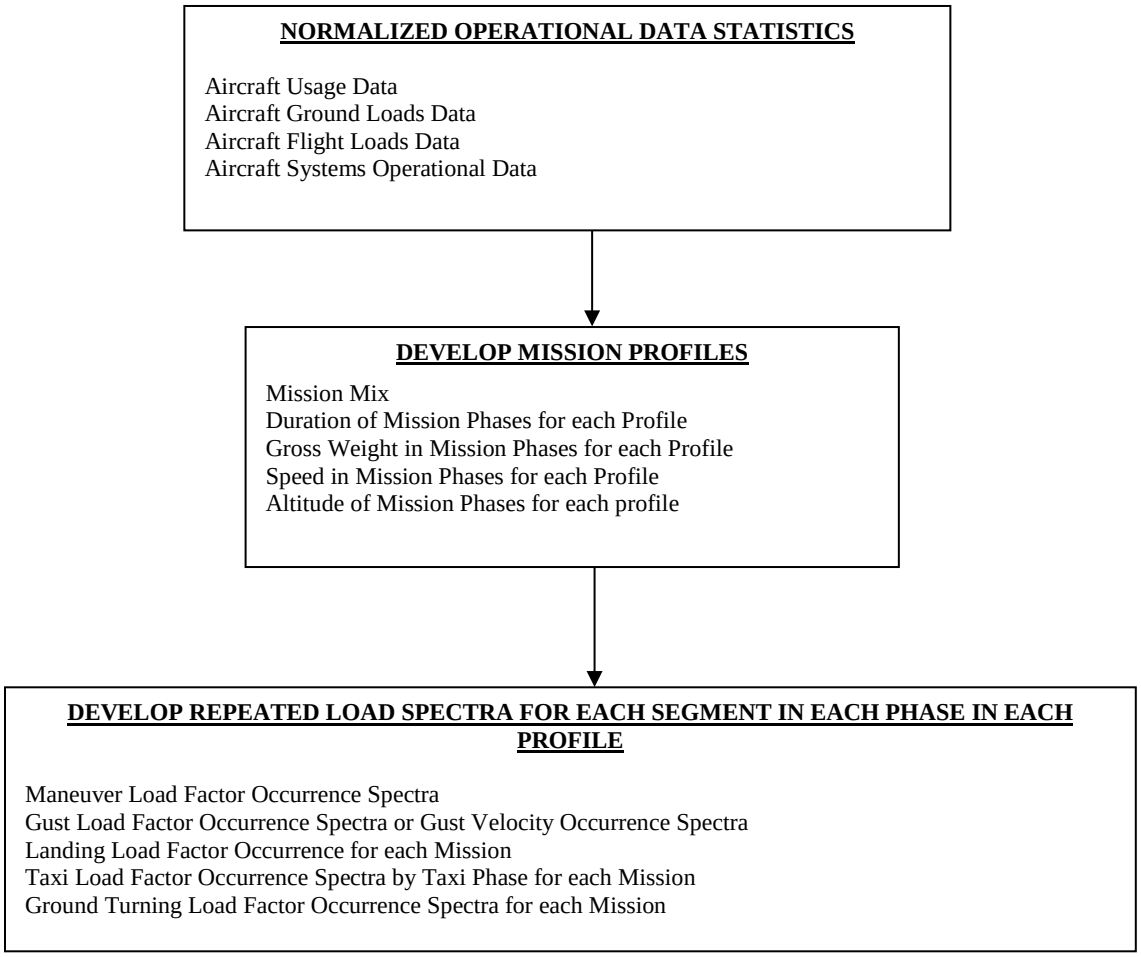

FIGURE 1. Repeated load spectra development.

2. APPLICABLE DOCUMENTS

2.1 General.

The documents listed below are not necessarily all of the documents referenced herein, but are needed to understand the information provided by this handbook.

2.2 Government documents.

None listed.

2.2.1 Other Government documents, drawings, and publications.

The following other Government documents, drawings, and publications form a part of this document to the extent specified herein.

Reference 1. Houbolt, John C., "Design Manual for Vertical Gusts Based on Power Spectral Techniques," Technical Report AFFDL-TR-70-106, December 1970.

(Copies of this document are available online at http://www.dtic.mil/dtic/.)

Reference 2. Houbolt, John C., "Status Review of Atmospheric Turbulence and Aircraft Response," AGARD Report No. 734, "The Flight of Flexible Aircraft in Turbulence-State of the Art in the Description and Modeling of Atmospheric Turbulence", December 1987.

(Copies of this document are available online at http://ntrs.nasa.gov/ and https://www.cso.nato.int/Pubs/rdp.asp?RDP=AGARD-R-734-ADD.)

Reference 3. Coupry, Gabriel (Daniel), "Improved Reduction of Gust Load Data for Gust Intensity," Houbolt, John C., "Manual on the Flight of Flexible Aircraft in Turbulence", AGARD 317.

(Copies of this document are available online at https://www.cso.nato.int/Pubs/rdp.asp?RDP=AGARD-AG-317.)

Reference 4. Fink, R.D., "USAF Stability and Control DATCOM," Flight Control Division, Air Force Flight Dynamics Laboratory, Wright-Patterson Air Force Base, Ohio, October 1960, Revised April 1978.

(Copies of this document are available online at http://www.dtic.mil/dtic/.)

Reference 5. de Jong, B., "Reduction of Incremental Load Factor Acceleration Data to Gust Statistics," DOT/FAA/CT-94/57, August 1994.

(Copies of this document are available online www.dtic.mil/dtic/tr/fulltext/u2/a284764.pdf.)

3. DEFINITIONS

$\overline{A}$ Aircraft PSD gust response factor

a Speed of sound (ft./sec)

$\overline{c}$ Wing mean geometric chord (ft.)

$\overline{C}$ Aircraft discrete gust response factor

C_{L_α}	Aircraft lift-curve slope per radian
$C_{L_{max}}$	Maximum lift coefficient
CAS	Calibrated air speed
cg	Center of gravity
EAS	Equivalent airspeed
F(PSD)	Continuous gust alleviation factor
g	Gravity constant, 32.17 ft./sec^2
H_p	Pressure altitude, (ft.)
K_g	Discrete gust alleviation factor, $0.88\ \mu/(5.3 + \mu)$
KCAS	Knots calibrated air speed
KEAS	Knots equivalent air speed
KIAS	Knots indicated air speed
kts	Knots
L	Turbulence scale length (ft.)
n	Load factor (g)
N	Number of occurrences for U_σ (PSD gust procedure)
nm	Nautical mile
n_x	Longitudinal load factor (g)
n_y	Lateral load factor (g)
n_z	Normal load factor (g)
N_0	Number of zero crossings per nautical mile (PSD gust procedure)
PSD	Power spectral density
q	Dynamic pressure (lbs./ft^2)
S	Ding area (ft^2)
TAS	True airspeed
UDRI	University of Dayton Research Institute
U_{de}	Derived gust velocity (ft./sec, EAS)
U_σ	Continuous turbulence gust intensity (ft./sec, TAS)
V_B	Design speed for maximum gust
V_C	Design cruise speed
V_D	Design dive speed
V_e	Equivalent airspeed

V_T	True airspeed
W	Gross weight (lbs.)
Δm	Incremental acceleration due to a turning maneuver
Δn_z	Incremental normal load factor, n_z - 1
$\Delta n_{z_{man}}$	Incremental maneuver load factor
$\Delta n_{z_{gust}}$	Incremental gust load factor
μ	Aircraft mass ratio, $\frac{2(W/S)}{\rho g \bar{c} C_{L_\alpha}}$
μ_p	Statistical mean of p (parameter on plots)
ρ	Air density, slugs/ft^3 (at altitude)
ρ_0	Standard sea level air density, 0.0023769 slugs/ft^3
σ_p	Standard deviation of p (parameter on plots)
φ	Bank angle (degrees)

4. OPERATIONAL DATA STATISTICS

4.1 Development of operational data statistics.

Development of the operational data statistics involves the processing of parameter data provided by the user of the aircraft in accordance with predefined processing criteria. The end product of this processing phase consists of normalized operational statistics. The recorded parameter data as made available by the user may consist of directly acquired values as well as calculated values and varies between aircraft types. A listing of the actual parameters, both directly acquired and calculated as provided by the user for each aircraft is shown under the pertinent aircraft section of the handbook.

Certain information and supplementary parameters are needed in subsequent data reduction that are not available in either the acquired or calculated formats provided by the user and need to be computed from other provided parameter data.

This section describes how parameter data are processed through a series of computer software programs, describes the data reduction criteria used to extract the statistical data from the parameters provided by the user, and describes the formulations used to compute supplementary parameters that are not provided but are needed in compiling the desired presentation formats.

4.2 Data reduction operations.

The data reduction phase retrieves operational data from the aircraft operator, processes it through a series of computer programs that convert the data to UDRI compatible formats, and provides statistical information on aircraft usage, ground loads, flight loads, and systems operation. The data processing flow chart is illustrated on Figure 2 and the flow of the processed data is discussed in subsequent paragraphs.

4.2.1 Initial quality screening.

All incoming data files are screened for acceptability. Individual flights are edited to remove erroneous or meaningless data such as discontinuous elapsed time data, evidence of nonfunctional channels or sensors, incomplete flight phases, and duplicate data sets. Files with excessive missing, incomplete, erroneous or duplicate data are excluded from further consideration.

4.2.2 Time-history files.

The parameter data files provided by the aircraft user contain multiple flights for each aircraft. The files are separated into individual parameter time history files for each flight. Then these time history files are compressed and filed for later recall by the flight loads processing software. Data editing and verification are performed on the data as the time histories are being prepared. This data editing and verification aims to detect logical inconsistencies in the data by evaluating parameter magnitudes against aircraft and system design capabilities. Message alerts indicate that obviously erroneous data have been removed and/or that questionable data have been retained but need to be manually reviewed prior to their acceptance.

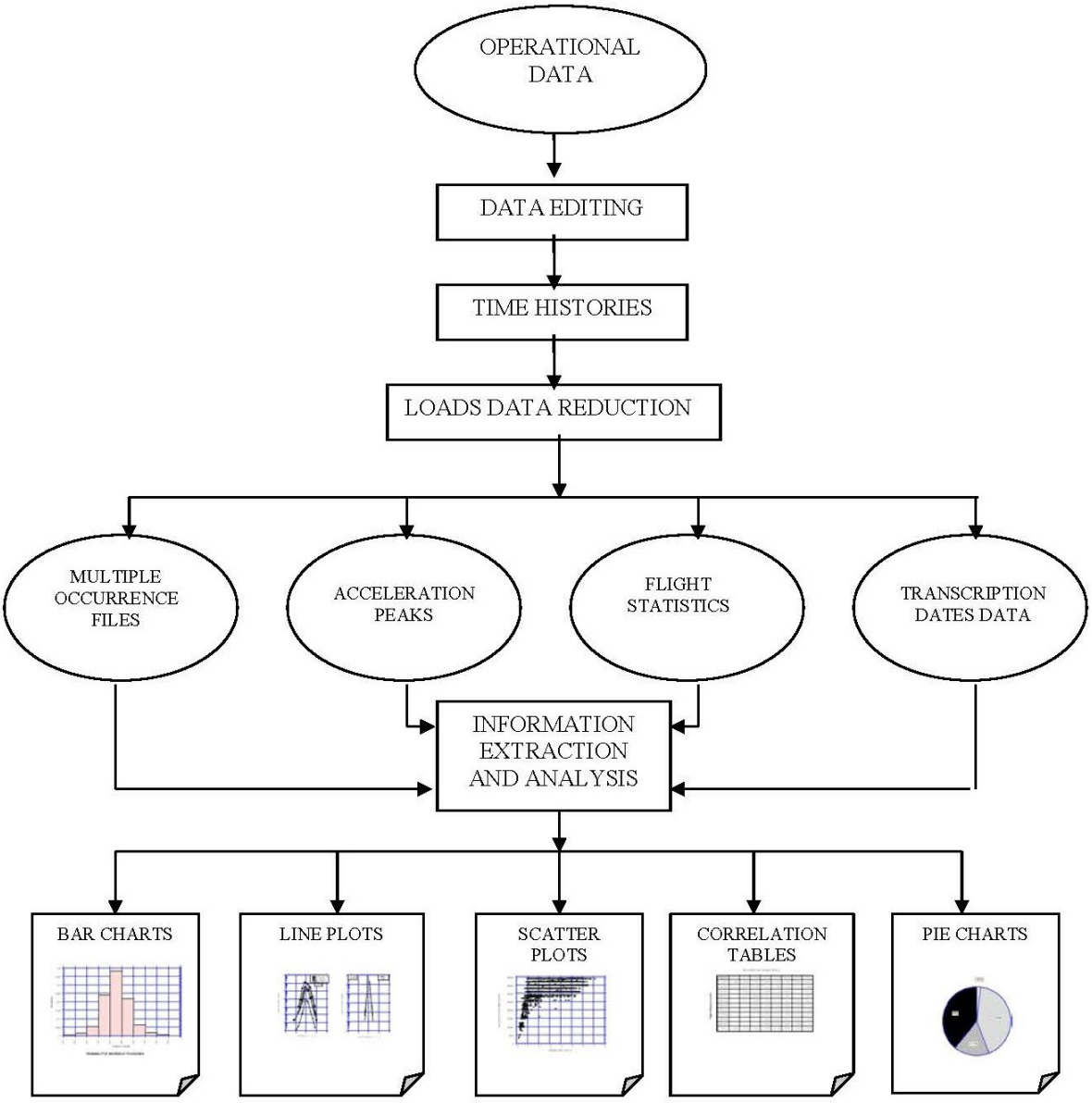

FIGURE 2. Data processing flow chart.

4.2.3 Relational database.

Important characteristics about each set of flights received from the aircraft user are recorded in a relational database. Aircraft user, aircraft tail number, and data source file are identified in the data. Each flight is assigned a unique flight sequence number.

4.2.4 Permanent data files.

In addition to the time history files, two other files are created and permanently stored with the time history files. The first file contains the chronologically sorted list of the phases of flight and their corresponding starting times. This file provides the means to separate flight by flight phases in subsequent data analysis processing. The second file contains the accumulated time and distance for various combinations of phase of flight and altitude band. This file provides the capability to present data results in terms of normalized unit time and/or distance.

4.2.5 Loads data reduction.

The loads data reduction program derives statistical information on aircraft usage, ground loads, flight loads, and systems operations from the compressed time history files. These data are then reduced in accordance with specific data reduction criteria.

4.3 Computed parameters.

Derived gust velocity, $U_{de,}$ and continuous gust intensity, $U_{\sigma,}$ are important statistical load parameters, which are derived from measured vertical accelerations. This derivation of U_{de} and U_{σ} involves values of atmospheric density, equivalent airspeed, and dynamic pressure. These values are calculated using equations that express relationships between atmospheric density and speed as a function of altitude based on the International Standard Atmosphere.

4.3.1 Atmospheric density.

For altitudes below 36,089 feet, the density ρ is expressed as a function of altitude by:

$$\rho = \rho_o (1 - 6.876 \times 10^{-6} \times H_p)^{4.256} \tag{1}$$

And the square root of the relative density ratio is:

$$\sqrt{\frac{\rho}{\rho_0}} = \left(1 - 6.876x10^{-6} xH_p\right)^{2.128} \tag{2}$$

Where ρ_0 is the standard density at sea level (0.0023769 slugs/ft^3) and H_p is pressure altitude (ft.). Pressure altitude is a recorded parameter.

For altitudes from 36,089 to 65,717 feet, the density ρ is calculated as follows:

$$\rho = \rho_0 \cdot 0.297076 e^{-4.80614x10^{-5}(Hp - 36,089)} \tag{3}$$

And the square root of the relative density ratio is:

$$\sqrt{\frac{\rho}{\rho_0}} = \left[0.297076 e^{\left(-4.806x10^{-5}(H_p - 36,089)\right)}\right]^{0.5} \tag{4}$$

4.3.2 Equivalent airspeed.

Equivalent air speed (V_e) is a function of true air speed (V_T) and the square root of the ratio of air density at altitude (ρ) to air density at sea level (ρ_0) and is expressed as

$$V_e = V_T \sqrt{\frac{\rho}{\rho_0}} \tag{5}$$

True airspeed (V_T) is derived from Mach number (M) and speed of sound (a):

$$V_T = Ma \tag{6}$$

Mach number is dimensionless and is a recorded parameter.

4.3.2.1 Equivalent airspeed at altitudes below 36,089 feet.

The speed of sound (a) is a function of pressure altitude (H_p) and for altitudes below 36,089 feet is expressed as

$$a = a_0 \sqrt{(1 - 6.876 \times 10^{-6} \times H_p)} \tag{7}$$

where the speed of sound at sea level a_0 is 1116.4 fps or 661.5 knots.

Using the recorded Mach number, substituting Equation 7 into Equation 6, and Equations 6 and 2 into Equation 5 gives the equivalent airspeed.

$$V_e = M \times a_0 \times (1 - 6.876 \times 10^{-6} \times H_p)^{2.626} \tag{8}$$

4.3.2.2 Equivalent airspeed at altitudes from 36,089 feet to 65,617 feet.

For altitudes from 36,089 to 65,617 feet the speed of sound (a) in knots is calculated as follows:

$$a = 38.968(-56.5 + 273.15)^{0.5} \tag{9}$$

Using the recorded Mach number, substituting Equation 9 into Equation 7, and Equations 7 and 4 into Equation 5 gives the equivalent airspeed in knots.

$$V_e = 573.571\left[0.297076 e^{\left(-4.806 \times 10^{-5}(H_p - 36{,}089)\right)}\right]^{0.5} \tag{10}$$

4.3.3 Dynamic pressure (q).

The dynamic pressure (q) is calculated from the air density and velocity as

$$q = \frac{1}{2} \rho V_T^2 \tag{11}$$

Where:

ρ = air density at altitude (slugs/ft^3)
V_T = true air speed (ft./sec)

a. True airspeed in fps at altitudes below 38,069 feet.

$$V_T = Ma_0\sqrt{1-6.876x10^{-6}H_p} \tag{12}$$

b. True airspeed in fps at altitudes from 36,089 to 65,517 feet.

$$V_T = 968.762M \tag{13}$$

4.3.4 Derived gust velocity (U_{de}).

The derived gust velocity, U_{de}, is computed from the peak values of gust incremental vertical acceleration as

$$U_{de} = \frac{\Delta n_z}{\overline{C}} \tag{14}$$

where Δn_z is gust peak incremental vertical acceleration and $\overline{C}$ is the aircraft response factor considering the plunge-only degree of freedom and is calculated from

$$\overline{C} = \frac{\rho_0 V_e C_{L_\alpha} S}{2W} K_g \tag{15}$$

Where:

ρ_0 = 0.002377 slugs/ft^3, standard sea level air density

V_e = equivalent airspeed (ft./sec)

C_{L_α} = aircraft lift-curve slope per radian

S = wing reference area (ft^2)

W = gross weight (lbs.)

$$K_g = \frac{0.88\mu}{5.3+\mu} = \text{gust alleviation factor, dimensionless} \tag{16}$$

$$\mu = \frac{2W}{\rho g \bar{c} C_{L\alpha} S} \tag{17}$$

ρ = air density, slug/ft^3, at pressure altitude (Hp), from Equation 1 or 3

g = 32.17 ft./sec^2

$\bar{c}$ = wing mean geometric chord (ft.)

4.3.5 Continuous gust intensity (U_σ).

The continuous gust intensity U_σ values are computed from the gust vertical acceleration values using the power spectral density formulations developed in References 1, 2, and 3 (see 2.2.1) as shown.

$$U_\sigma = \frac{\Delta n_z}{\overline{A}} \tag{18}$$

Where:

Δn_z = gust peak incremental vertical acceleration

$\overline{A}$ = aircraft PSD gust response factor = $\frac{\rho V_T C_{L\alpha} S}{2W} F(PSD)$ *in* $\frac{1}{ft/sec}$ (19)

$\bar{c}$ = wing mean geometric chord (ft.)

C_{L_α} = aircraft lift-curve slope per radian

$$F(PSD) = \frac{11.8}{\sqrt{\pi}}\left[\frac{\bar{c}}{2L}\right]^{\frac{1}{3}}\sqrt{\frac{\mu}{110+\mu}},\ dimensionless \quad (20)$$

g = 32.17 ft./sec^2

L = turbulence scale length, 2500 ft.

$$\mu = \frac{2W}{\rho g \bar{c} C_{L_\alpha} S},\ \text{dimensionless} \quad (21)$$

ρ = air density (slugs/ft^3) at pressure altitude from Equation 1 or 3

S = wing reference area (ft^2)

V_T = true airspeed (ft./sec)

W = gross weight (lbs.)

4.3.6 Lift-curve slope.

Unfortunately, lift-curve slope data is often not available and aircraft manufacturers are reluctant to provide such information on the basis of proprietary considerations. As a result, UDRI has found it necessary to determine lift-curve slopes from empirical relationships.

For the rigid aircraft, the calculation of the lift-curve slope is based on an extension of the one-dimensional approximation for the wing lift-curve slope presented in the USAF Stability and Control DATCOM, (see 2.2.1 Reference 4). The rigid wing lift-curve slope derivative for the subsonic speed regime in reference is given as:

$$C_{l_\alpha} = \frac{2\pi A_r}{2+\left(4+A_r^2\beta^2\left(1+\frac{tan^2\Lambda}{\beta^2}\right)\right)^{1/2}} \quad (22)$$

A_r = Wing aspect ratio

Λ = Wing span

β = $\sqrt{1-M^2}$

$C_{l\alpha}$ = Lift-curve slope per radian

Λ = Quarter chord sweep angle

M = Mach number

Equation 22 provides an estimate of the wing lift-curve slope. Aircraft gust response calculations are based on the use of the total aircraft lift-curve slope. A comprehensive evaluation of the total aircraft lift-curve slope for a number of aircrafts using the USAF Stability and Control DATCOM (see Reference 4) methodology showed that the wing lift-curve slope underestimated the aircraft lift-curve slope by approximately 14 percent. Therefore, the wing lift-curve slope value obtained from Equation 20 needs to be multiplied by 1.14 to derive the untrimmed rigid lift-curve slope for the entire aircraft.

4.3.7 Flight distance.

The flight distance was obtained by integrating the range with respect to changes in aircraft velocity as a function of time. The integrated flight distance D is obtained by the numerical integration from the time at liftoff (t_0) to the time of touchdown (t_n), and V_T is the average true velocity during Δt.

$$D = \sum_{t_0}^{t_n} \Delta t \cdot V_T \tag{23}$$

4.3.8 Rate of climb.

The rate of climb is obtained by numerical differentiation of the change in pressure altitude with time.

$$RC = \sum_{t_1}^{t_2} \frac{\Delta H_p}{\Delta t} \tag{24}$$

4.4 Data reduction criteria.

To process the measured data into statistical loads formats, specific data reduction criteria were developed for separating the phases of ground and flight operations, identifying specific events associated with operation of the aircraft and its onboard systems, assigning sign conventions, determining maximum and minimum values and load cycles, and distinguishing between gust and maneuver load factors. These criteria are discussed in this section.

4.4.1 Phases of flight profile.

The ground and flight phases are determined from the recorded data. Each time-history profile is divided into major ground and flight phases. The ground phases consist of taxi-out, takeoff roll, landing roll, and taxi-in, and possibly touch and goes. The primary airborne phases are departure, climb, cruise, descent, and approach. Depending on the aircraft type, additional phases may be required. Figure 3 shows an example flight profile for a refueling aircraft.

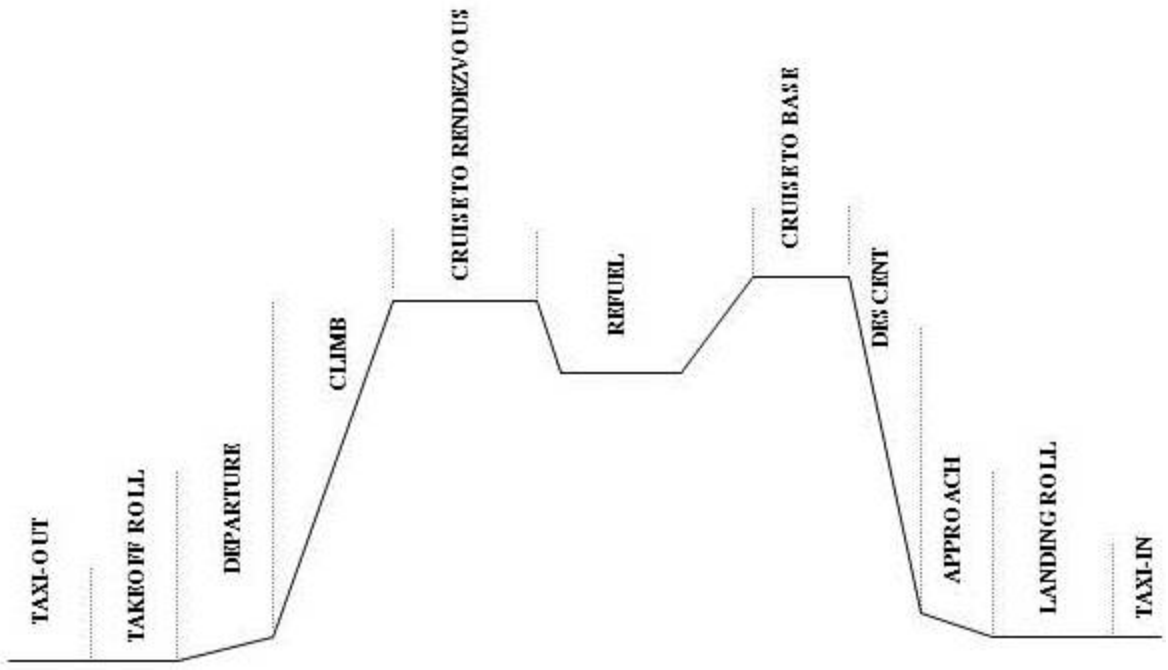

FIGURE 3. Description of flight profile phases.

The criteria used to define each of these phases are summarized in Table I and discussed in more detail in the following paragraphs.

TABLE I. Flight phase criteria.

Phase of Flight	Defining Condition at Start of Phase
Taxi-out	From initial aircraft movement.
Takeoff Roll	Ground acceleration >2kts./sec in a 20 second duration sequence.
Departure	Liftoff, Squat switch off.
Climb	***Rate of Climb ≥ 250 ft./min maintained for at least 1 minute with flaps retracted.***
Cruise, refuel	Rate of climb is between ±250 ft./min and flaps retracted.
Descent	Rate of descent ≥250 ft./min occurs for at least 1 minute and flaps retracted.
Approach	Rate of descent ≤250 ft./min occurs for at least 1 minute with flaps extended.
Landing roll	Touchdown, Squat switch on.
Taxi-in	End of runway turnoff, parked at the gate, or flight data recorder shutdown.

4.4.1.1 Ground phases.
Specific data reduction criteria were developed and used to identify the beginning and end of each ground phase of operation (taxi-out, takeoff roll, landing roll with and without thrust reverser deployed and taxi-in).

The taxi-out phase begins when the ground speed exceeds 1 knot. All aircraft movement until the aircraft begins its takeoff roll is defined as taxi-out.

The beginning of the takeoff roll is found by searching for ground speeds that accelerated at rates greater than 2 kts/sec for a minimum duration of 20 seconds. Then, when these values are found, the beginning of the takeoff roll is assigned as the time slice when the first ground speed rate change is greater than 2 kts/sec for the sequence that occurred. The takeoff roll ends at liftoff with the squat switch off signal.

The landing roll phase is defined as beginning 1 second after the squat switch signaled that the landing touchdown had occurred and ending when the aircraft begins its turnoff from the active runway. The criterion for the turnoff is based on a magnetic heading change following landing (see 4.4.2.4 for additional, detailed discussion).

Taxi-in is defined as the point where the aircraft completed its turnoff from the active runway after its landing roll to the point when the aircraft was either parked at the gate or the flight data recorder has shut down. The criterion for completion of the turnoff uses magnetic heading to identify when the aircraft has either returned to taxiing in a straight line or has turned in the opposite direction (see 4.4.2.4 for additional, detailed discussion).

4.4.1.2 Airborne phases.
The airborne portion of each flight profile was separated into phases called departure, climb, cruise, descent, and approach. These phases occur between the times that the squat switch turns off at liftoff until it turns on again at landing touchdown. The beginning of each flight phase is defined based on combinations of the squat switch position, flap settings, and/or the calculated rate of climb or descent over a period of at least 1 minute as shown in Table I. Also by definition, the departure phase cannot be less than 1 minute in length.

It should be noted that an airborne phase could occur several times per flight because it is determined by the rate of climb and the position of the flaps. When this occurs, the flight loads data are combined and presented as a single flight phase. The UDRI software then creates a file that chronologically lists the phases of flight and their corresponding starting times.

4.4.2 Specific events.
In addition to the ground and airborne phases, a unique set of criteria was also required to identify certain specific events such as liftoff, landing touchdown, thrust reverser deployment and stowage, and start and completion of turnoff from the active runway after landing. Figure 4 shows a sketch depicting these phases and events.

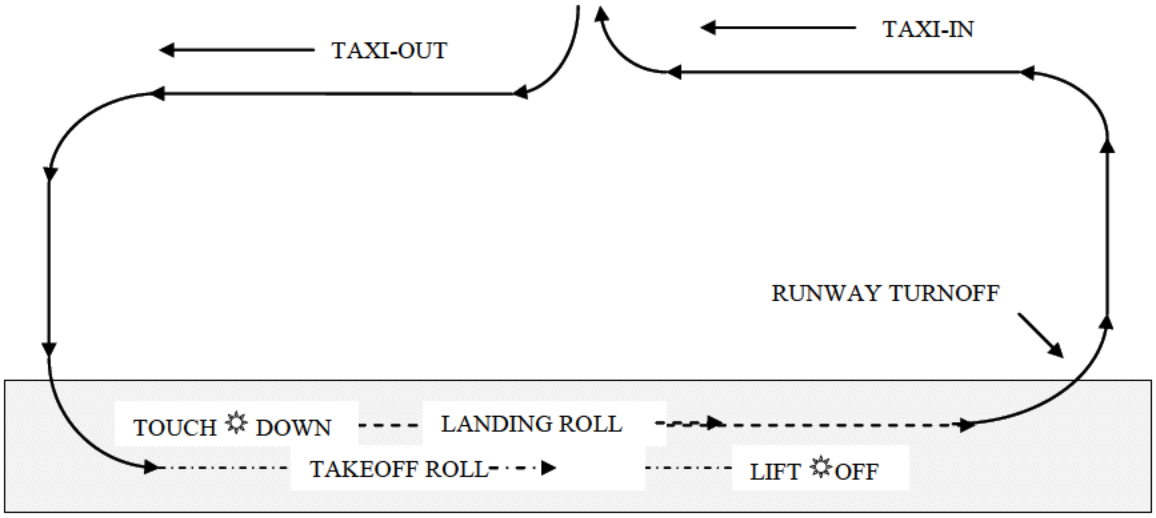

FIGURE 4. Ground operation events.

The criteria used to define each of the specific events are summarized in Table II and discussed in more detail in AGARD Report No. 734 and the following paragraphs.

TABLE II. Summary of specific events criteria.

Phase/Event	Defining Conditions
Liftoff	Point of first reading in series of increasing radio altitude values greater than 4 feet higher than the average radio altitude value calculated during the takeoff roll.
Landing touchdown	From 5 seconds prior to squat switch on to 1 second afterwards.
Thrust reverser deployment/stowage	Thrust reverser switch on for deployment and off for stowage.
Runway turnoff	From first sequential magnetic heading change in same direction from runway centerline and heading sequence changes >13.5 degrees to a straight line heading or turn in opposite direction.

4.4.2.1 Liftoff.
Observations using other parameters such as radio altitude and pitch angle as indicators of liftoff and touchdown have shown that the squat switch signal does not provide an accurate indication of when liftoff (or touchdown) actually occurs. To determine when liftoff actually occurs, an algorithm identifies the liftoff point as the first reading in the series of increasing radio altitude values was greater than 4 feet higher than the average radio altitude value it calculated during the takeoff roll is used.

4.4.2.2 Touchdown.
As noted (see 4.4.2.1), the squat switch signal does not provide an accurate indication of when liftoff (or touchdown) actually occurs. To ensure that the maximum vertical and side load factors associated with touchdown were identified, the actual touchdown event is deemed to occur within a time frame from 5 seconds prior to until 1 second following squat switch closure. The 5 second interval is based on the consideration it is important to ensure capturing the maximum load factor

associated with the touchdown event even if this results in some loss of load factor peaks in the approach phase. The 1 second time after squat switch was chosen somewhat arbitrarily, but was intended to ensure that sufficient time was allowed for the aircraft to respond to the touchdown and for the vertical and side load accelerations to build to their maximum values.

4.4.2.3 Thrust reverser deployment/stowage.
An on/off switch identifies when deployment or stowage of the thrust reverser occurs. Thus, by identifying when this occurs as a special event, load factor acceleration data can be obtained at the instant of thrust reverser deployment and during the time of thrust reverser usage and stowage.

4.4.2.4 Runway turnoff.
Changes in the aircraft's magnetic heading were used to identify the beginning and end of the aircraft's turnoff from the active runway after the landing roll. After the aircraft touched down, subsequent magnetic heading readings were averaged and this average heading was defined as the runway centerline. Subsequent magnetic heading changes were then tested to identify continuous movement in the same direction away from this centerline. When the aircraft's sequential magnetic heading change exceeded 13.5 degrees from the direction of the landing centerline, the time slice associated with the first sequential heading change from the landing centerline in the direction of the turn was defined as the beginning of the turnoff from the runway.

An alternate method was used to identify flights involving "shallow" turns from the runway that did not exceed the 13.5 degree turn criteria. This method utilizes aircraft ground speed and magnetic heading to calculate the aircraft's position relative to the runway centerline by identifying when the aircraft's position perpendicular to the runway centerline exceeded 100 feet. The time slice associated with the first aircraft movement away from the landing centerline in the direction of the turn was defined as the beginning of the aircraft's turnoff from the runway.

The end point of the first turnoff from the active runway was also identified using magnetic heading readings. An algorithm was developed that uses the changes in magnetic heading, while the aircraft was in its turn, to identify when the aircraft had either returned to taxiing in a straight line or was turning in the opposite direction. The first point that provided this indication was then defined as the end point of the turnoff from the runway. This point is also the beginning of the taxi-in phase.

4.4.3 Sign conventions.
Acceleration data are recorded in three directions: vertical (z), lateral (y), and longitudinal (x). As shown on Figure 5, the positive z direction is up; the positive y direction is aircraft starboard; and the positive x direction is forward.

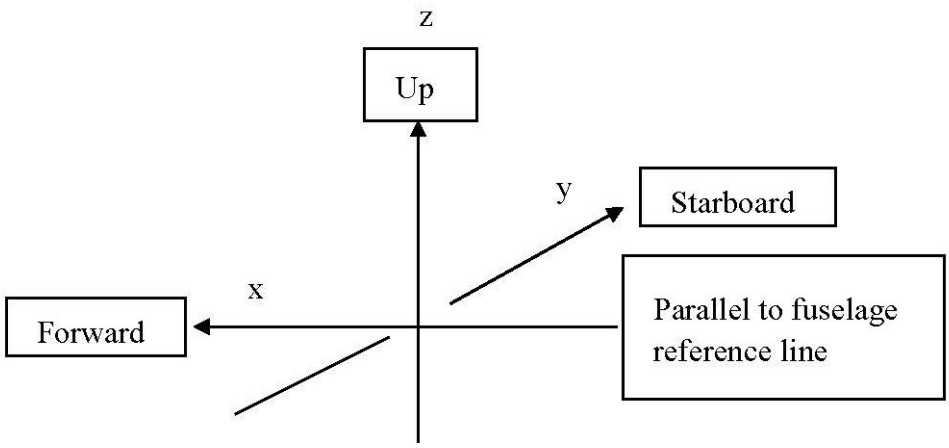

FIGURE 5. Sign convention for aircraft accelerations.

4.4.4 Peak selection technique.

The peak-between-means method presented in DOT/FAA/CT-94/57 (see 2.2.1 Reference 5) is used to identify positive and negative peaks in the acceleration data. This method is consistent with past practices and pertains to all accelerations (n_x, n_y, Δn_z, $\Delta n_{z_{gust}}$, $\Delta n_{z_{man}}$). A brief description of the peak-between-means technique follows.

One peak is identified between each two successive crossings of the mean acceleration, which is the 0-g condition for lateral, longitudinal, and incremental vertical accelerations. Peaks greater than the mean are considered positive, and those less than the mean are considered negative. A threshold zone is defined around the mean, within which acceleration peaks are ignored because they have been shown to be irrelevant. The threshold zone is ±0.05 g for the vertical accelerations Δn_z, $\Delta n_{z_{gust}}$, and $\Delta n_{z_{man}}$, ±0.005 g for lateral acceleration n_y, and ±0.0025 g for longitudinal acceleration n_x.

Figure 6 below demonstrates the acceleration peak selection technique. The sample acceleration trace contains eight zero crossings, which are circled, set off by vertical dashed lines, and labeled as C_i, i =0 to 7. For each of seven intervals between successive mean crossings, C_{i-1} to C_i, i = 1 to 7, one peak, which is located at P_i, is identified. Those peaks lying outside of the threshold zone (P_1, P_2, P_5, P_6, and P_7) are accepted and retained; whereas, those peaks lying inside the threshold zone (P_3 and P_4) are ignored.

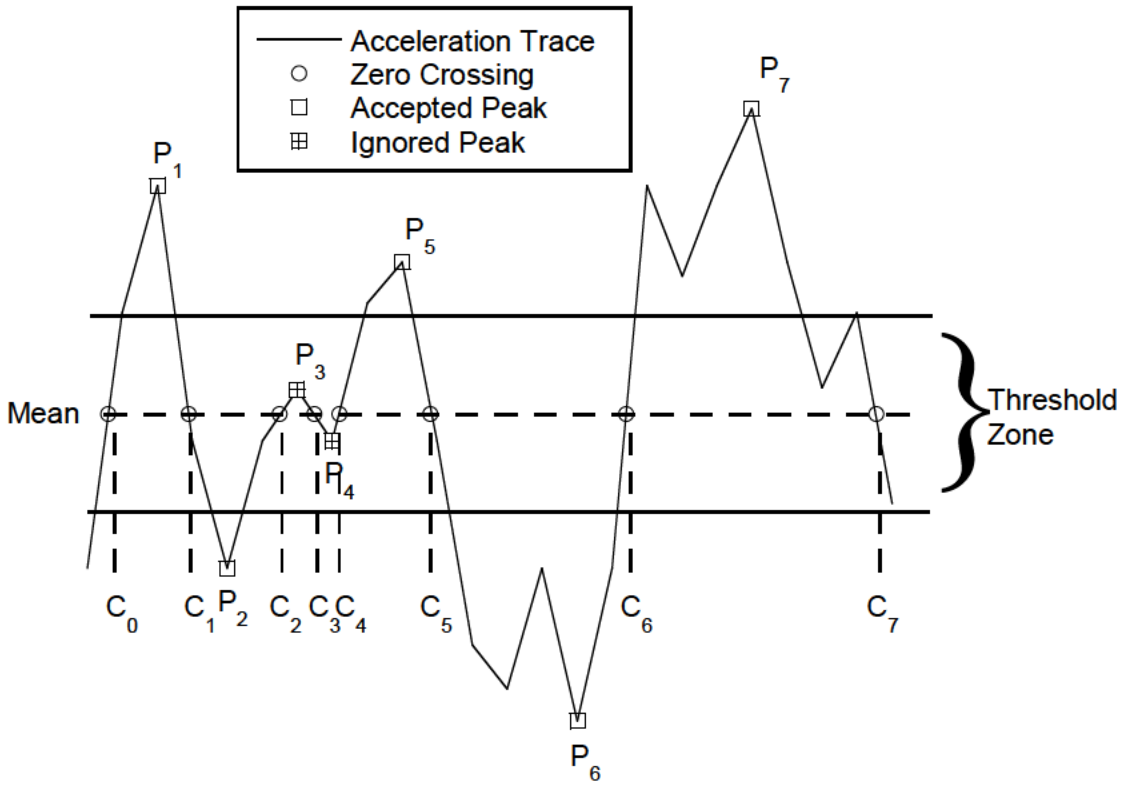

FIGURE 6. Peak-between-means classification criteria.

4.4.5 Separation of maneuver and gust load factors.

Vertical acceleration, n_Z, is measured at the center of gravity (CG) of the aircraft and incremental vertical acceleration, Δn_Z, results from removing the 1-g condition from n_Z. The incremental acceleration measured at the cg of the aircraft in flight may be the result of either maneuvers or gusts. In order to derive gust and maneuver statistics, the maneuver induced acceleration ($\Delta n_{Z_{man}}$) and the gust response acceleration ($\Delta n_{Z_{gust}}$) requires separation from the total acceleration history. Appendix A presents the UDRI development of an improved method of separating maneuver and gust load factors from measured acceleration time histories using a peak cycle duration associated with an aircraft's short period frequency. This method allows for differences in the response of an individual aircraft to turbulence throughout a flight as well as differences between aircraft types. The method developed shown in Appendix A includes a normalization process to account for differences in aircraft type. This normalization results in a simple polynomial equation that requires only Mach number and aircraft gross weight as inputs and provides a cycle duration criterion for any acceleration peak. The equation is as follows:

$$t = (0.020825-0.06514M+0.093663M^2-0.044067M^3)\ W^{0.46} \qquad (25)$$

If the cycle duration of an acceleration peak is equal to or less than the calculated value the peak is considered a gust response. If the cycle duration of an acceleration peak is longer than the calculated cycle response the peak is classified as a maneuver.

5. STATISTICAL DATA PRESENTATION

5.1 Statistical data presentation.

The aircraft usage and service loads statistics are presented in separate volumes by aircraft category as shown in Table III.

TABLE III. Aircraft classification list.

AIRCRAFT CATEGORY	VOLUME
REFUELING	-2
CARGO	-3
BOMBER	-4
ATTACK	-5
TRAINER	-6
FIGHTER	-7
SPECIAL	-8

For each aircraft within a category the specific handbook volume contains basic information on gross weight and engine characteristics as well as the major physical dimensions of the aircraft. A three view drawing showing the front, side, and top views of the aircraft is also presented. For each aircraft, a listing of the recorded or derived parameters that are available to develop the statistical data is also included. Because the available parameters are different for each aircraft, the derived statistical data formats will not be identical for each aircraft.

For each aircraft, the statistical data is arranged to cover four primary areas of statistical information consisting of:

a. Aircraft usage statistical data.
b. Ground operation statistical data.
c. Flight operation statistical data.
d. System operation statistical data.

The statistical data is presented in fundamental parameter form, such as speed, gross weight, altitude, load factor, surface deflection etc. The statistical formats available for an aircraft are in the form of tables, line plots, or scatter plots. The graphical formats are accompanied by the corresponding tabulated data to allow the direct derivation of load spectra without recourse to the graphical presentation. Scatter plots provide the means for characterizing pair-wise relationships between variables and can be used to determine the strength of the relationship between the two variables. The aircraft usage statistical data contains typical statistical data covering gross weight, flight distance, altitude, and speed statistics as well as aircraft attitude and rate data during liftoff, approach and touchdown. The gross weight, flight distance, altitude, and speed statistics can be

used to derive flight mix information as well as detailed operational flight profiles. A procedure to derive mission mix and mission profile information from the statistical usage data is presented in Appendix C of this volume.

The ground operation statistical data contains statistical loads data pertinent to ground operations. Of primary interest are the frequency and probability information on vertical, lateral, and longitudinal accelerations during taxi, takeoff, landing, and ground turning. The ground load parameter statistics for the parameters are presented in a normalized form in terms of exceedances per flight and are presented in both graphical and tabular format. An approach for mathematically predicting ground loads turning spectra based on the main gear track dimension and the distance between main and nose gears is presented in Appendix D of this volume.

The flight operation statistical data contains gust and maneuver load statistics for flight operations. The gust statistics includes both discrete gust as well as continuous turbulence data. The discrete gust information will be in the form of exceedances of derived gust velocities U_{de} per unit distance. The continuous turbulence data is in the form of generalized exceedance curves (N_y/N_o verses $y/\bar{A}$). The procedure used to derive the generalized exceedance curves is covered in Appendix B of this volume. As for the ground load statistics, the flight data is also presented in line plots and bi-variate scatter plots accompanied by the associated tabular data.

The system operation statistical data contains statistical information on systems operations, such as control surface deflections and thrust reverser operations.

6. NOTES

6.1 Intended use.

This handbook is intended to serve as a practical reference guide to aircraft usage and operational statistics that can be used to establish rational repeated loads criteria for aircraft structure.

6.2 Subject term (key word) listing.

Approach
Climb
Cruise
Damage tolerance
Departure
Descent
Durability
Flight operations
Flight phases
Ground operations
Landing weights
Maintenance requirements
Structure

System operations
Takeoff weights

APPENDIX A

AN IMPROVED MANEUVER-GUST SEPARATION CRITERION

A.1 SCOPE

A.1.1 Scope.

The DOT/FAA/AR-99/14 (see Reference A1) presented results of a study to evaluate of methods to separate maneuvers and gust load factors from measured acceleration time histories recorded on a Digital Flight Data Recorder (DFDR). The reference concluded that a cycle duration type of criterion for differentiating between gust and maneuvers response provided a reasonable and easily implemented technique for separating gusts and maneuvers in an acceleration time history. Inherent in this approach is the premise that the cycle duration is a function of the aircraft response to a continuous input. The response of the aircraft is influenced by its aerodynamic and structural characteristics and operating parameters such as speed and gross weight. Thus, the response is not a constant value but will vary throughout a flight and will be different for different aircrafts.

The DOT/FAA/AR-99/14 (see Reference A1) recommended that cycle duration of 2.0 seconds be used as a criterion for separating maneuvers and gust for the B-737 and MD-82/83 aircraft. For simplicity, this cycle duration criterion was applied to the entire time history from takeoff to landing. The reference also suggested that the validity of this cycle duration should be evaluated for its applicability to aircraft of different size. This appendix presents an extension of the earlier study, which considers differences in an aircraft's frequency response characteristics throughout a flight and using these differences in a procedure to separate maneuver and gust accelerations.

A.2 APPLICABLE DOCUMENTS

A.2.1 Other Government documents, drawings, and publications.

The following other Government documents, drawings, and publications form a part of this document to the extent specified herein.

A1. Rustenburg, John, Skinn, Donald, Tipps, Daniel O., "An Evaluation of Methods to Separate Maneuver and Gust Load Factors from Measured Acceleration Time Histories," University of Dayton Research Institute Report UDR-TM-1998-00011, November 1998. Also published as DOT/FAA/AR-99/14, April 1999.

(Copies of this document are available online at http://www.dtic.mil/get-tr-doc/pdf?AD=ADA363333 and www.tc.faa.gov/its/worldpac/techrpt/ar99-14.pdf.)

A2. Houbolt, J. C., Pratt, K. G., Steiner, R., Langley Research Center. (1964). Dynamic response of airplanes to atmospheric turbulence including flight data on input and response. Washington, D.C.: National Aeronautics and Space Administration.

(Copies of this document are available for purchase online at https://w95020.eos-intl.net/W95020/OPAC/Search/SimpleSearch.aspx and https://catalog.hathitrust.org/Record/011432947)

A3. Roskam, Jan, “Airplane Flight Dynamics and Automatic Flight Controls, Part 1,” Roskam Aviation and Engineering Corporation. 1979.

(Copies of this document are available for purchase online at http://www.darcorp.com/Books/.)

A4. Howford, John, “Personal Communication”, Past FAA Chief Scientific and Technical Advisor (CSTA) for Loads/Aeroelasticity, August 2007.

A.3 CONTINUOUS TURBULENCE REVIEW

A.3.1 Continuous turbulence review.

The basic continuous turbulence concept involves a) the power spectral density of the turbulence, b) the frequency response function of the aircraft, and c) the aircraft gust response spectrum. The turbulence power spectral density characterizes the atmosphere, the aircraft frequency response function characterizes the aircraft, and the aircraft response spectrum characterizes the aircraft response to the turbulence. In graphic format, as shown on Figure A-1.

The power spectral density provides information on how the energy in a patch of random turbulence of a given root mean square gust velocity varies with wavelength.

Atmospheric turbulence is caused by some form of instability. This instability can be thermal instability resulting from convection, or mechanical instability resulting from wind shear or flow moving over surface irregularities. In the case of thermal instability the turbulence results from differences in the ground and air temperatures and remains relatively stationary with respect to the ground. Turbulence resulting from mechanical instabilities is related to ground irregularities whether small or large such as hills or mountains, and is also considered stationary with respect to the ground. The turbulence generated by these phenomena is being continually broken down through inertial and viscous forces into smaller and smaller vortices. The turbulence is thus transformed from the longer wavelengths into progressively shorter ones. Thus, regardless of the origin of the turbulence the turbulence properties are best described in terms of distance, i.e. wavelength then frequency.

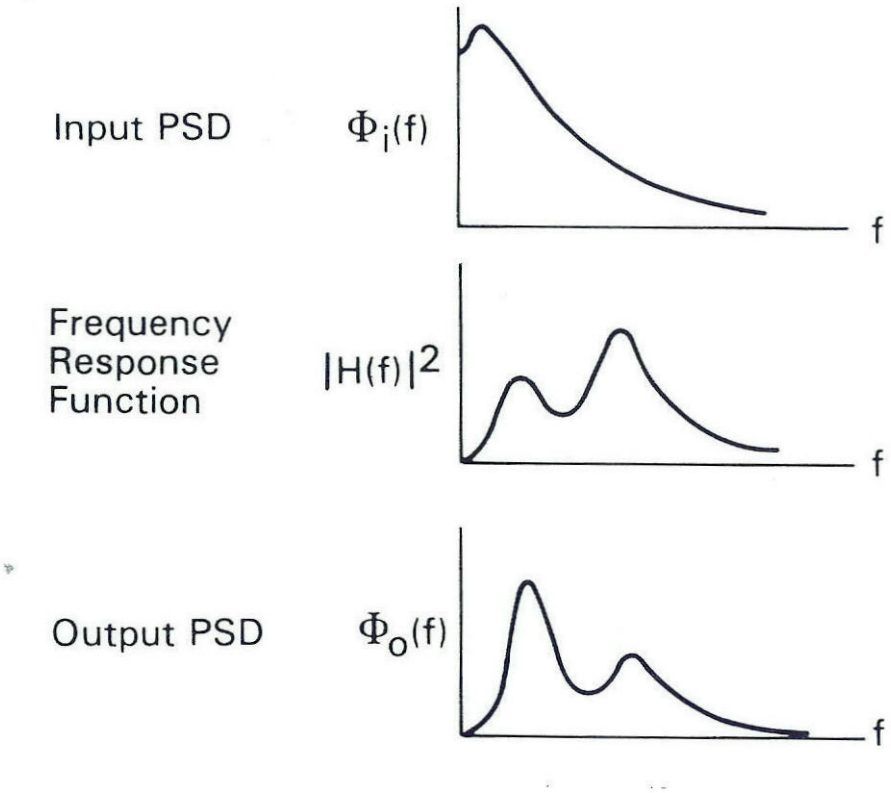

FIGURE A- 1. Input-output relationship for gust response.

The frequency response function describes the aircraft response to sinusoidal gust encounters of unit amplitude at varying frequencies.

The power spectral density provides information on how the energy in a patch of turbulence of a given root mean square gust velocity varies with wavelength. No single analytical model exists, which can accurately describe the atmospheric turbulence over all atmospheric conditions and scale lengths. Of the available power spectral density expressions the von Karman spectrum first suggested for the representation of isotropic turbulence in NASA Technical Report NASA TR R-199 (see Reference A2) is now generally accepted as providing the best overall representation of the measured gust velocity spectra. This is especially true for the inertial subrange represented by the asymptotic region of the spectrum, where most contemporary aircrafts' dynamic responses occur. The von Karman Power Spectral Density (PSD) expression used to describe continuous atmospheric turbulence takes the following form.

$$\Phi(\Omega) = \frac{2L}{\pi} \frac{1 + \frac{8}{3}(1.339L\Omega)^2}{\left[1 + (1.339L\Omega)^2\right]^{\frac{5}{6}}} \qquad \text{(A1)}$$

Figure A-2 shows the von Karman Power Spectral Densities normalized to unit gust velocity for different scale of turbulence values. At the low frequencies where flattening of the curve occurs no reliable gust measurements are available. Consequently, the analytical representation of any turbulence spectrum at these low frequencies has no real meaning.

For a given flight condition, the frequency response function describes the aircraft response to sinusoidal inputs of constant unit amplitude but varying frequencies. The frequency response function can be of varying levels of complexity and be based on the rigid body vertical translation only, or the rigid body short period mode only, or the rigid body modes plus any number of flexible modes. As an example, Figure A-3 shows the frequency response functions for different degrees of freedom. As can be seen the aircraft response is a function of the frequency of the input. These inputs can be sinusoidal gust or longitudinal elevator deflection inputs of varying frequencies. The peaks in the frequency response curves reflect the aircraft's natural frequencies when exited by gust or maneuver inputs. For instance, on Figure A-3 the first peak in curve number 5 corresponds to the rigid aircraft's short period natural frequency.

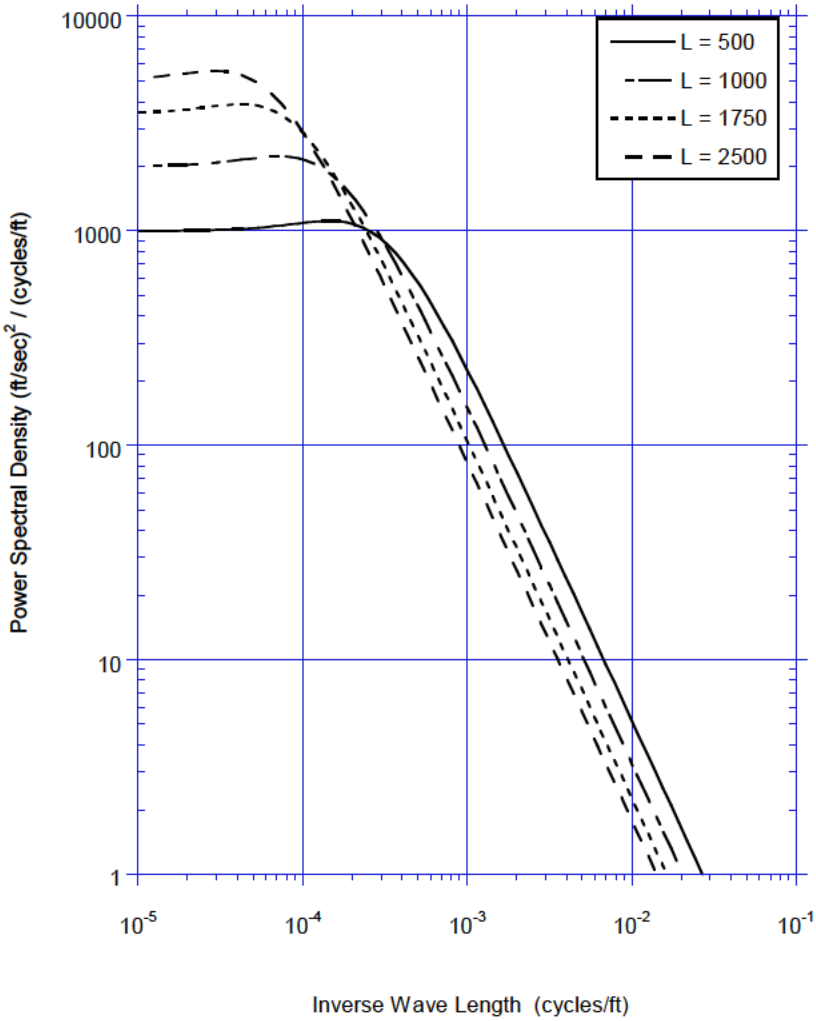

FIGURE A- 2. von Karman spectral densities for various L values.

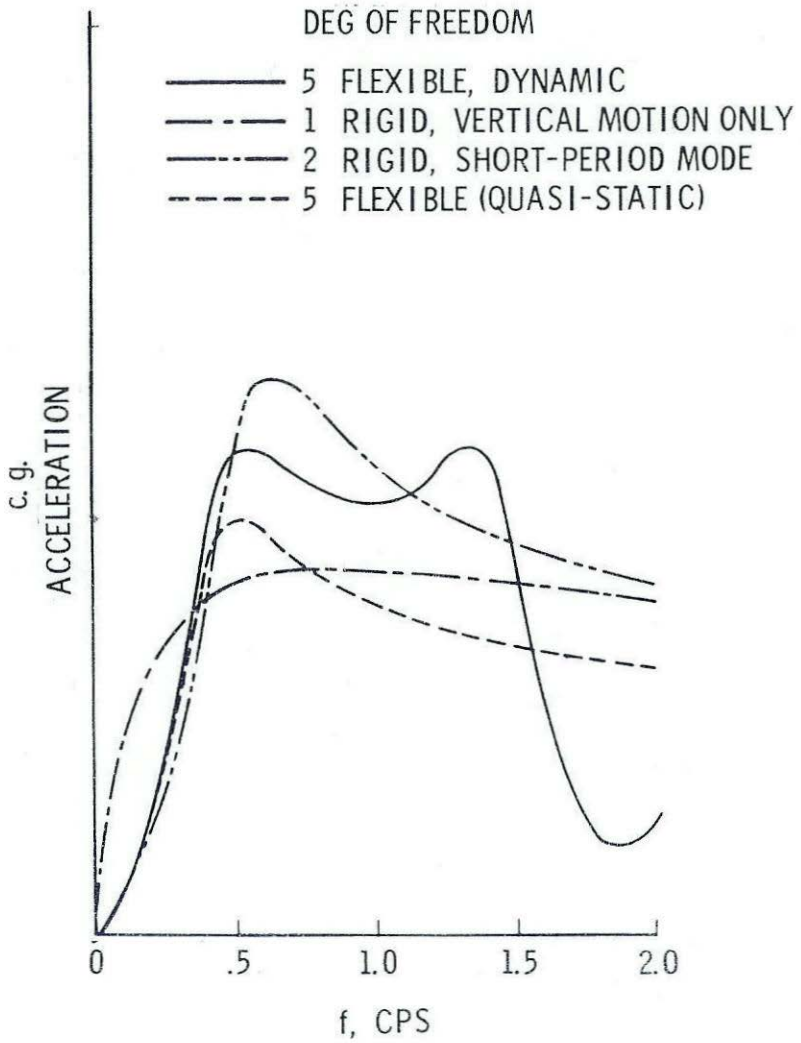

FIGURE A- 3. Center of gravity acceleration frequency response functions.

The response power spectrum is the product of the turbulence spectrum and the frequency response function squared. The frequency response function is representative of a given flight condition of speed, altitude, gross weight and cg position, and is normally given as a function of frequency. Since the turbulence spectrum represents the atmospheric turbulence as a function of gust wavelength, the turbulence input spectrum needs to be redefined as a function of frequency by multiplying the wavelength by the speed of the aircraft. The response power spectrum, as the product of the turbulence spectrum and the frequency response function squared, then reflects what the aircraft actually experiences for the specific flight condition in response to varying wavelengths and gust intensities as described by the gust input spectrum. As shown on Figure A-1, as frequency increases the turbulence exhibits reduced energy. At the same time, the frequency response function may exhibit increased attenuation of the response as frequency increases resulting in an overall reduction in the power level with increasing frequency. Thus the aircraft response to turbulence is significant over a limited range of frequencies.

A.4 MANEUVER-GUST SEPARATION CRITERION

A.4.1 Development of maneuver-gust separation criterion.

The basic measured aircraft flight load parameter of interest to gust loads consists of recorded time histories of vertical acceleration, about its mean while the aircraft is being subjected to turbulence and maneuvers. Figure A-4 presents a snapshot of such a history.

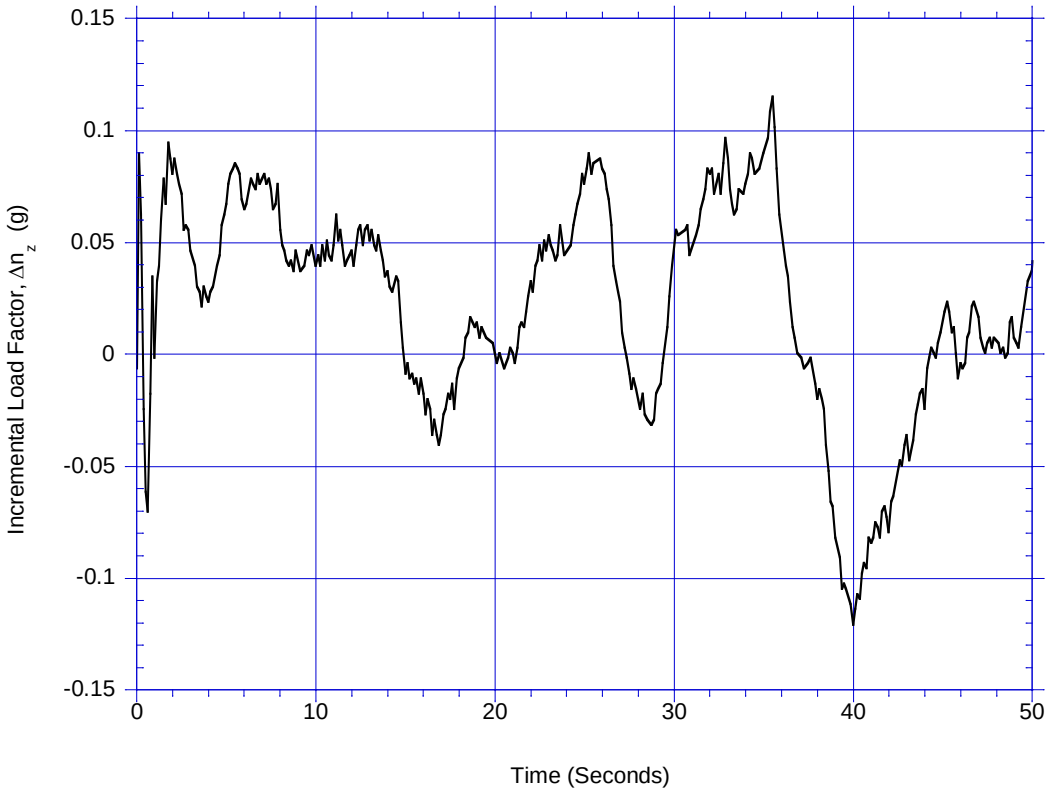

FIGURE A- 4. Load factor time-history.

The accelerations shown on Figure A-4 may be the result of turbulence as well as maneuvers. Because design requirements specify gusts and maneuvers requirements separately, recorded acceleration peaks need to be separated into those resulting from turbulence and those resulting from maneuvers. In order to accomplish this task a maneuver-gust separation technique using basic aircraft response frequencies was developed. Customary pilot inputs for maneuvering an aircraft such as those associated with banking, pulling up and pushing over will generally be of a longer duration than those from individual gusts or continuous turbulence. Figures A-5, A-6, and A-7 present load factor time histories associated with these three maneuver types. Clearly, the durations of such maneuvers associated with changing the flight path are relatively long and at very low frequencies. These frequencies do not excite the normal aircraft rigid body response modes or flexible modes.

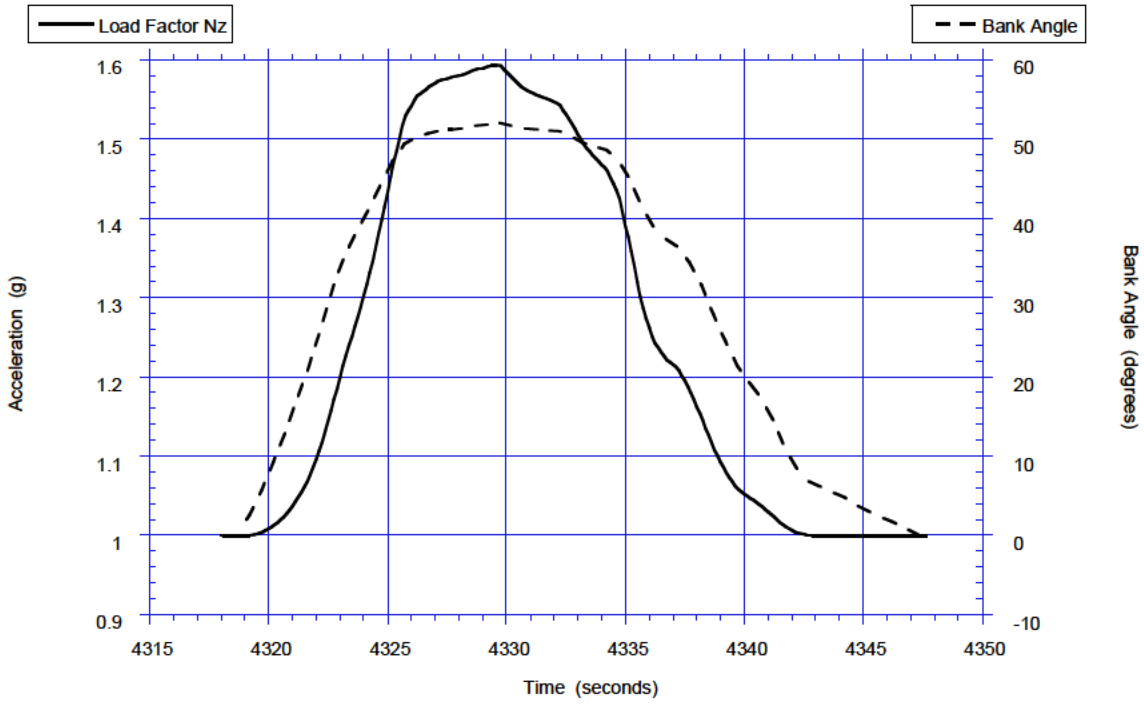

FIGURE A- 5. Banking maneuver time-history.

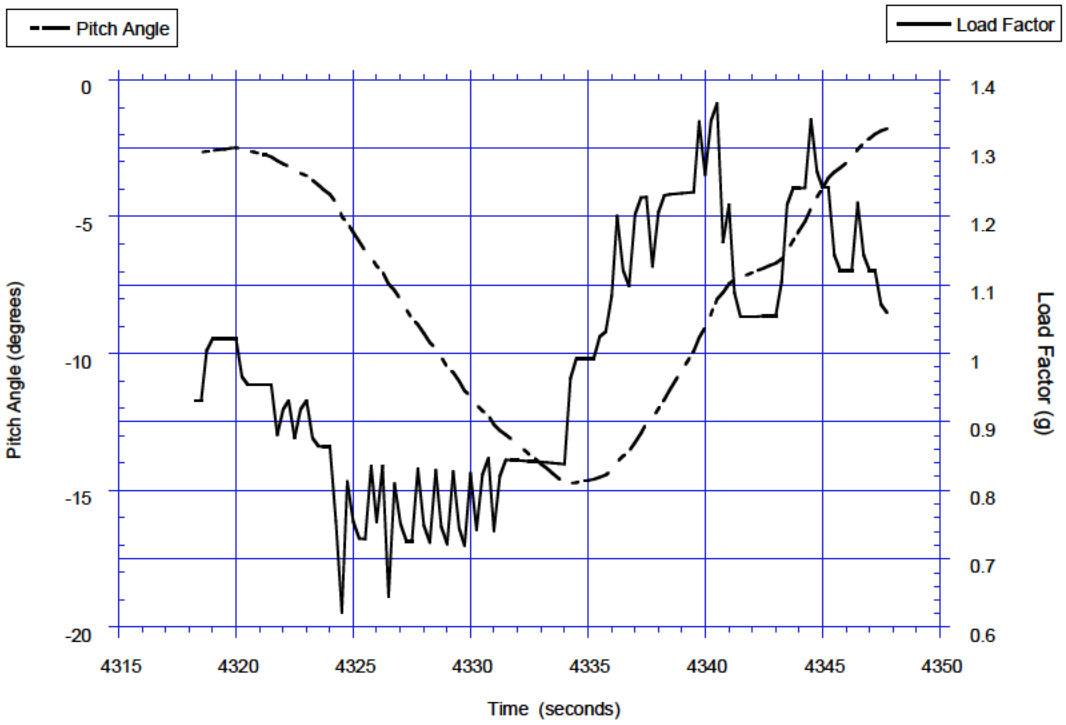

FIGURE A- 6. Push-over maneuver time-history.

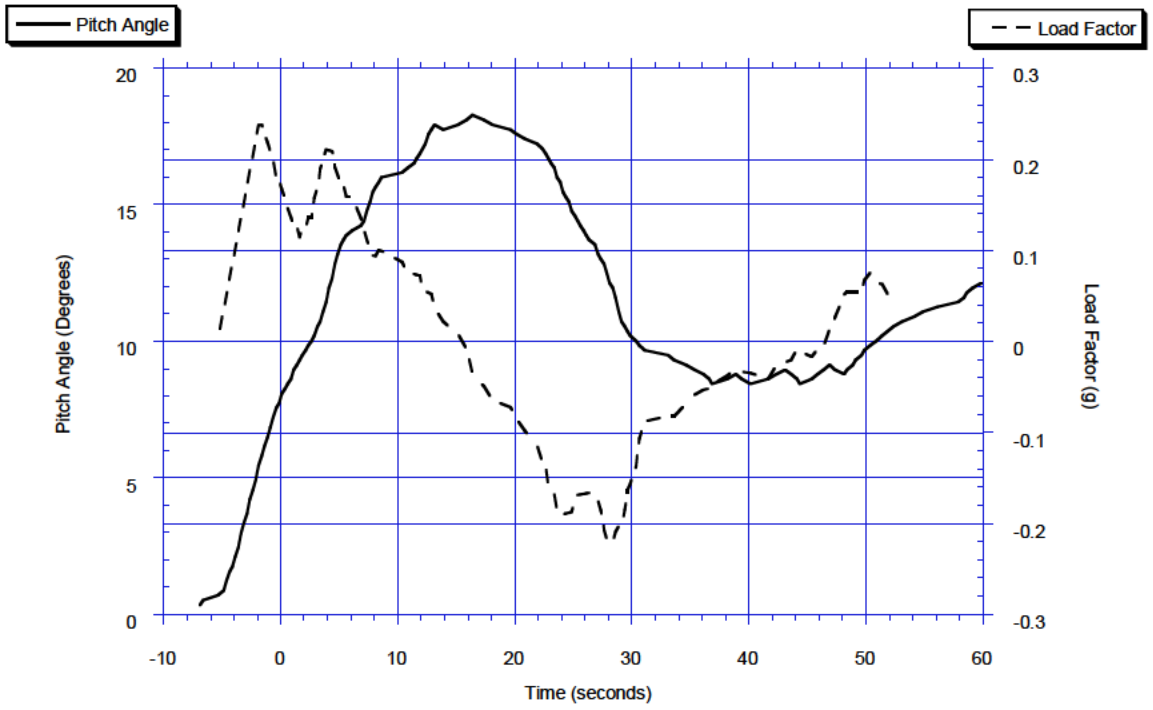

FIGURE A- 7. Pull-up maneuver time-history.

The normal rigid aircraft response modes consist of the short period higher frequency mode and the phugoid lower frequency mode. These modes can be excited by either a maneuver or a gust input. In the case of a maneuver input, the short period mode is excited by a longitudinal control input impulse of a second or less. Whereas, the phugoid mode is of a lower frequency, it would be excited by control inputs more representative of a step type input of several seconds' duration. From a maneuver input perspective, excitation of the short period mode would be a reflection of aggressive maneuvering inputs not expected during normal operational procedures of commercial or military transport aircraft. Flight through choppy air will easily excite the short period oscillations for these aircraft. However, unless abrupt control inputs are made, short period oscillations are highly unlikely to occur due to pilot maneuver inputs. With the aircraft in level flight the main source of excitation will be the turbulence disturbance. Also, the short period mode is relatively well damped and the oscillations damp out very quickly with no pilot effort. Therefore, for our purposes it is assumed that all short period excitations are the result of turbulence and that regardless of the wavelength of the gust no significant acceleration would ordinarily occur at frequencies much slower than the short period frequency.

The phugoid mode is a low frequency oscillation following a small maneuver or gust disturbance. The mode is usually very slow and is rather independent of aircraft characteristics and altitude. A rough approximation of the phugoid mode is:

$$\omega_p = \frac{g}{V_t}\sqrt{2} \qquad \text{(A2)}$$

For speeds of 250 to 800 fps, the frequency of the phugoid mode would typically be from 0.18 to 0.06 radians/sec, 0.0007 to 0.000075 radians per foot or 0.0001 to 0.000012 cycles per foot. These frequencies are in the gust power spectrum frequency range where no reliable gust measurements

are available because the gust velocities have no appreciable effect on aircraft response. It appears reasonable to assume that any phugoid response is initiated by a maneuver input or changes in aircraft state.

Consolidating the previously discussed frequency considerations the maneuver vs gust frequency regimes are defined:

a. Frequencies below the short period frequency as being associated primarily with maneuvers.
b. Frequencies at or above the short period frequency as being associated with gust disturbances.

Having established this baseline for the separation of maneuvers and gusts it now becomes necessary to develop a practical methodology that can be applied to measured time histories of vertical load factor.

A.5 MANEUVER-GUST SEPARATION METHODOLOGY

A.5.1 Development of a maneuver-gust separation methodology.

A rough approximation to the undamped aircraft short period frequency is obtained from:

$$\omega_{sp} = \sqrt{\frac{-qS\bar{c}C_{m\alpha}}{I_{yy}}} \tag{A3}$$

Where:

ω_{sp} = the short period frequency (rad/sec).

q = dynamic pressure (lbs./ft^2).

S = wing area (ft^2).

c = mean aerodynamic chord (mac) (ft.).

$C_{m\alpha}$ = pitching moment curve slope (1/rad).

I_{yy} = Airplane moment of inertia about the yy axis

The total aircraft pitching moment curve slope is:

$$C_{m\alpha} = \frac{\delta C_m}{\delta \alpha_{wb}} = (C_{L\alpha})_{wb}\left[h_{cg} - h_{wb}\right] - V_H (C_{L\alpha})_t \left[1 - \frac{\delta \varepsilon}{\delta \alpha}\right] \tag{A4}$$

Where:

h_{cg} = the cg location in terms of % mac.

h_{wb} = the location of the wing-body aerodynamic center in terms of percent mac.

$$V_H = \frac{l_h S}{\bar{c} S_w}$$

= the volume ratio of the horizontal stabilizer.

l_h = horizontal distance from the cg to the 0.25 MAC of the horizontal tail.

As can be seen in Equation A4, the aircraft pitching moment curve slope is related to the lift-curve slope of the wing and horizontal tail. The lift-curve slope was estimated using the procedures described in USAF Stability and Control DATCOM (see Reference 4). This reference provides the methodology to determine stability and control derivatives without resort to outside information. Determination of the lift-curve slope for this study included considerations of the wing-body contribution with associated wing-body interference factors and the horizontal tail contribution with associated downwash correction.

A.5.2 Aircraft lift-curve slope derivation.
For the rigid aircraft the calculation of the lift-curve slope is based on an extension of the one-dimensional approximation for the wing lift-curve slope presented in the USAF Stability and Control DATCOM, (see Reference 4). The rigid wing lift-curve slope derivative for the subsonic speed regime in USAF Stability and Control DATCOM (see Reference 4) is given as:

$$C_{l_\alpha}(w) = \frac{2\pi A_r}{2 + \left(4 + \frac{A_r^2 \beta^2}{k^2}\left(1 + \frac{\tan^2 \Lambda}{\beta^2}\right)\right)^{1/2}} \qquad \text{(A5)}$$

Where:

$C_{l_\alpha}(w)$ = Wing lift-curve slope per radian.

$A_r = \frac{b^2}{S}$ = Wing aspect ratio based on total plan form area.

b = Wing span.

$\beta = \sqrt{1 - M}$

Λ = 50 percent chord sweep.

M = Mach number.

k = is the ratio of the section lift-curve over 2π.

The factor k in Equation A5 requires knowledge of the wing section lift-curve slope. Since the actual section lift-curve for specific aircrafts is not known, an average value of 0.996 based on 120 NACA wing sections shown in USAF Stability and Control DATCOM (see Reference 4) was used.

The aspect ratio used in Equation A4 is based on the total wing area from tip to the fuselage centerline. Unfortunately, the aircraft industry does not use a fixed definition of the wing reference area used in aerodynamic calculations and the aspect ratio may not always be based on the total wing area. For instance, the definition used by Airbus uses a gross reference area that considers exposed wing area + (area of rectangle inside the fuselage between the leading and trailing edges at the root), while Boeing uses a “wimpress” definition that includes the trapezoidal area + (exposed ''ehudi''break area) + (covered ''ehudi''break area) * (fraction of exposed span at the break). The reference area used by the Engineering Sciences Data Unit (ESDU) is the area of a notional trapezoid having the same exposed area as the actual exposed wing, and with the same tip chord and span. (This notional trapezoid is intended as a rough aerodynamic equivalent to the entire wing and differs from the basic trapezoidal wing). Figure A-8 shows the different wing areas that may be used as the reference area.

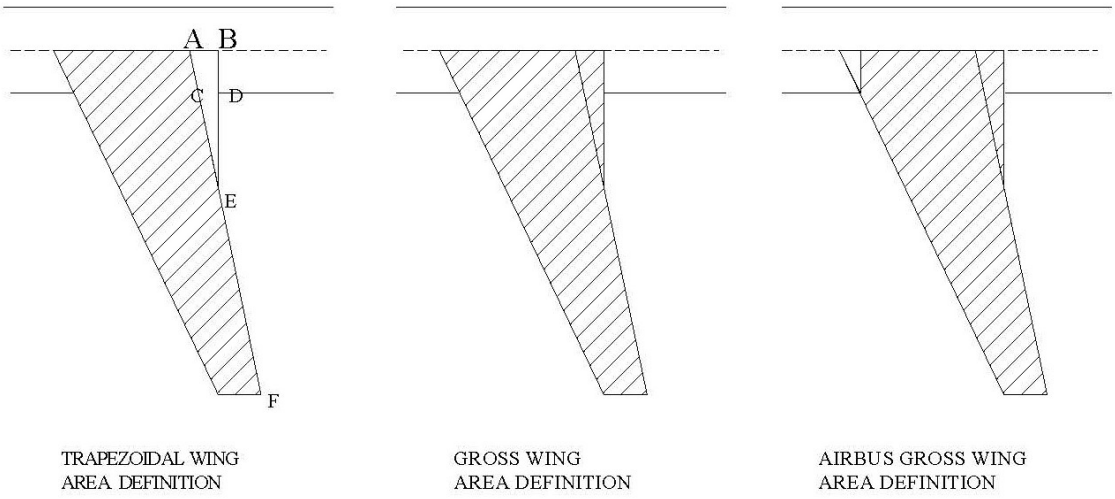

FIGURE A- 8. Wing area definitions.

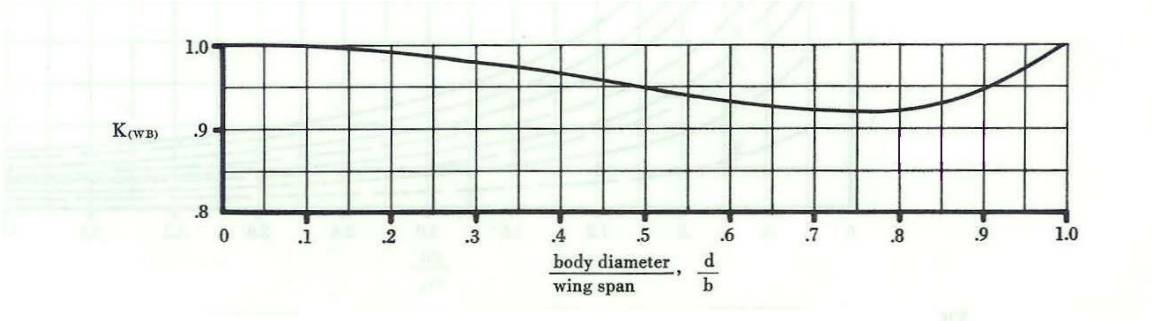

FIGURE A- 9. Wing-body lift ratio.

The methodology of USAF Stability and Control DATCOM (see Reference 4) requires the use of the total wing area. For this study the gross wing area definition as shown in the center of Figure A-8 was used in the derivation of the lift-curve slope. Figure A-9 presents a wing-body correction factor to account for the wing lift in the presence of the body.

This curve can be represented by an equation of the form:

$$K(wb) := 1.0065 - 0.13583\cdot\frac{df}{bw} + 0.20113\cdot\left(\frac{df}{bw}\right)^2 - 3.7697\cdot\left(\frac{df}{bw}\right)^3 + 3.7218\cdot\left(\frac{df}{bw}\right) \quad \text{(A6)}$$

The lift-curve slope for the wing-body then becomes:

$$C_{l_\alpha}(wb) = K(wb)\frac{2\pi A_r}{2+\left(4+\frac{A_r^2\beta^2}{k^2}\left(1+\frac{\tan^2\Lambda}{\beta^2}\right)\right)^{1/2}} \quad \text{(A7)}$$

To calculate the total aircraft lift-curve slope, the effects of the horizontal tail needs to be added. The horizontal tail contribution is expressed by the following equation.

$$Cl_\alpha(ht) = \frac{S_{HT}}{S_W}\eta\left(1-\frac{d\varepsilon}{d\alpha}\right)Cl_{\alpha HT} \quad \text{(A8)}$$

Where:

$Cl_{\alpha HT}$ = Basic horizontal tail lift-curve slope.

$Cl_\alpha(ht)$ = Horizontal tail contribution to total aircraft lift-curve slope.

S_{HT} = Total horizontal tail area.

S_W = Total wing area.
$d\varepsilon/d\alpha$ = The rate of change in downwash with wing angle of attack.

The basic horizontal tail lift-curve slope Cl_{HT} can be calculated using Equation A4 as was done for the wing, but using the proper parameters for the horizontal tail.

The value of the wing downwash parameter $d\varepsilon/d\alpha$ can be calculated Equation A9 as obtained from NASA Technical Report NASA TR R-199 (see Reference A2):

$$\frac{d\varepsilon}{d\alpha} = 4.44\left(K_a K_\lambda K_h \sqrt{\cos(\Lambda_w)}\right)^{1.19} \quad \text{(A9)}$$

Where:

$$K_a = \frac{1}{AR_w} - \frac{1}{1 + AR_w^{1.7}} \tag{A10}$$

$$K_\lambda = \frac{10 - 3\lambda_w}{7} \tag{A11}$$

$$K_H = \frac{1 - \frac{v_h}{b_w}}{\sqrt[3]{\frac{2l_h}{b_w}}} \tag{A12}$$

To obtain the total aircraft lift-curve slope the lift-curve slope for the wing-body and the horizontal tail are added as show in the following equation.

$$Cl_\alpha = Cl_\alpha(wb) + \frac{S_{HT}}{S_W}\eta\left(1 - \frac{d\varepsilon}{d\alpha}\right)Cl_\alpha(ht) \tag{A13}$$

To validate the above procedure for calculating the lift-curve slope the equations were used to derive the rigid aircraft lift-curve slope values for five aircrafts for which these values were available. Figures A-10 – A-14 show the comparison between the known and calculated lift-curve slopes for these five aircrafts. In each case the lift-curve slopes are referenced to the wing reference areas used by the aircraft manufacturer rather than the total wing area.

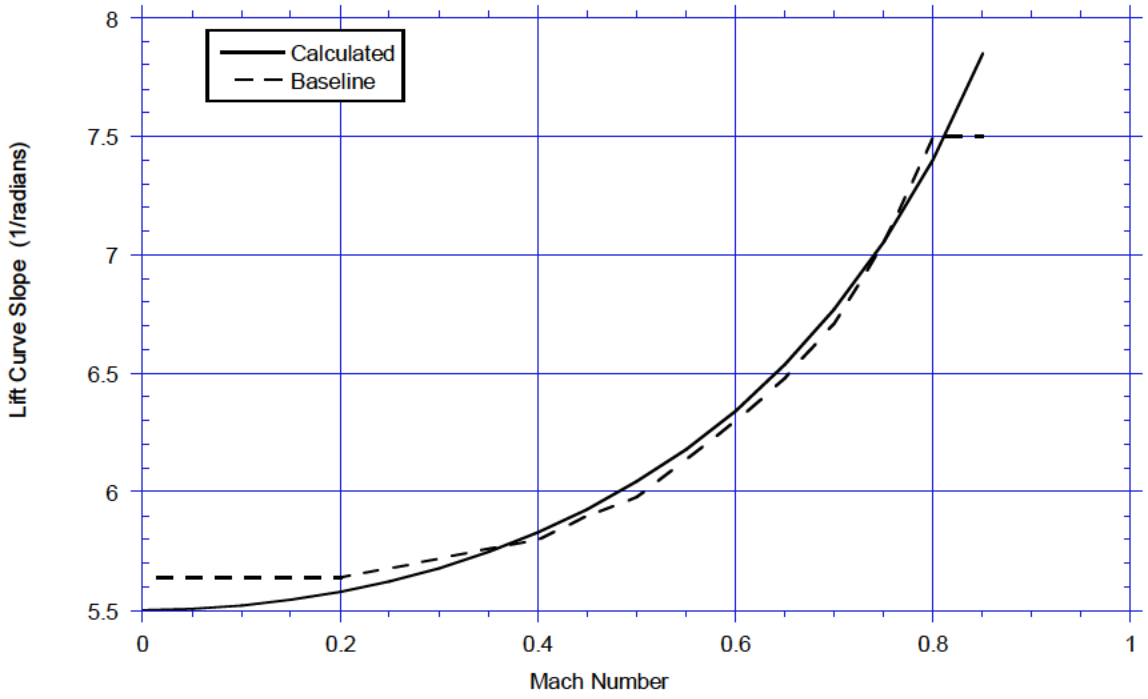

FIGURE A- 10. A-320 calculated vs baseline total aircraft lift-curve slope comparison.

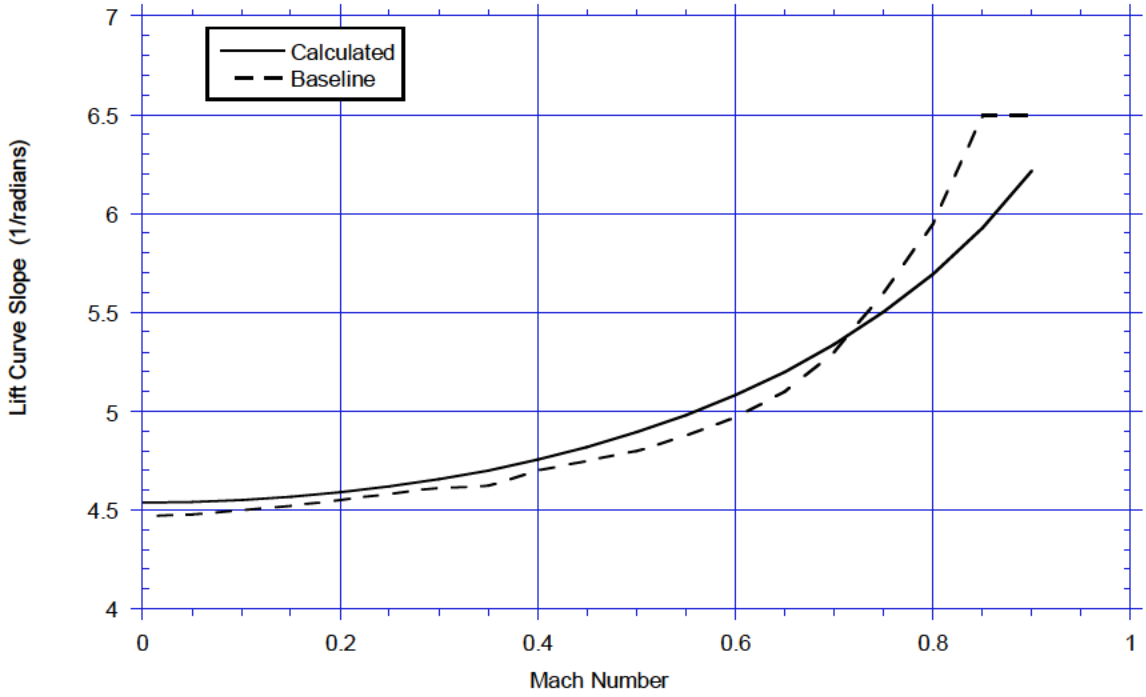

FIGURE A- 11. DC-10-10 calculated vs baseline wing-body lift-curve slope comparison.

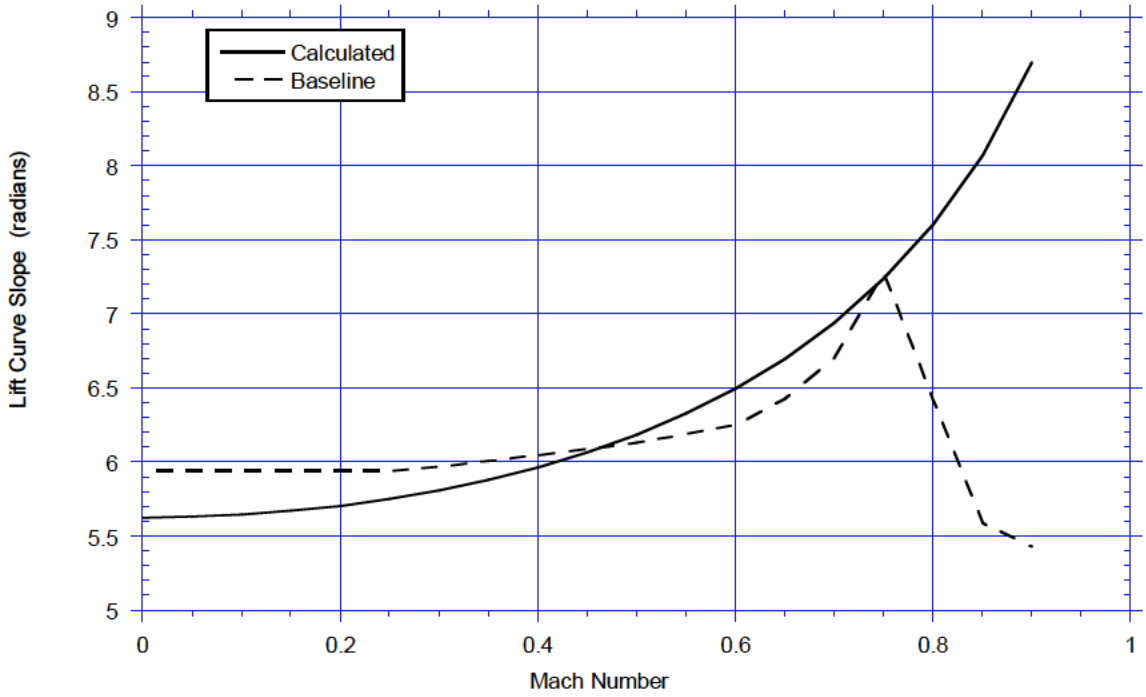

FIGURE A- 12. MD-82 calculated vs baseline total aircraft lift-curve slope comparison.

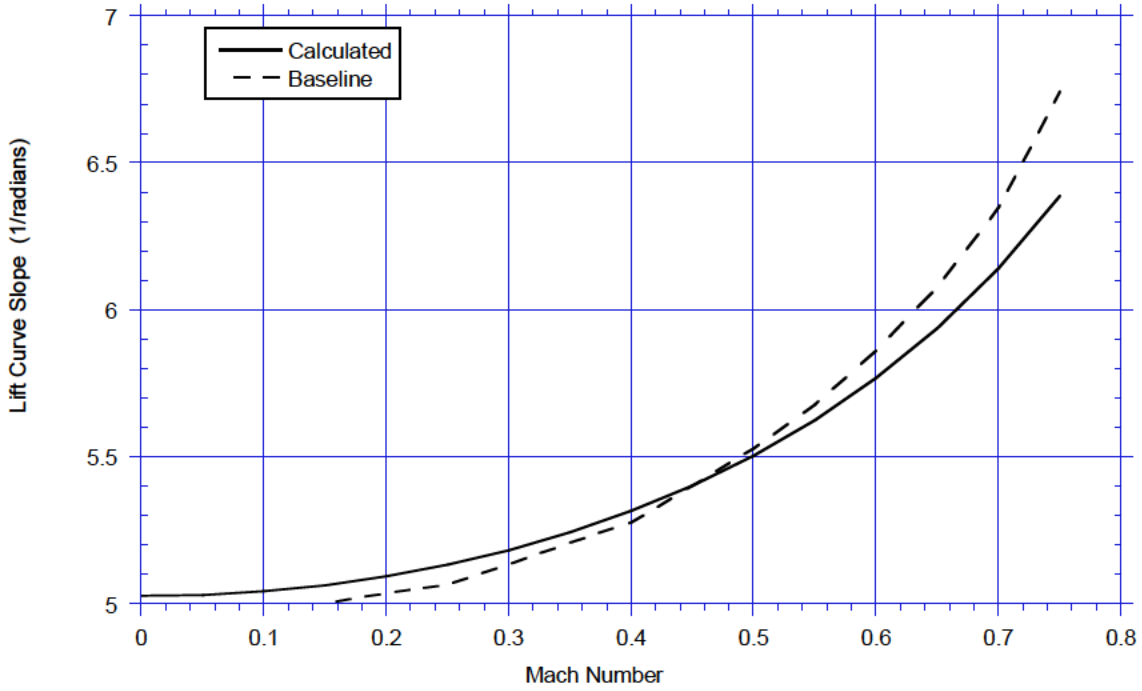

FIGURE A- 13. C-141A calculated vs baseline total aircraft lift-curve slope comparison.

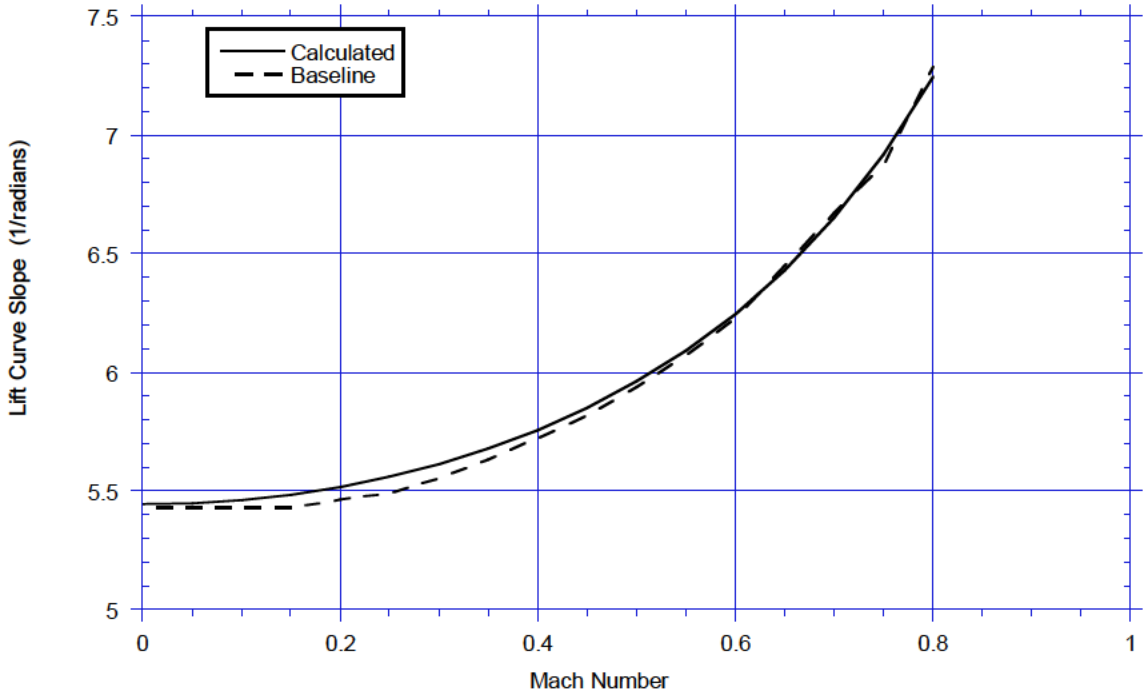

FIGURE A- 14. C-5A calculated vs baseline total aircraft lift-curve slope comparison.

A.5.3 Aircraft short period frequency derivation.

As can be seen in Equation A4 the aircraft pitching moment curve slope, or the pitching stiffness, is a function of the center of the lift-curve slope and gravity location. The derivation of the lift-curve slope was discussed in the previous section. It is difficult to define a cg location that is

representative for any aircraft for any flight. Attempts to define the cg location based on a fixed percent mac ahead of the aircraft's neutral point during a flight were found to be inconclusive. For all transport aircrafts, it was decided to assume the cg location to be at 25 percent of the mean aerodynamic chord. Taking the wing-body aerodynamic center at 25 percent mac the pitching moment becomes a function of the horizontal stabilizer effectiveness only.

As can be seen in Equation A3, derivation of the short period frequency also requires the aircraft moment of inertia about the aircraft's y-y axis. The aircraft moment of inertia can be estimated from Figure A-15 obtained from Airplane Flight Dynamics and Automatic Flight Controls, Part 1 (see Reference A4). The regression line shown on Figure A-15 can be reproduced using the following equation.

$$I_{yy} = .000070348*GW^{2.0337} \qquad \text{(A14)}$$

A.5.4 Separation criterion derivation.

The short period frequency was calculated for the flight conditions of speed, altitude, and gross weight which existed at the coincident time of each positive or negative load factor peak in the recorded load factor time histories from two randomly selected flights for each of the aircraft identified in Table A-I.

TABLE A- I. Aircraft in study.

AIRCRAFT
ERJ-145XR
B-737-400
B-737-700
A-320
B-767-200ER
B-777-200ER
B-747-400

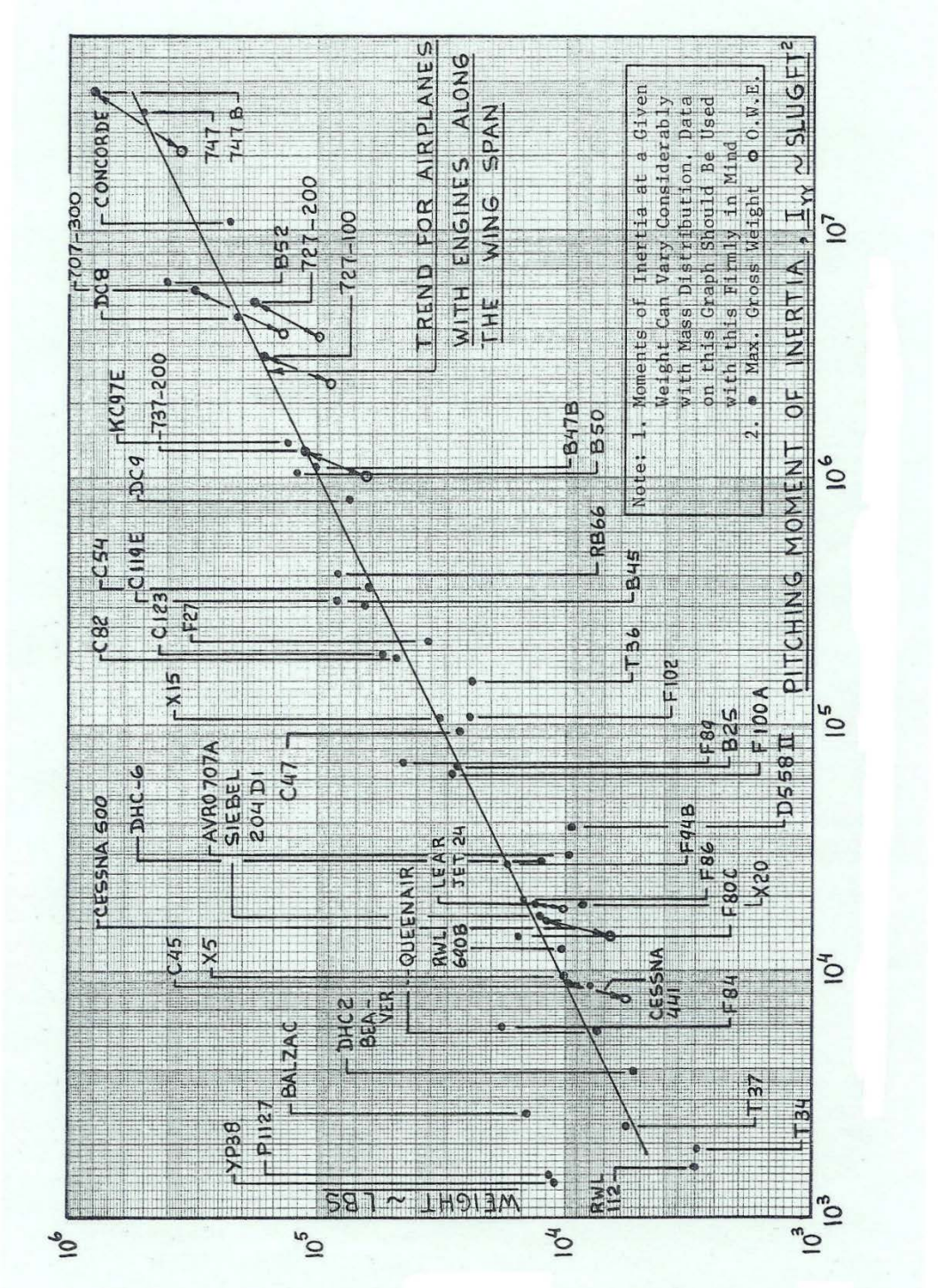

FIGURE A- 15. Variation of pitching moment of inertia with aircraft weight.

Figure A-16 shows the variation of the short period frequency of the aircraft for the flight conditions coincident with the time at the vertical acceleration peaks throughout two flights for each of the aircrafts identified in Table A-I. From this figure it can easily be observed that the value of the short period frequency varies not only with flight phase but also between aircraft. The figure shows that the response frequency is in inverse proportion to the size of the aircraft. The

inverse of half of the short period frequency value provides the characteristic wavelength of the aircraft response peak to a maneuver or gust input. Figure A-17 shows the average cycle lengths that can be expected at any time during the flight for each of the aircrafts. Figure A-18 presents the cycle duration for the 14 flights as a function of Mach number. From these figures it is clear that a fixed cycle duration criterion, such as 2 seconds, is not appropriate for all aircrafts or for all phases of flight.

Figure A-18 also shows that except for the magnitude level, the shapes of the cycle time curves as a function of Mach number are quite similar with the cycle time getting shorter with increasing Mach number. In itself this is not surprising because for a gust input of a fixed length the gust duration will be shorter as the speed at which the gust is traversed increases, i.e. gust duration = gust length/speed. The shorter gust duration input (higher frequency) will excite the higher response frequencies resulting in shorter duration response peaks. The differences in cycle length for different aircraft at a fixed Mach number are of course the result of differences in the aircraft frequency response characteristics. For a fixed Mach number the smaller aircraft are more sensitive to higher frequency gusts then the larger aircraft. Hence, the lower cycle times as aircraft size decreases.

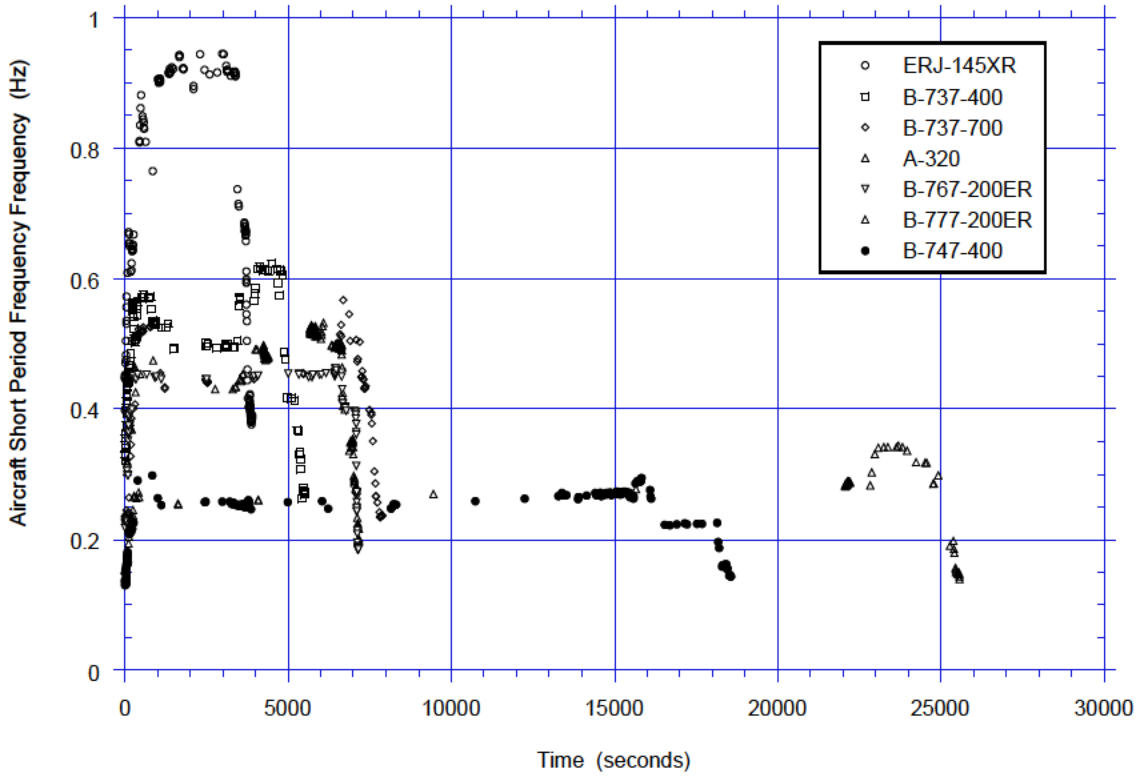

FIGURE A- 16. Aircraft short period frequency vs flight time.

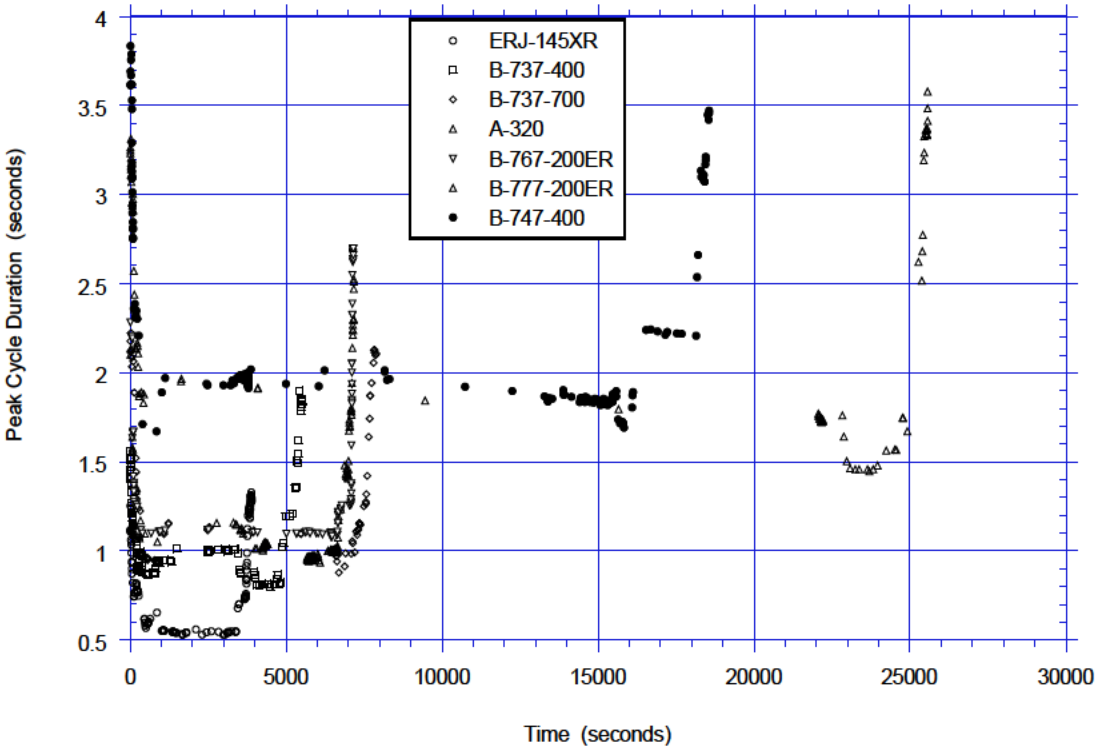

FIGURE A- 17. Peak cycle duration vs flight time.

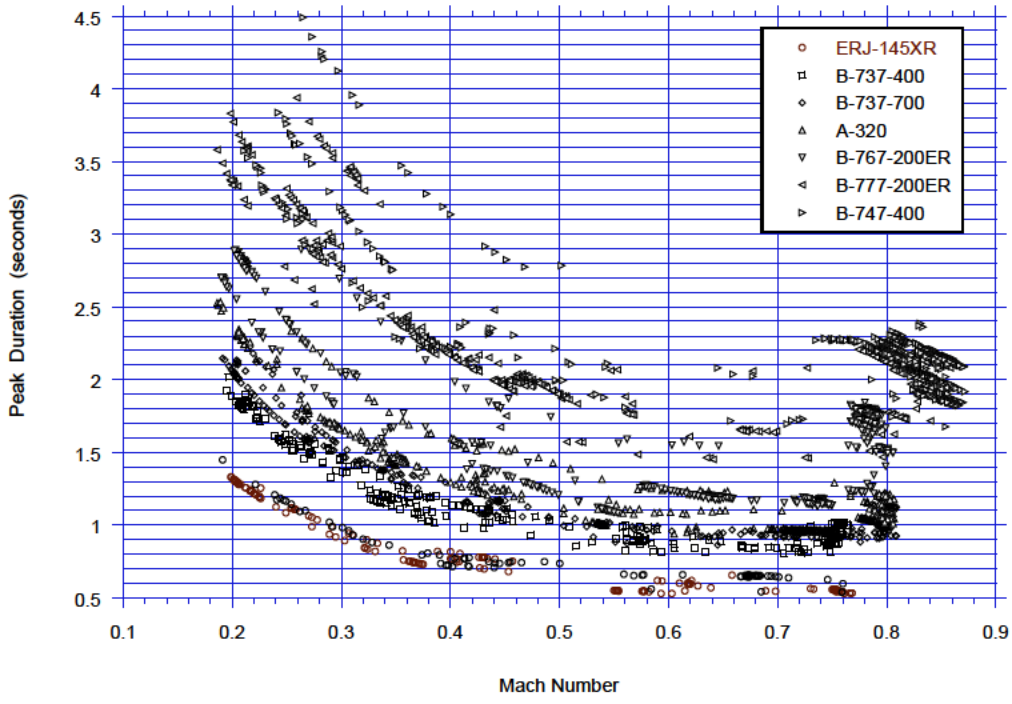

FIGURE A- 18. Peak cycle duration vs mach number.

It was found that the data scatter shown on Figure A-18 can be reduced by dividing the cycle time for each aircraft by the aircraft's gross weight raised to the 0.46 power. The data on Figure A-18 then collapses into a closely banded series of curves that can be represented by a third order polynomial equation. Figure A-19 shows the final normalized cycle duration as a function of Mach number.

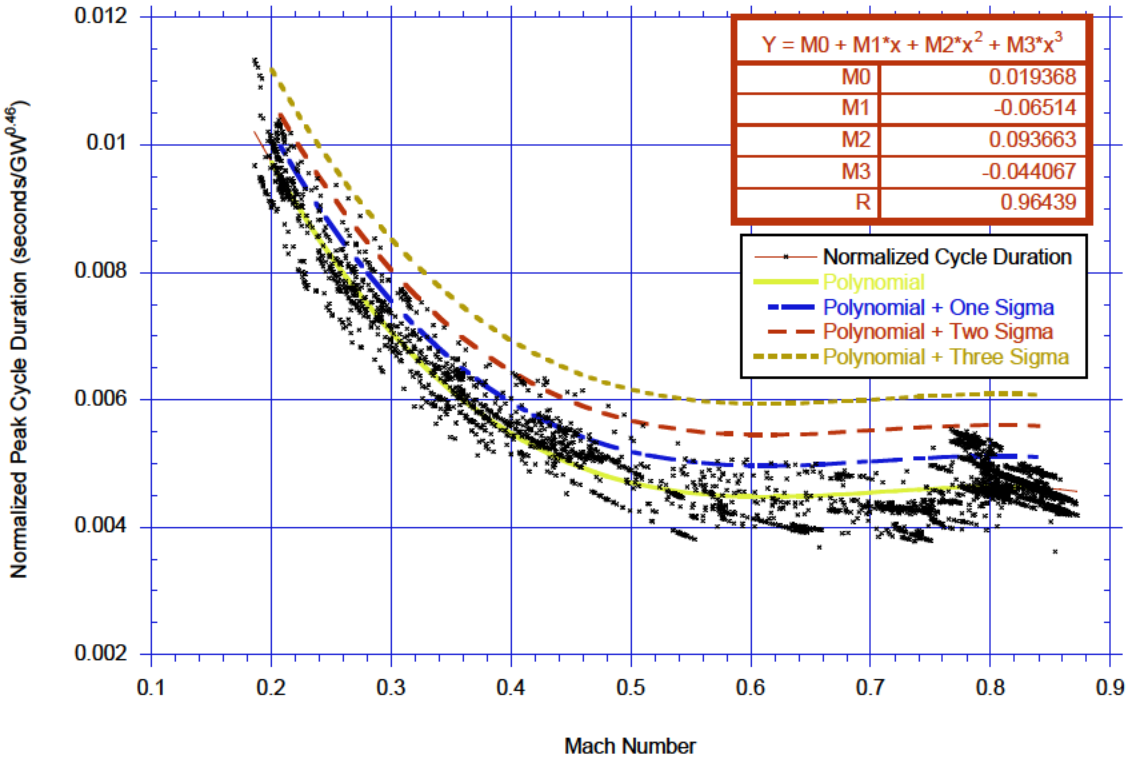

FIGURE A- 19. Normalized peak cycle duration vs mach number.

The value of 0.46 for the gross weight exponent was selected based on the maximum correlation coefficient obtained from a series of polynomial curve fits of the data at increasing fractional exponent values to which the gross weight was raised. Figure A-20 shows the variation in correlation coefficient with the gross weight exponent level.

The data points on Figure A-19 and the associated polynomial curve fit suggests an approach that can be used during data processing to determine the cycle duration for a maneuver-gust separation criterion throughout a flight. As suggested by Personal Communication (see Reference A5) and as portrayed on Figure A-21, for some frequency increment below the short period frequency the response may be due to either gusts or maneuvers.

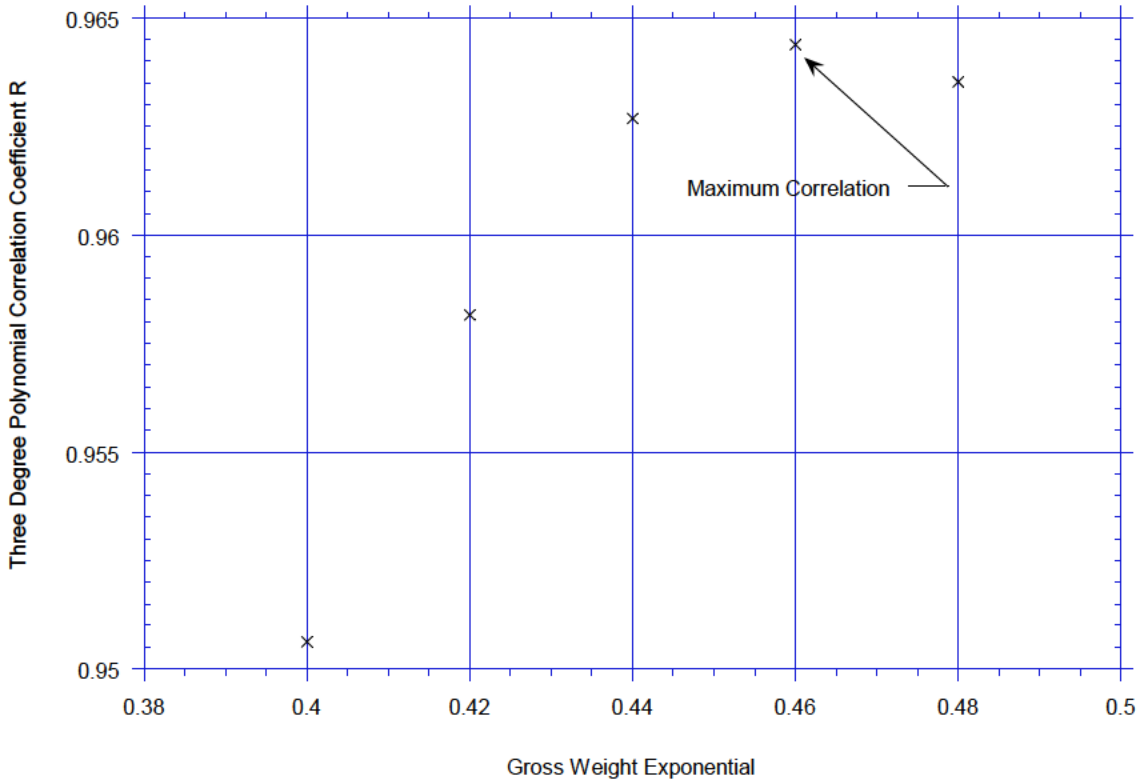

FIGURE A- 20. Correlation factor vs gross weight exponent value.

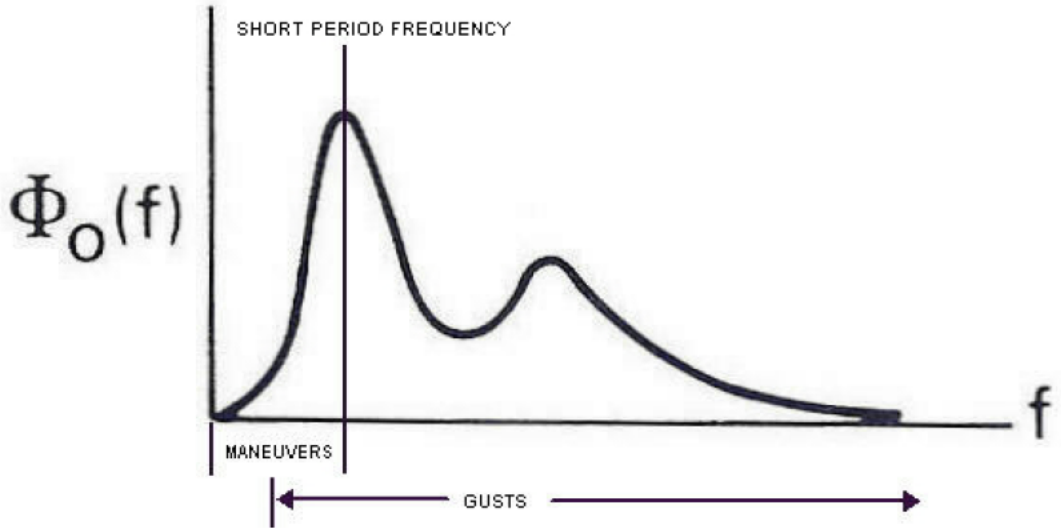

FIGURE A- 21. Aircraft response power spectral density.

Therefore as suggested by Personal Communication (see Reference A5), it seems rational to bias the maneuver-gust separation criterion to somewhat longer cycle durations than would be obtained from average curve based on the polynomial equation. The standard deviation of the data points from the polynomial on Figure A-19 above is 0.0004857. Therefore, Figure A-19 also shows

curves that represents the polynomial plus one, two and three standard deviations. In order to account for lower frequency gusts below the average short period frequency it is suggested that the polynomial plus three standard deviations be used to determine the cycle length for the separation of maneuvers and gusts. The use of this curve or algorithm in data reduction will provide the feasibility of adjusting the maneuver-gust separation cycle time to account for aircraft size differences and speed variations.

Cycle duration for this peak equal to or less than the calculated value would be considered a gust response. A cycle duration longer than the average calculated cycle response would be classified as a maneuver. The final polynomial equation including the three sigma spread would be as follows:

$$t = (0.020825-0.06514M+0.093663M^2-0.044067M^3)\, W^{0.46} \qquad \text{(A13)}$$

A.6 CONCLUSIONS

A.6.1 Conclusions.

Accurate durability and damage tolerance analyses of an aircraft structure are needed to: (1) validate existing certification criteria, (2) design repairs, (3) implement engineering changes, or (4) to establish capability for a new design. This accuracy can be enhanced by improved understanding and reliability of the available maneuver and gust spectra. This accuracy can be improved by refinement of the maneuver-gust separation techniques used, while the reliability is improved by the reduction of larger amounts of measured flight loads data for different classes and types of aircrafts. Improvements in accuracy of maneuver and gust spectra from measured data needs to be measured against the many other variables in the design process influencing the final structural integrity. Improvements in the accuracy of defining maneuver and gust spectra from measured data needs to be measured against the many variables in the design process, which influence the final structural integrity. Improvements in the reliability of the maneuver and gust spectra needs to be measured against the ease or difficulty of processing large amount of data. To accomplish this, the method used to separate maneuver and gust accelerations from measured acceleration time histories should provide consistent estimates of the frequency distribution of maneuvers and gust. The process should also require minimal human interface and be general enough to allow the efficient processing of large amounts of data without requiring changes to account for differences in aircraft type and any data parameters.

Maneuver-gust separation using a cycle duration criteria has been used in government and industry for many years. The DOT/FAA/AR-99/14 (see Reference A1) suggested the use of a 2-second cycle duration time for the separation of gusts and maneuvers from acceleration time histories. The study described in this report indicates that aircraft gust response frequency characteristics are considerably different between both aircraft types and the different phases of flight. Since the variation in gust response frequency characteristics results in corresponding variations in cycle duration, a gust-maneuver separation criterion based on single cycle duration of 2 seconds applicable to all aircraft types and flight phases is not considered appropriate. This study developed a variable peak cycle duration criterion for gust-maneuver separation that will account for the variations in cycle time by aircraft size and flight phase. The new cycle duration criterion

can be programmed with a simple algorithm that requires only Mach number and aircraft gross weight as inputs and is easily implemented for use in separating gusts and maneuvers in large numbers of time histories. The new criterion provides an improved method of using the time honored cycle duration as a means for separating gusts and maneuvers.

APPENDIX B

DERIVATION OF CONTINUOUS TURBULENCE FIELD PARAMETERS

B.1 SCOPE

B.1.1 Scope.

The continuous turbulence model used in the airworthiness requirements is described by a power spectral density function and a mathematical equation expressing the distribution of continuous gust intensity magnitudes. The distribution of continuous gust intensities is described in the form of generalized exceedance curves that may be used to determine any gust response load parameter for any other aircraft. The generalized gust intensity exceedance curves are represented by an equation that contains two probability parameters (P) that represent the proportions of time spent in two turbulence levels of two different root mean square (rms) intensity levels as indicated by a parameter (b). The P and b parameters are often referred to as turbulence field parameters. This appendix describes the derivation of generalized exceedance curves from measured load factor exceedances and the associated turbulence field parameters. The appendix also contains the generalized exceedance curves and associated turbulence field parameters based on actual B-737-400/700 operational load factor measurements.

B.2 APPLICABLE DOCUMENTS

B.2.1 Other Government documents, drawings, and publications.

The following other Government documents, drawings, and publications form a part of this document to the extent specified herein.

B1. Press, Harry, Meadows, May T., and Hadlock, Ivan, “A Re-evaluation of data on Atmospheric Turbulence and Airplane Gust Loads for Application in Spectral Calculations,” NACA Report 1272, 1956.

B2. Press, Harry, Steiner, Roy, “An Approach to the Problem of Estimating Severe and Repeated Gust Loads for Missile Operations, NACA Note 4332, September 1958.

B3. Rice, S. O., “Mathematical Analysis of Random Noise,” Bell Systems Technical Journal, Volume XXIII, No. 3, July 1944, pp282-332, and Volume XXIV No. 1 January 1945, pp 46-156.

B4. Press, William H, Brian P. Flannery, Saul A. Teukolskyand, William T. Vetterling, “Numerical Recipes in C, the Art of Scientific Computing,” Cambridge University Press, 1993.

B.3 GENERALIZED EXCEEDANCE EXPRESSION

B.3.1 Generalized exceedance expression.

The probability of the rms gust velocities in the various continuous turbulence patches is described by the probability density function. If it is assumed that the form of the power spectral density does not change, the turbulence experienced by an aircraft can be defined by the probability distribution of the rms gust velocity as a function of altitude. Based on the approach presented in

NACA Report 1272 (see Reference B1), NACA Note 4332 (see Reference B2) introduced a mathematical expression for the probability distribution of rms gust velocity of the following form.

$$\hat{f}(\sigma_w) = P_1 \frac{1}{b}\sqrt{\frac{2}{\pi}} e^{-\frac{\sigma_w^2}{2b_1^2}} + P_2 \frac{1}{b}\sqrt{\frac{2}{\pi}} e^{-\frac{\sigma_w^2}{2b_2^2}} \qquad \text{(B1)}$$

Mathematical Analysis of Random Noise (see Reference B3) presents an expression that relates the number of positive slope zero crossing in a time history to the rms gust velocity of the continuous turbulence.

$$N_y = N_0 e^{-\frac{y^2}{2\sigma_y^2}} \qquad \text{(B2)}$$

Entering the mathematical formulation of the probability density distribution of the rms gust velocities of Equation B2 in Equation B1 provides a convenient description of the probability of exceedance of any response quantity.

$$\frac{N_y}{N_0} = P_1 e^{-\frac{y/\bar{A}}{b_1}} + P_2 e^{-\frac{y/\bar{A}}{b_2}} \qquad \text{(B3)}$$

The equation describes the turbulence experienced in normal operations as consisting of two general types. One type consisting of light to moderate turbulence termed "nonstorm" turbulence and one consisting of more severe turbulence termed "storm" turbulence. However, the distinction of nonstorm and storm turbulence is misleading because the curves represent all types of turbulence from light to severe regardless of its causes, and in fact may include very little, if any true storm data.

The P values represent the proportion of total flight time spent in each type of turbulence, and the b values are indicative of the overall intensity of each type. $\bar{A}$ and N_0 are aircraft response characteristics where $\bar{A}=\sigma_y/\sigma_w$ and N_0= the number of zero crossings or the number of exceedances of y=0. Ny represents the cumulative occurrences per unit time of the value y where y can be any response peak, such as acceleration, stress, bending moment etc. The value of $y/\bar{A}$ represents the true gust velocity. A semilog plot of Ny/N_0 versus $y/\bar{A}$ results in a generalized exceedance curve that describes the probability of exceeding the continuous turbulence gust intensity peaks.

B.3.2 Aircraft gust response factor.

If the quantity "y" in Equation B3 is defined as the incremental load factor from 1.0 g then the rms gust velocity U_σ is:

$$U_\sigma = \frac{\Delta n_z}{\bar{A}} \qquad \text{(B4)}$$

$\bar{A}$ in Equation B3 represents the incremental load factor response to unit rms gust velocity and is obtained by integration of the dynamic response function H_y squared times the von Karman power spectral density for unit gust velocity.

$$\bar{A} = \left[\int_0^{\Omega_c} \left| H_y \right|^2 \Phi_w(\Omega) d\Omega \right]^{\frac{1}{2}} \tag{B5}$$

An accurate determination of $\bar{A}$ requires a detailed dynamic analysis to calculate the aircraft dynamic response function H_y and involves aircraft aerodynamic, mass, and stiffness data that are not available for this analysis. In Technical Report AFFDL-TR-70-106 (see Reference 1), Houbolt presented a procedure for atmospheric data reduction that included a simplified approach for calculating $\bar{A}$ values based on continuous gust and spectral density approach considerations. The response transfer coefficient $\bar{A}$ is defined as shown in Equation B6 where the value K_Φ represents an alleviation factor. This factor as originally proposed was a function of gust length L and mean aerodynamic chord as shown on Figure B-1. Based on an analysis of a number of different aircrafts, in AGARD-R-734-ADD (see Reference 2), Houbolt presented an acceptable approximation of the continuous gust alleviation factor using a single equation. Subsequently, Houbolt derived another approximation that gave more accurate results. This final simplified formulation of K_Φ was presented in AGARDograph (see Reference 3) and is shown in Equation B7.

$$\bar{A} = \frac{\rho V C_{L\alpha} S}{2W} K_\Phi \tag{B6}$$

$$K_\Phi = \frac{11.8}{\sqrt{\pi}} \left[\frac{\bar{c}}{2L} \right]^{\frac{1}{2}} \sqrt{\frac{\mu}{110 + \mu}} \tag{B7}$$

Where:

$$\mu = \frac{2W}{\rho g \bar{c} C_{L\alpha} S} \tag{B8}$$

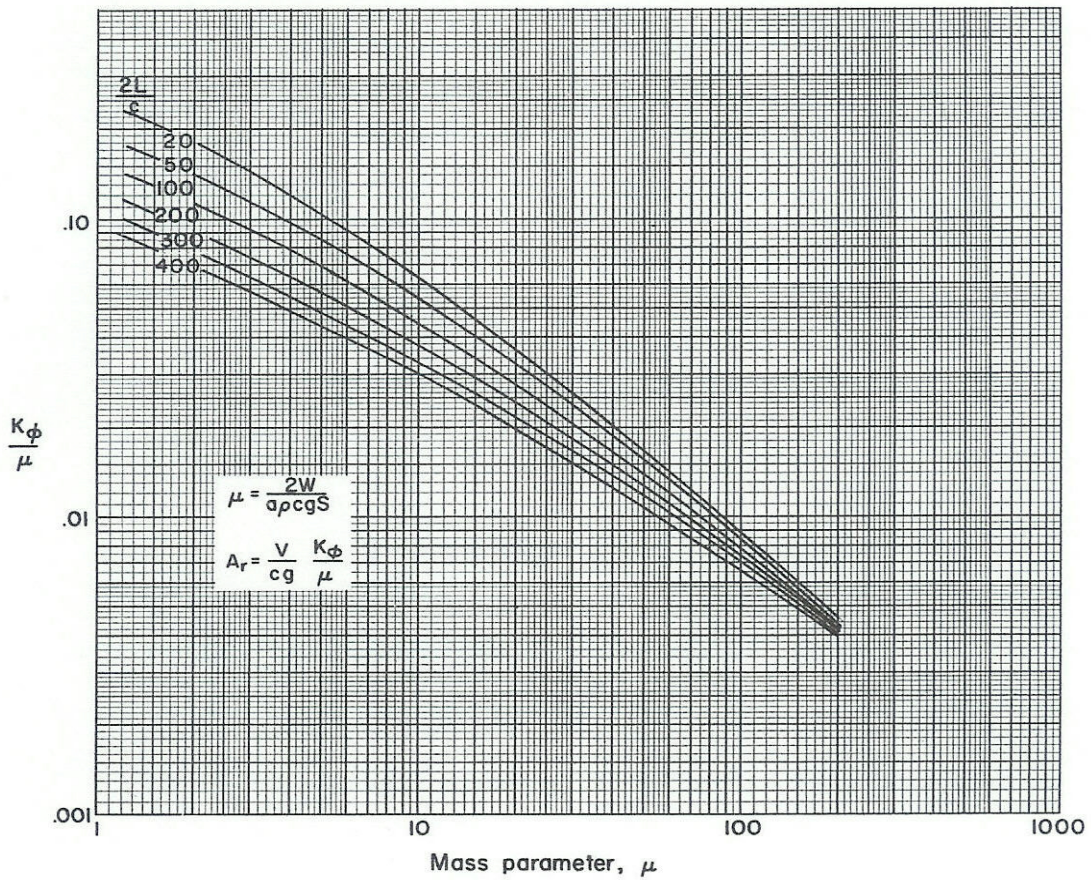

FIGURE B- 1. Variation of K_Φ / μ with μ.

B.3.3 Aircraft characteristic response frequency.

The parameter N_0 in Equation B3 is representative of the aircraft's characteristic response frequency to continuous turbulence. This value is obtained by:

$$N_0 = \left[\frac{\int_0^{\Omega_c} |H_y|^2 \, \Phi_w(\Omega) d\Omega}{\int_0^{\Omega} \Phi_w(\Omega) d\Omega} \right]^{\frac{1}{2}} \qquad \text{(B9)}$$

As with the calculation of $\bar{A}$ an accurate calculation for N_0 also requires a detailed dynamic analysis to calculate the aircraft dynamic response function H_y and involves aircraft aerodynamic, mass, and stiffness data that is not available for this analysis. In accordance with Equation B3 the value of N_0 also represents the total number of zero crossings of the acceleration trace with positive or negative slope. This equates to the total number of positive or negative peaks in terms of cycles per second. This then provides an approach to derive the value of N_0 through extrapolation of the peak count distribution curve from the counts at the threshold level to the zero gust velocity level. The approach provides values for N_0 that are more directly related to the actual flight conditions

that existed during the flight in turbulence. This extrapolation can be performed using a general curve fit equation based on the mathematical formulation of Equation B3. Figure B-2 provides an example of such an extrapolation. In this case the ordinate of the figure shows $2N_0$ because both positive and negative gust peaks are included. Since the continuous gust approach is based on the assumption that the number of negative slope crossings is equal to the number of positive slope crossings dividing the value $2N_0$ by 2 will provide the number of occurrences for either positive or negative gusts.

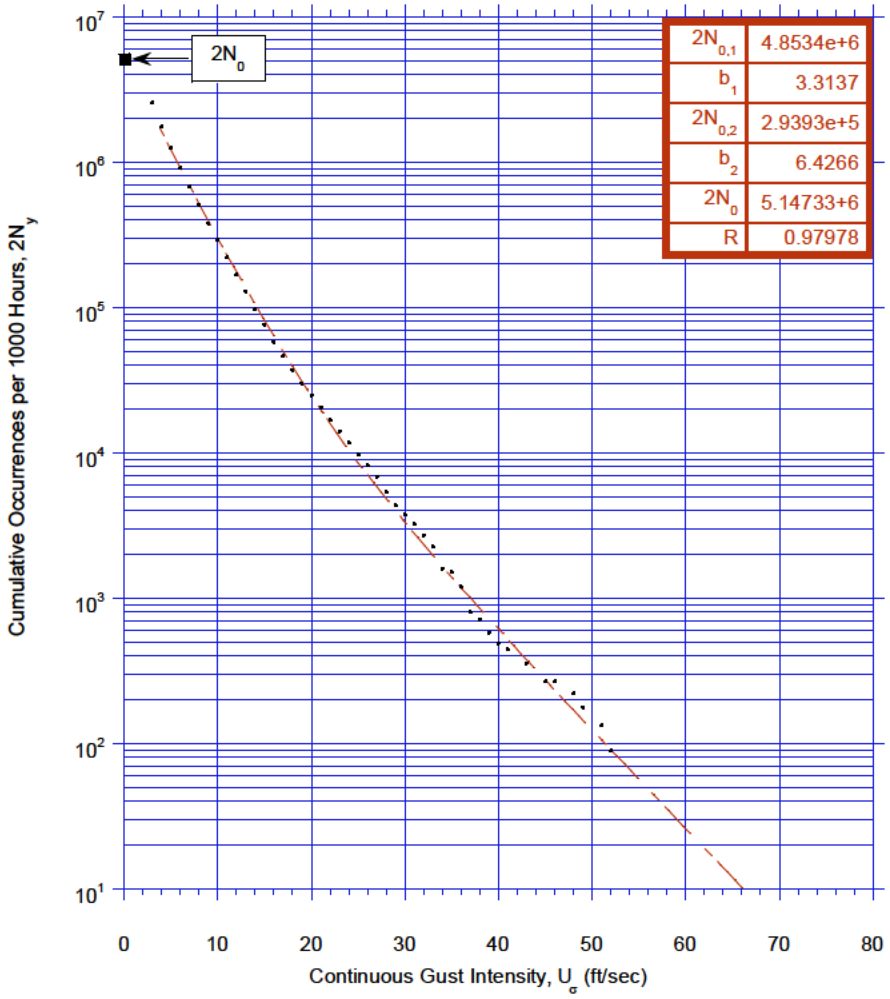

FIGURE B- 2. Example of zero intercept extrapolation.

B.4 GENERALIZED EXCEEDANCE CURVE DERIVATION

B.4.1 Generalized exceedance curve derivation.

Derivation of the generalized exceedance curve first requires the determination of cumulative frequency distribution of combined positive and negative gust intensities from peak counts. Load factor time history data obtained during normal operations are used to obtain peak counts of $U_\sigma = \Delta n_z / \bar{A}$. The peak counts of U_σ can be summed and plotted to provide cumulative frequency distributions of U_σ peaks per unit time while in turbulence. The time in turbulence is obtained by summing the times of all gust peaks. These times are available from the duration criterion used in the separation of gusts and maneuvers. Figure B-2 shown earlier also serves as an example of such

a distribution. Such frequency distributions are derived for selected altitude bands as shown in Table B-I.

TABLE B- I. Altitude bands.

0 – 500 Feet
500 – 1,000 Feet
1,000 – 2,500 Feet
2,500 – 5,000 Feet
5,000 – 10,000 Feet
10,000 – 20,000 feet
20,000 – 30,000 Feet
30,000 – 40,000 Feet
40,000 – 50,000 Feet

The cumulative frequency distributions of gust intensity peaks are then transformed into cumulative probability distributions. Dividing the number of gust intensity peaks $2N_y$ per unit time by $2N_0$ provides a cumulative probability or generalized exceedance curve of Ny/N_0 versus $y/\bar{A}$ based on the total time in turbulence in each altitude bracket. The value of $2N_0$ is derived by extrapolation as shown earlier. Figure B-3 provides an example of the cumulative probability of Ny/N_0 versus $y/\bar{A}$ based on the time in turbulence. In other words, the cumulative probability if all flight time were spent in turbulence. Since not all time spent in the altitude bracket is subject to flight in turbulence the exceedances N_y/N_0 are multiplied by the ratio of the time in turbulence in the altitude bracket over the total time in the altitude bracket so that:

$$\left(\frac{N_y}{N_0}\right)_{turb} = \frac{N_y}{N_0}\frac{T_{turb}}{T_{total}} \qquad \text{(B10)}$$

Thus, for an arbitrary ratio of 22.563 hours in turbulence over 276.019 total flight hours the final cumulative probability curve, or more generally known generalized exceedance curve, would be as shown on Figure B-4.

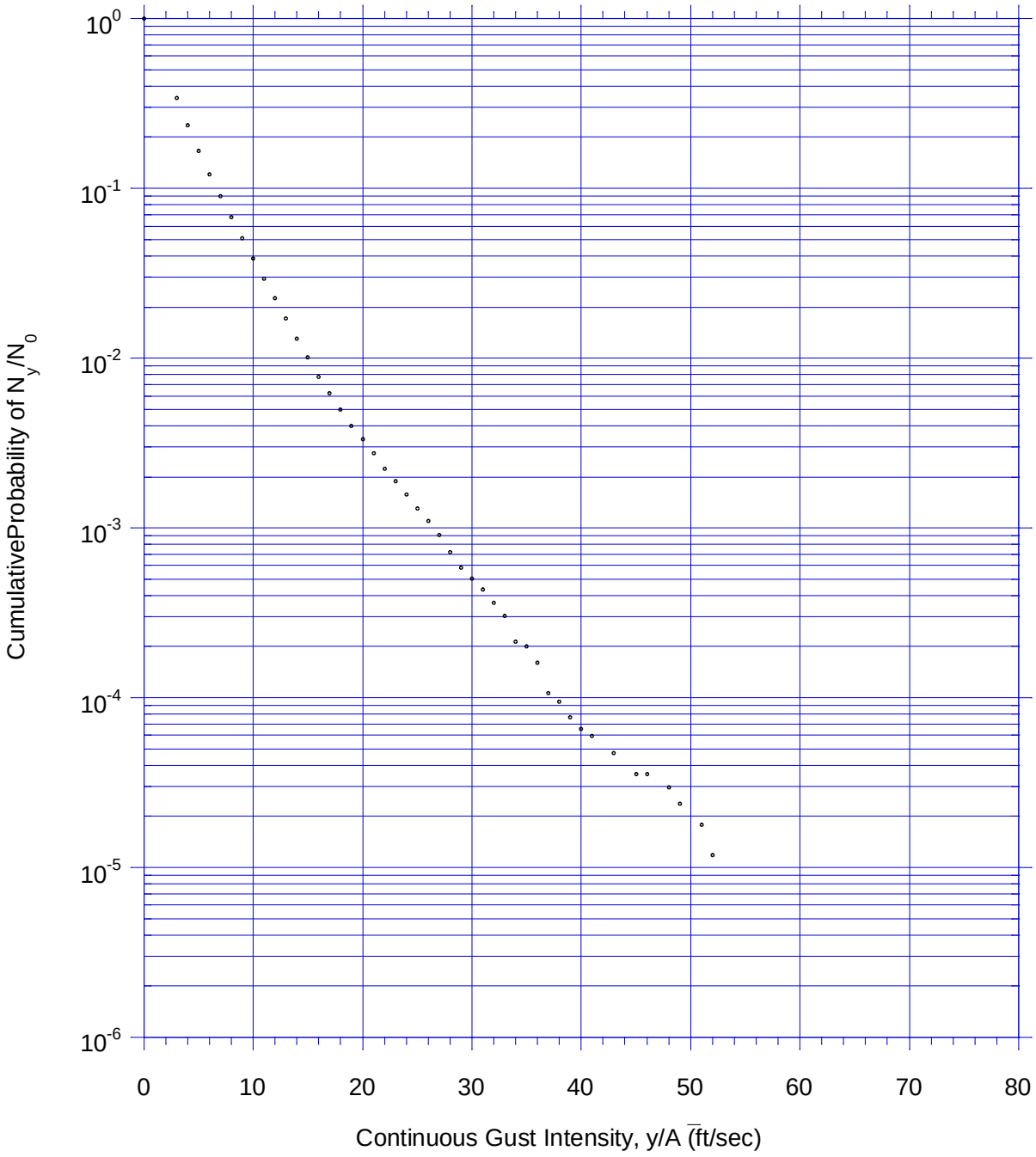

FIGURE B- 3. Cumulative probability of gust intensity while in turbulence.

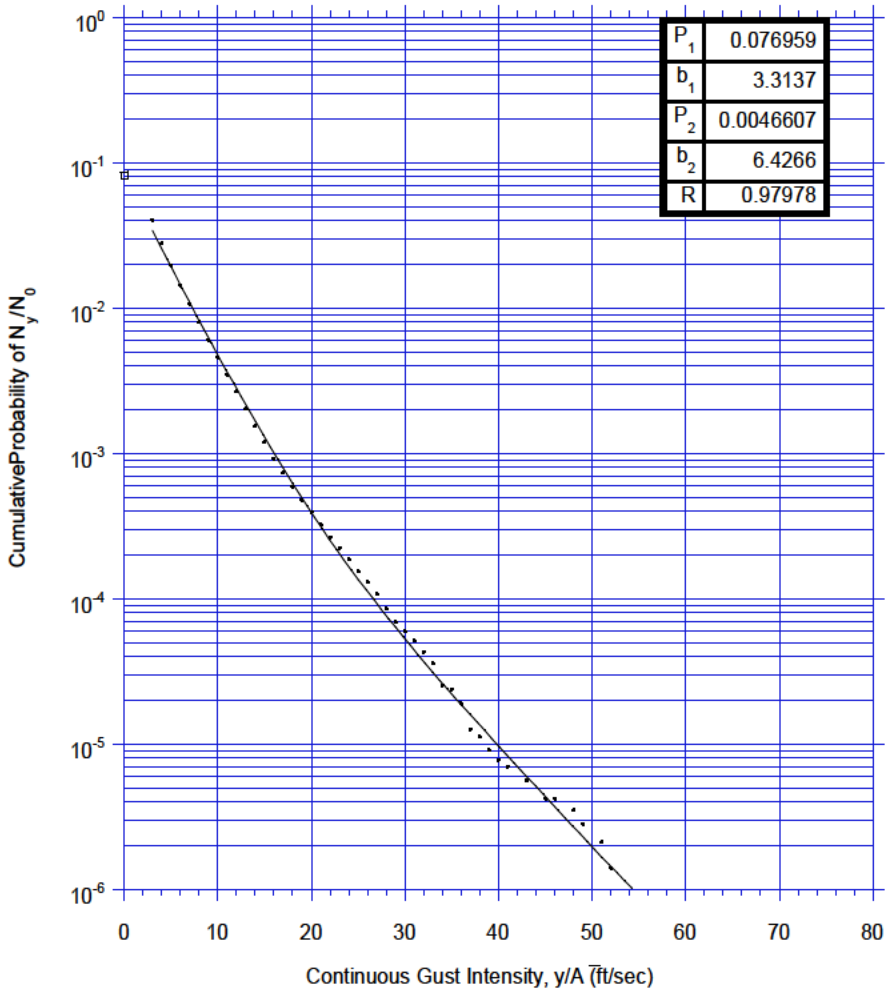

FIGURE B- 4. Generalized exceedance curve.

B.5 DERIVATION OF TURBULENCE FIELD PARAMETERS

As mentioned previously the generalized exceedance curves derived from the measured data can be represented by an empirical equation. Based on the work by Rice in Mathematical Analysis of Random Noise (see Reference B3) as given by Equation B3 and repeated here:

$$\frac{N_y}{N_0} = P_1 e^{-\frac{y/\bar{A}}{b_1}} + P_2 e^{-\frac{y/\bar{A}}{b_2}} \qquad \text{(B11)}$$

The equation describes the turbulence experienced during flight as consisting of the sum of two turbulence distributions sometimes referred to as non-storm and storm turbulence.

The P and b values for a generalized exceedance distribution such as shown on Figure B-4, can be derived through the use of a general curves fit that represents Equation B11 using the Levenburg-Marquardt algorithm. This algorithm uses an iterative procedure to produce a curve fit until the Chi-square does not change for a number of iterations or the percent change in the normalized Chi-

square is less than a specified allowable error. Discussion of the procedure is beyond the scope of this report, but can be found in Numerical Recipes in C, the Art of Scientific Computing (see Reference B4). Figure B-4 shows a comparison of the measured data and the fitted curve based on Equation B11. The legend on the figure shows the P and b values for the fitted curve.

The steps shown in procedure (see Reference 3) described are more detailed than necessary to provide an understanding of the approach and suggest the need for using a curve fit twice. Once for determining the extrapolated value for N_0 and once for obtaining the P and b parameters. The procedure can be simplified by using the information obtained from the curve fit used to extrapolate to N_0. The b_1 and b_2 parameters do not change throughout the steps from Figure B-2 to Figure B-4. The P_1 value can be obtained as follows:

$$P_1 = \frac{T_{turb}}{T_{total}} \frac{N_{0,1}}{(N_{0,1} + N_{0,2})} \tag{B12}$$

Similarly, the value for P2 can be calculated. In one sense, this approach is preferred because the curve fit process uses an iterative approach from initial starting values, which while providing identical correlations for different starting values (resulting in small although insignificant differences in the answers for the parameters during the second curve fit).

The final $P_{1,2}$ values may be considered composite values of all the flight experience over various topographies, seasons, time of day, etc. Still, if based on data for a single aircraft type from a single operator, the P values may not be representative from a global perspective. To obtain a more global representation of the turbulence field parameters they should be based on the overall gust experience of a variety of aircrafts and operators. The results from different aircraft models can be combined because any differences in aircraft response are accounted for in the gust-maneuver separation process and the calculation of N_0 and $\bar{A}$, just as they are accounted for within the same aircraft type.

With the individual aircraft generalized exceedance curves established for a given altitude bracket the individual curves are added to obtain a composite generalized exceedance curve covering the experience of a variety of aircraft. To add the curves they need to be ratioed by the percent of time that each aircraft has operated in the altitude bracket. Let the total flight time in the altitude bracket for all aircrafts equal T_T where T_1, T_2, T_3, to T_n are the times for each aircraft thus:

$$T_T = T_1 + T_2 + T_3 + \cdots \cdot T_n \tag{B13}$$

To obtain the composite curve the individual curves are added so that:

$$\left(\frac{Ny}{No}\right)_{composite} = \frac{T_1}{T_T}\left(\frac{N_y}{N_0}\right)_{turb\ 1} + \frac{T_2}{T_T}\left(\frac{N_y}{N_0}\right)_{turb\ 2} + \cdots\cdots \frac{T_n}{T_T}\left(\frac{N_y}{N_0}\right)_{turb\ n} \tag{B14}$$

The composite curve represents the continuous turbulence statistics in the form of a generalized exceedance curve based on the operational experience of a number of different aircraft covering a

variety of geographical and seasonal differences. Turbulence field parameters can now be derived using a general curve of the form as defined by Equation B11.

APPENDIX C

DERIVATION OF FLIGHT MIX AND PROFILE DESCRIPTION

C.1 SCOPE

C.1.1 Scope.

The durability and damage tolerance analysis of aircraft structure requires the definition of repeated load spectra consistent with the operational usage of the aircraft. The operational usage of the aircraft is defined by mix of flight profiles of varying durations and distances. Each profile is further broken down to show the approximate duration, altitude, airspeed, and gross weights of the various segments in the profile. For passenger and cargo carrying aircraft the segments are generally identified as takeoff, departure, climb, cruise, descent, approach, and touchdown. Segmentation for military aircraft may be more complicated to account for specific segments associated with weapon delivery, target attack, low level terrain following, on station surveillance, etc.

The data in this handbook can be used to extract the information needed to describe the average aircraft usage in terms of the profile mix and profile segment variables of approximate duration, altitude, airspeed, and gross weight. This appendix describes an approach of how this may be accomplished using example data similar to that contained in this handbook.

C.2 FLIGHT USAGE DERIVATION

C.2.1 Flight usage derivation.

The development of flight by flight repeated loading-stress spectra for durability and damage tolerance analyses of aircraft structural repairs or modifications requires knowledge of the aircraft's typical usage.

One aspect of this usage is the mix of flight lengths or flight durations expected to be experienced during normal operations. This mix of flight lengths/durations is expanded into a number of flight profiles that include information on gross weight, speed, and altitude throughout the various phases of flight, such as departure, climb, cruise, descent, and approach. Figure C-1 shows an example of a flight profile. The resulting flight profiles are used in conjunction with normalized load exceedance spectra to derive flight by flight repeated load spectra.

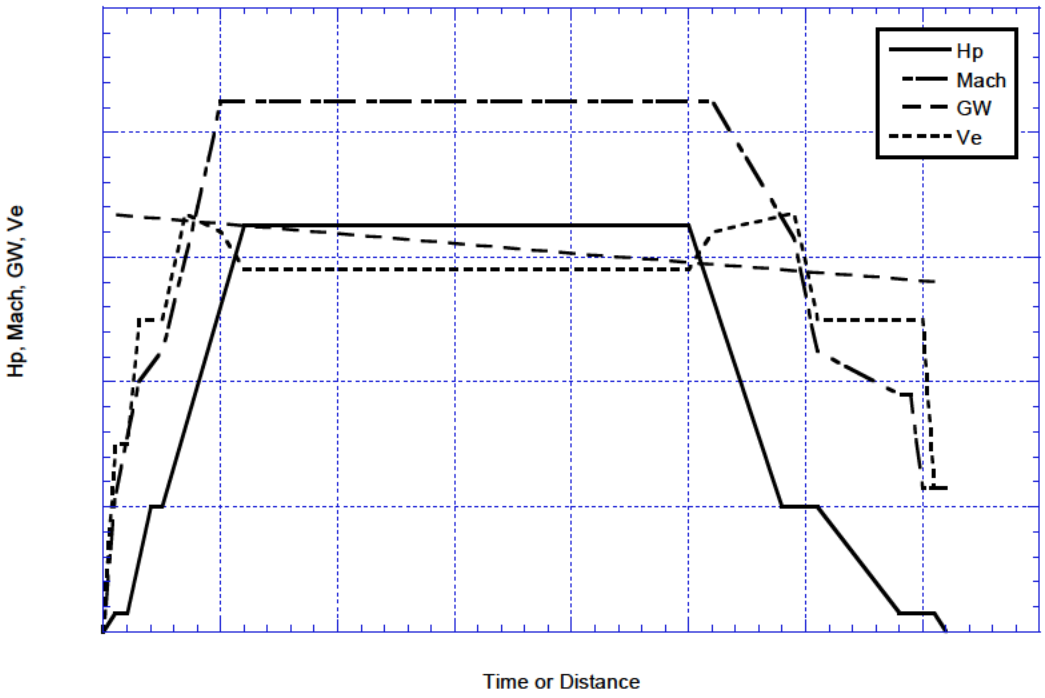

FIGURE C- 1. Typical flight profile description.

Statistical loads data presented in this handbook can be used to derive flight profile mix information as well as detailed operational flight profiles.

C.2.2 Flight mix estimation.

The first step in establishing the aircraft usage is to define the flight profile mix in terms of the expected average flight length or duration and the percentage of the total flights that each will be flown. Aircraft usage data collected during normal operations contains information on the flight distance for each flight flown by the user. These data are presented in statistical loads reports as a cumulative probability of flight distance as shown on Figure C-2. The figure also shows the cumulative probability in tabular form at 100 nautical mile increments. The statistical data as shown on Figure C-2 can be used to derive a distribution of the number or percent of flights for a number of representative flight profile distances. Because the statistical data is provided in terms of distance flown rather than duration, the profile mix will be derived in terms of flight distance.

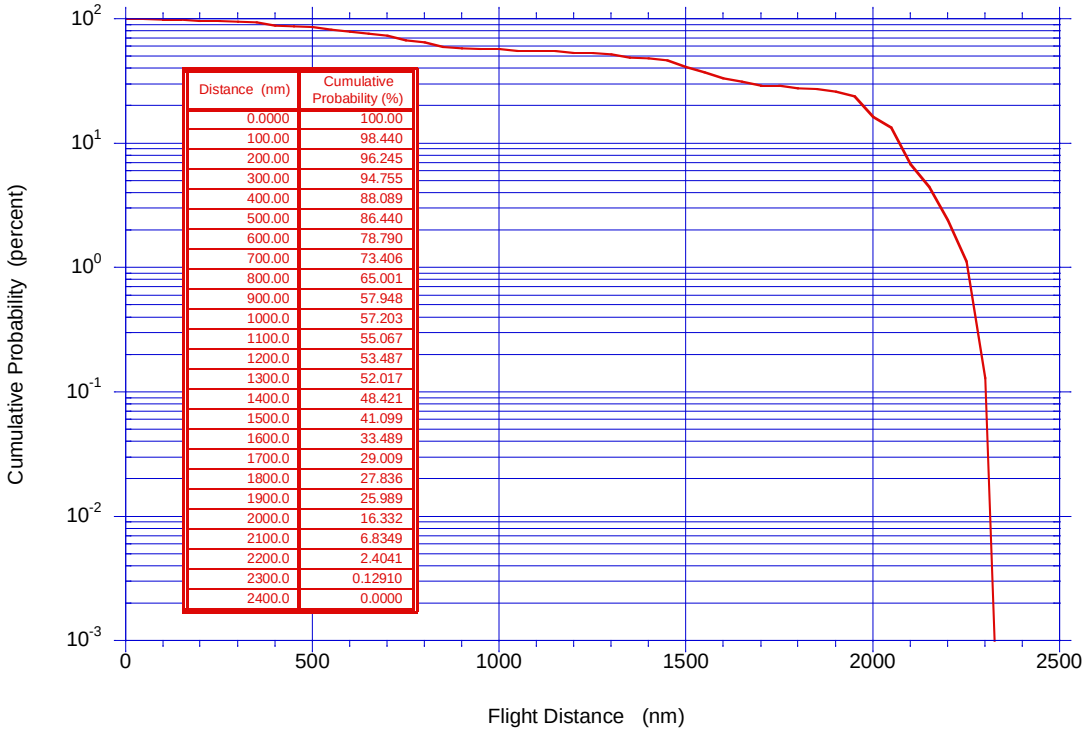

Distance (nm)	Cumulative Probability (%)
0.0000	100.00
100.00	98.440
200.00	96.245
300.00	94.755
400.00	88.089
500.00	86.440
600.00	78.790
700.00	73.406
800.00	65.001
900.00	57.948
1000.0	57.203
1100.0	55.067
1200.0	53.487
1300.0	52.017
1400.0	48.421
1500.0	41.099
1600.0	33.489
1700.0	29.009
1800.0	27.836
1900.0	25.989
2000.0	16.332
2100.0	6.8349
2200.0	2.4041
2300.0	0.12910
2400.0	0.0000

FIGURE C- 2. Cumulative probability of flight distance.

The selection process of representative flight profiles requires the breakdown of the cumulative probability data into a preselected number of flight distance increments. Some engineering judgment is required in the selection of the distance increment. A small increment will result in too many flight profiles of lengths that do not vary much from one to another and could have been combined in fewer, but more distinct profiles. An increment that is too large will result in the combination of profiles that are different enough to be counted as distinct separate profiles. A useful rule of thumb is to select an increment approximately $1/25^{th}$ of the distance of the longest flights in the database. The increments in the table on Figure C-2 reflect this approximation. To determine a flight mix the cumulative probability data presented on Figure C-2 needs to be translated into the percent probability of having flown a flight of various average flight lengths. The probability of having flown a flight of some average distance is obtained by taking the difference between two successive cumulative probabilities as shown in columns C and D in Table C-I. The results when plotted provide a chart showing the distribution of flight distances. The distribution is shown on Figure C-3 in a bar chart format and provides insight into the predominant flight distances that were experience during the operation of the aircraft and is used in the selection of representative flight profiles. As shown on the figure, four representative flight profile distances were selected. Table C-I also presents the procedure for calculating the probability of flights and the average flight length for each of the selected profiles. Table C-II shows the selected profile mix.

TABLE C- I. Flight profile selection (example).

(A) FLIGHT DISTANCE (nm)	(B) CUMULATIVE PROBABILITY (percent)	(C) MEAN DISTANCE (nm)	(D) PROBABILITY OF OCCURRENCE (percent)	(E) FLIGHT PROFILE DESIGNATION	(F) PERCENT OF TOTAL FLIGHTS IN PROFILE (percent)	(G) FLIGHT DISTANCE IN INCREMENT (nm)	(H) AVERAGE DISTANCE IN PROFILE (nm)
	From Figure C-2	((Col A, Row$_n$) + (Col A, Row$_{n-1}$))/2	(Col B, Row$_n$) - (Col B, Row$_{n-1}$)	Selected from Figure C-3	SUM (Col D, Row$_n$ to Row$_{n-1}$)	(Col C, Row$_n$ x Col D, Row$_n$) / Col F	(Sum(Col C x Col D)) / Col F
0	100.00						
100	98.44	50	1.56			5.75	
200	96.25	150	2.19	PROFILE #1		24.28	
300	94.76	250	1.49			27.47	
400	88.09	350	6.67			172.06	
500	86.44	450	1.65		13.56	54.72	284.28
600	78.79	550	7.65			143.91	
700	73.41	650	5.38	PROFILE #2		119.70	
800	65.00	750	8.41			215.61	
900	57.95	850	7.05			205.05	
1000	57.20	950	0.74		29.24	24.21	708.47
1100	55.07	1050	2.14			76.37	
1200	53.49	1150	1.58			61.87	
1300	52.02	1250	1.47	PROFILE #3		62.57	
1400	48.42	1350	3.60			165.31	
1500	41.10	1450	7.32			361.52	
1600	33.49	1550	7.61			401.66	
1700	29.01	1650	4.48			251.71	
1800	27.84	1750	1.17		29.37	69.90	1450.92
1900	25.99	1850	1.85			122.75	
2000	16.33	1950	9.66	PROFILE #4		676.50	
2100	6.83	2050	9.50			699.42	
2200	2.40	2150	4.43			342.23	
2300	0.13	2250	2.28			183.89	
2400	0.00	2350	0.13		27.84	10.90	2035.69
TOTAL			100.00		100		

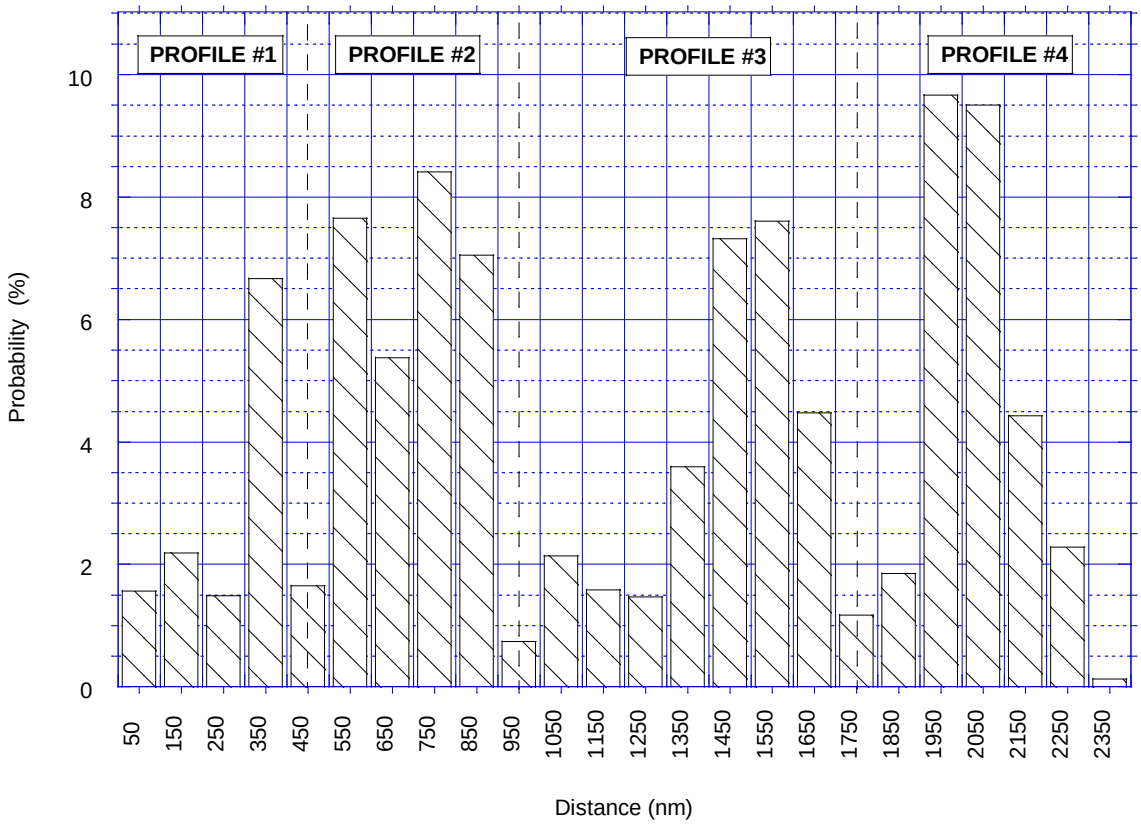

FIGURE C- 3. Flight profile utilization.

TABLE C- II. Profile mix.

FLIGHT PROFILE	PERCENT OF FLIGHTS	MEAN DISTANCE (NM)
1	13.56	285
2	29.24	710
3	29.37	1450
4	27.83	2036

C.3 FLIGHT PROFILE DESCRIPTION

C.3.1 Flight profile description.

The expected aircraft utilization in terms of the distribution of flights and flight lengths was established above. Each flight profile in the flight profile mix is further described by the various phases such as takeoff, climb, cruise, descent etc. Figure C-4 describes the various phases for a simple flight from taxi-out to taxi-in that needs to be considered in the determination of repeated loads.

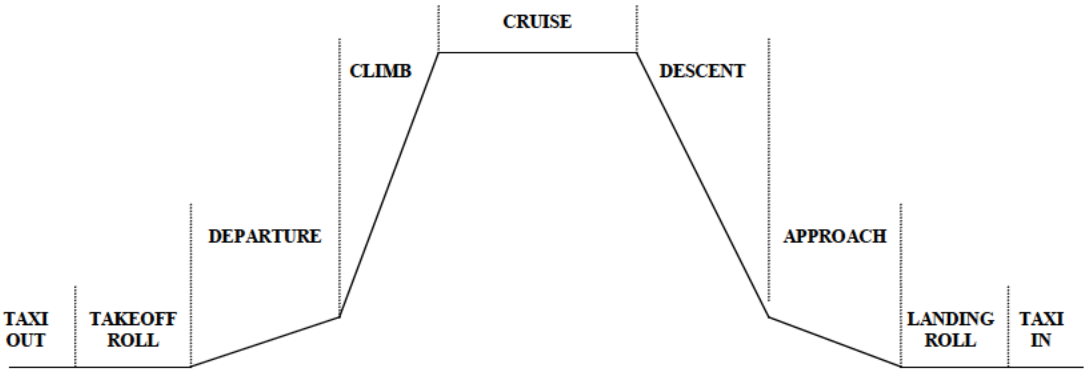

FIGURE C- 4. Flight profile description.

As shown on Figure C-1, for each phase in the profile the variation in gross weight, speed, and altitude need to be defined. This data can be extracted from gross weight, speed and altitude statistical data such as presented in this handbook.

C.3.2 Gross weight derivation.

Information about the variation in gross weight can be deduced from the correlation tables showing the gross weight as a function of flight distance by percent of flights. Table C-III shows such a table. The last column shows how the data can be binned to reflect the distances within the individual profiles as shown in Table C-II.

TABLE C- III. Correlation of takeoff gross weight and flight length, percent of flights.

Takeoff Gross Weight (1000 lbs)

Flight Length (nm)	100-110	110-120	120-130	130-140	140-150	150-160	160-170	Total	Flight Profile
0- 250	0.089	1.838	1.321	0.487	0.139	0.020	0.010	3.904	PROFILE #1
250- 500	0.010	0.864	2.752	3.924	2.086	0.010	0.010	9.656	
500- 750		0.368	4.371	6.338	7.510	0.825		19.412	PROFILE #2
750-1000		0.139	0.944	2.424	4.947	1.371		9.825	
1000-1250		0.010	0.228	1.033	1.212	1.431	0.020	3.934	
1250-1500			0.109	1.202	2.861	6.666	1.331	12.170	PROFILE #3
1500-1750			0.070	0.874	2.503	6.030	2.643	12.120	
1750-2000				0.437	2.444	4.729	5.037	12.647	
2000-2250				0.209	2.027	5.722	7.252	15.210	PROFILE #4
2250-2500				0.099	0.278	0.457	0.288	1.123	
Total	0.099	3.219	9.795	17.028	26.008	27.260	16.591	100 000	

To calculate the average takeoff gross weight, the rows and columns of the table are transposed and broken down by flight profile. Tables C-IV through C-VII show the result for profiles 1

through 4 respectively. The value at the bottom of the last column shows the mean takeoff gross weight for the profile.

TABLE C- IV. Takeoff gross weight calculation, profile #1.

	P	Q	R	S	T	U	V
38	TOGW (Klbs)	Mean TOGW (lbs)	DISTANCE INCREMENT 0-250 NM	DISTANCE INCREMENT 250-500 NM	TOTAL PROBABILITY OF OCCURRENCE (%)	RELATIVE PROBABILITY OF OCCURRENCE (%)	MEAN GROSS WEIGHT FOR PROFILE 1 (lbs)
39							
40	100-110	105000	0.089	0.01	0.099	0.007300885	766.5929204
41	110-120	115000	1.838	0.864	2.702	0.199262537	22915.19174
42	120-130	125000	1.321	2.752	4.073	0.300368732	37546.09145
43	130-140	135000	0.487	3.924	4.411	0.325294985	43914.82301
44	140-150	145000	0.139	2.086	2.225	0.164085546	23792.40413
45	150-160	155000	0.02	0.01	0.03	0.002212389	342.920354
46	160-170	165000	0.01	0.01	0.02	0.001474926	243.3628319
47							
48	TOTAL				13.56	1	129278.0236

TABLE C- V. Takeoff gross weight calculation, profile #2.

	P	Q	R	S	T	U	V
53	TOGW (Klbs)	Mean TOGW (lbs)	DISTANCE INCREMENT 500-750 NM	DISTANCE INCREMENT 750-1,000 NM	TOTAL PROBABILITY OF OCCURRENCE (%)	RELATIVE PROBABILITY OF OCCURRENCE (%)	MEAN GROSS WEIGHT FOR PROFILE 2 (lbs)
54							
55	100-110	105000					1
56	110-120	115000	0.368	0.139	0.507	0.01734104	0.98265896
57	120-130	125000	4.371	0.944	5.315	0.181790197	0.800868762
58	130-140	135000	6.338	2.424	8.762	0.299688751	0.501180012
59	140-150	145000	7.51	4.947	12.457	0.426069706	0.075110305
60	150-160	155000	0.825	1.371	2.196	0.075110305	
61	160-170	165000			0	0	0
62							
63	TOTAL				29.237	1	

TABLE C- VI. Takeoff gross weight calculation, profile #3.

	P	Q	R	S	T	U	V	W
84	TOGW (Klbs)	Mean TOGW (lbs)	DISTANCE INCREMENT 1,000 - 1,250 NM	DISTANCE INCREMENT 1,250-1,500 NM	DISTANCE INCREMENT 2,250-2,500 NM	TOTAL PROBABILITY OF OCCURRENCE (%)	RELATIVE PROBABILITY OF OCCURRENCE (%)	MEAN GROSS WEIGHT FOR PROFILE 3 (lbs)
85								
86	110-120	115000	0.01			0.01	0.000354321	40.74690855
87	120-130	125000	0.228	0 109	0.07	0.407	0.014420862	1802.607802
88	130-140	135000	1.033	1 202	0.874	3 109	0.110158381	14871.3815
89	140-150	145000	1.212	2.861	2.503	6 576	0.233001453	33785.21064
90	150-160	155000	1.431	6.666	6.03	14 127	0.500549197	77585.12561
91	160-170	165000	0.02	1 331	2.643	3 994	0.141515785	23350.10452
92								
93						28 223	1	151435.177

TABLE C- VII. Takeoff gross weight calculation, profile #4.

(A) TOGW (Klbs)	(B) Mean TOGW (lbs)	(C) DISTANCE INCREMENT 1,750-2,000 NM	(D) DISTANCE INCREMENT 2,000-2,250 NM	(E) DISTANCE INCREMENT 1,500-1,750 NM	(F) TOTAL PROBABILITY OF OCCURRENCE (%)	(G) RELATIVE PROBABILITY OF OCCURRENCE (%)	(H) MEAN GROSS WEIGHT FOR PROFILE 4 (lbs)
110-120	115000						
120-130	125000						
130-140	135000	0.437	0.209	0.099	0.745	0.025708272	3470.616653
140-150	145000	2.444	2.027	0.278	4.749	0.16387729	23762.20712
150-160	155000	4.729	5.722	0.457	10.908	0.376410504	58343.62814
160-170	165000	5.037	7.252	0.288	12.577	0.434003934	71610.64909
	85000						
TOTAL					28.979	1	157187.101

Table C-VIII provides statistical correlation data between the takeoff gross weight and the landing gross weight. This data can be used to derive a relationship between a mean takeoff gross weight and a mean landing gross weight. Table C-IX shows the procedure using the data from Table C-VIII. The mean takeoff and landing gross weight in the table are plotted on Figure C-4. A polynomial curve fit to the data points provide a convenient method to calculate the expected landing gross weights for the four profiles.

TABLE C- VIII. Correlation of takeoff and landing gross weights, percent of flights.

Takeoff Gross Weight (1000 lbs)

Landing Gross Weight (1000 lbs) 10066 Fits	100-110	110-120	120-130	130-140	140-150	150-160	160-170	Total
100-110	0.099	0.984	0.169	0.030				1.282
110-120		2.235	7.500	3.209	2.434	0.417		15.796
120-130			2.126	11 862	9.160	9.011	1.053	33 211
130-140				1.927	14.206	16.759	14.385	47 278
140-150					0.209	1.073	1.142	2.424
150-160								
160-170							0.010	0.010
Total	0.099	3.219	9.795	17 028	26.008	27 260	16.591	100.000

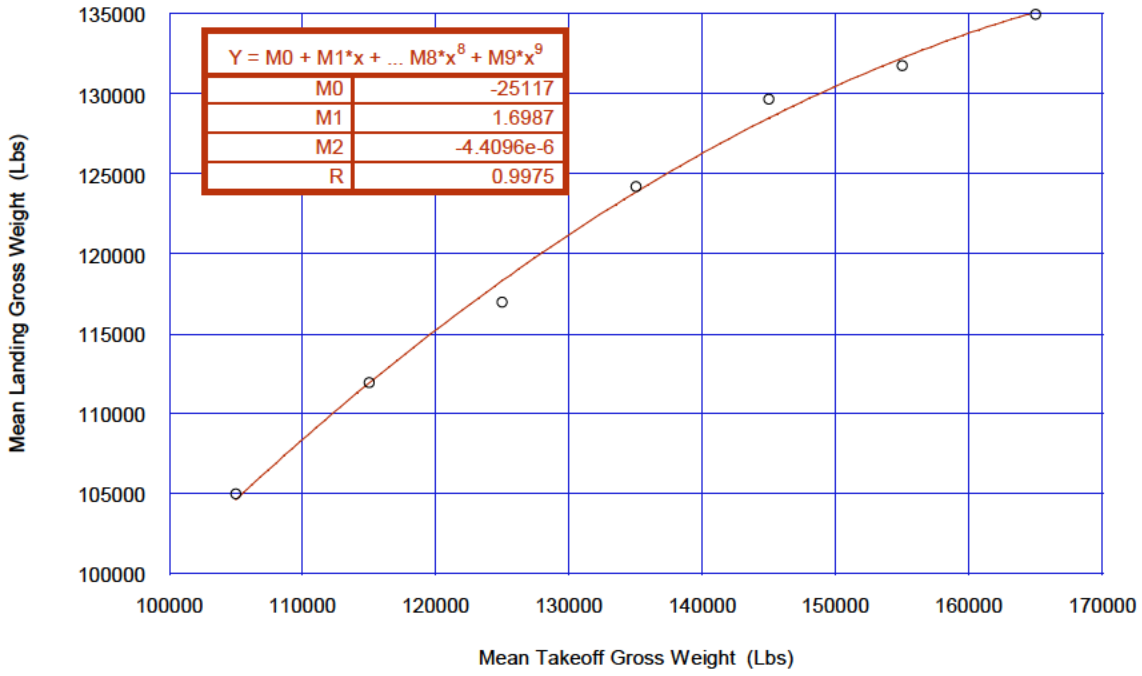

FIGURE C- 5. Mean landing gross weight vs mean takeoff gross weight.

TABLE C- IX. Calculation of mean landing gross weight vs mean takeoff gross weight.

	AC	AD	AE	AF	AG	AH	AI	AJ	AK	AL	AM	AN	AO	AP	AQ
38	MEAN LANDING GW (Lbs)	PROBABILITY FOR MEAN TOGW 105,000 Lbs (%)	MEAN LANDING GW FOR 105,000 TOGW (Lbs)	PROBABILITY FOR MEAN TOGW 115,000 Lbs (%)	MEAN LANDING GW FOR 115,000 TOGW (Lbs)	PROBABILITY FOR MEAN TOGW 125,000 Lbs (%)	MEAN LANDING GW FOR 125,000 TOGW (Lbs)	PROBABILITY FOR MEAN TOGW 135,000 Lbs (%)	MEAN LANDING GW FOR 135,000 TOGW (Lbs)	PROBABILITY FOR MEAN TOGW 145,000 Lbs (%)	MEAN LANDING GW FOR 145,000 TOGW (Lbs)	PROBABILITY FOR MEAN TOGW 155,000 Lbs (%)	MEAN LANDING GW FOR 155,000 TOGW (Lbs)	PROBABILITY FOR MEAN TOGW 165,000 Lbs (%)	MEAN LANDING GW FOR 165,000 TOGW (Lbs)
39															
40	105000	0.099	105000	0.984	32096.92451	0.169	1811.638591	0.03	184.9894292		0		0		0
41	115000		0	2.235	79846.22554	7.5	88055.13017	3.209	21672.24571	2.434	10762.04391	0.417	1759.170946		0
42	125000		0		0	2.126	27131.18938	11.862	87077.16702	9.16	44023.22273	9.011	41319.69919	1.053	7933.996383
43	135000		0		0		0	1.927	15277.48414	14.206	73736.39894	16.759	82995.78136	14.385	117056.962
44	145000		0		0		0		0	0.209	1165.173594	1.073	5707.446809	1.142	9981.314045
45	155000		0		0		0		0		0		0		0
46	165000		0		0		0		0		0		0	0.01	99.45750452
47															
48	TOTAL %	0.099		3.219		9.795		17.028		26.009		27.26		16.59	
49	Mean LDGW		105000		111943.15		116997.9581		124211.8863		129686.8392		131782.0983		134972.2725

C.3.3 Maximum altitude derivation.

Figure C-6 provides information on the maximum altitudes as a function of flight duration. As mentioned previously, because the statistical data is provided in terms of distance flown rather than duration, the profile segment information will be derived in terms of flight distance. The data represented on Figure C-6 needs to be translated in terms of distance rather than duration. Since the data for the aircraft used in this example are based on a total time of 30,817 flight hours and a total distance of 12,517,104 nautical miles. Multiplying the abscissa of the plot by the ratio of nautical miles to duration transforms the plot into the maximum altitude as a function of flight distance. Figure C-7 shows the transformed plot. The average maximum altitude for each of the profiles was determined by calculating the average altitude within each distance band for each profile as shown on Figure C-7. Thus, for profile 1 the mean maximum altitude was calculated for all points within the distance band 50 to 450 nautical miles. Likewise for profile 2, the average maximum altitude is based on the points within the distance band from 450 to 950 nautical miles. The average maximum altitude for profiles 3 and 4 were obtained in the identical manner. The resulting mean maximum altitudes are shown on the graph as the large solid squares.

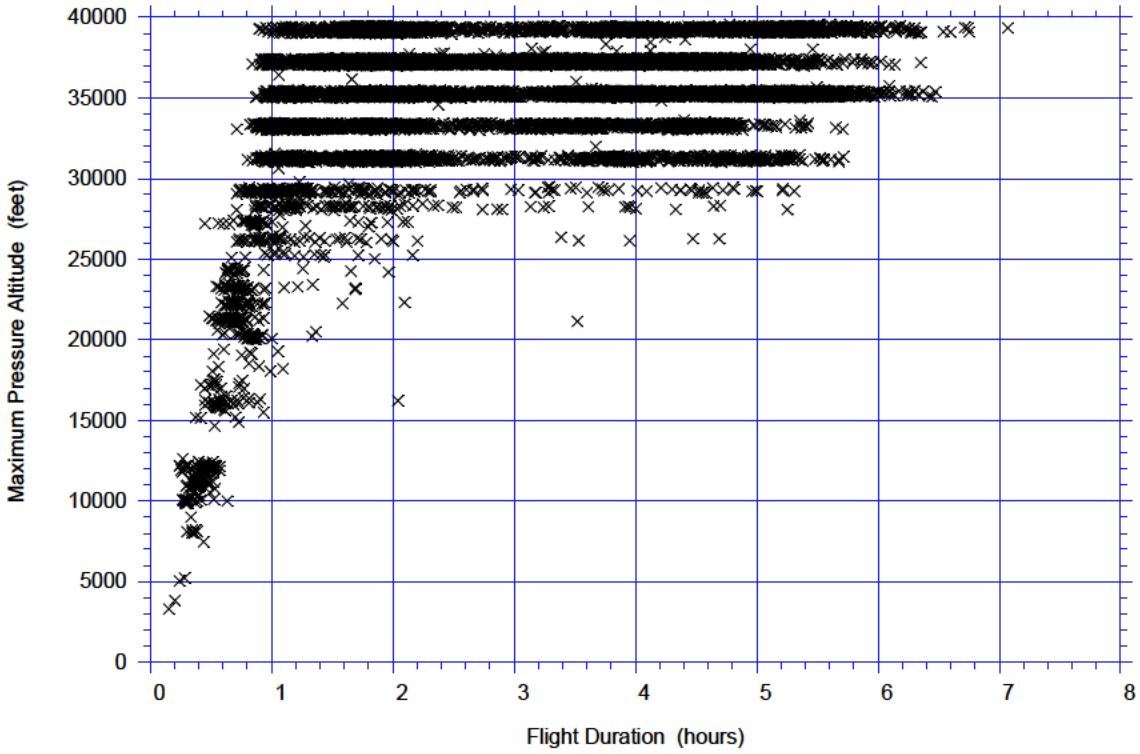

FIGURE C- 6. Correlation of maximum altitude and flight duration.

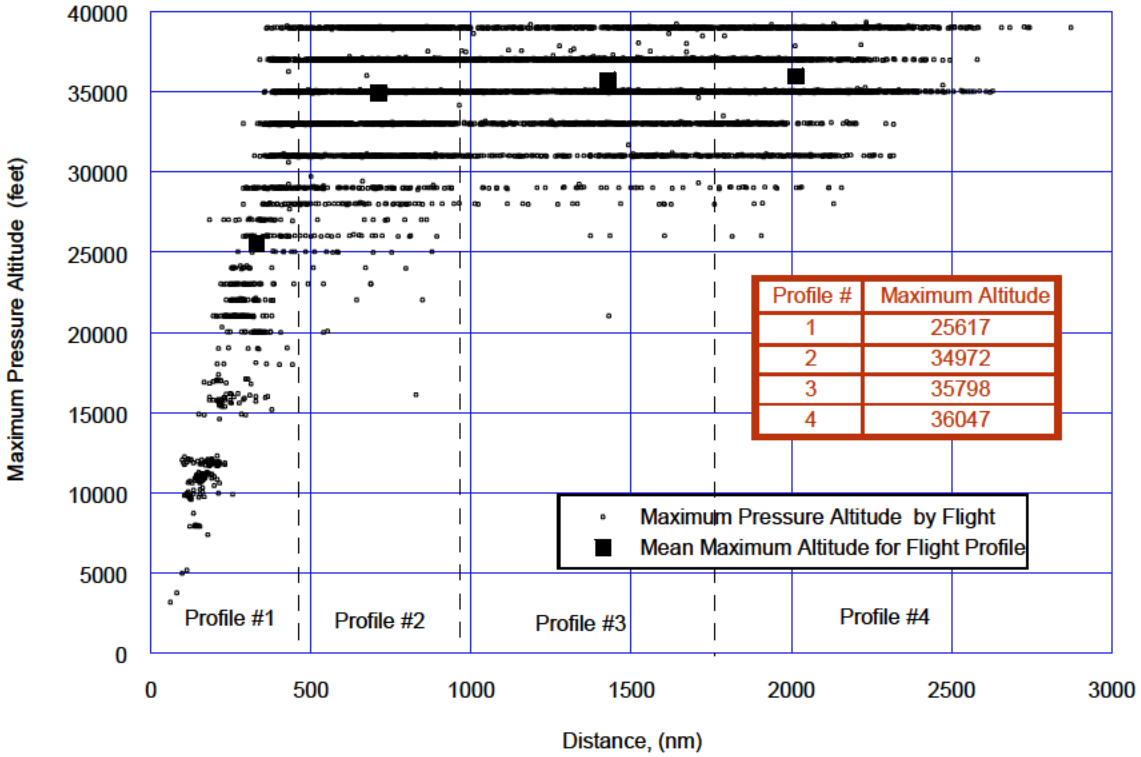

FIGURE C- 7. Correlation of maximum altitude and flight distance.

C.3.4 Phase of flight distance derivation.

Table C-IX provides information on the relative percent of all the flights within a specified distance range that fall within the selected altitude bands. These data can be used to derive estimates of distance spent in the departure, climb, cruise, descent, and approach phases of flight for each profile in the profile mix.

From the data in Table C-IX the accumulated distance to reach the various altitudes can be derived for each of the flight distance increments. Table C-X shows the calculations for determining the cumulative flight distances as a function of the total flight distances. It is assumed that the departure and approach phases occur at altitudes below 10,000 feet. The climb and descent phases are assumed to occur between 10,000 feet and 30,000 feet. The cumulative distance data for these altitude increments is plotted as shown on Figure C-7. Linear curve fits to the points provide information on the variation in the phase distance as a function of total flight distance.

TABLE C- X. Percent of flight distance in altitude bands.

Flight Distance (nautical miles)

Altitude Band (feet)	0-500	500-1000	1000-1500	1500-2000	2000-2500	2500-3000	3000-3500
29500-39500	29.230	63.420	77 340	82.410	85.700	89 320	89.720
19500-29500	32.190	19.650	12.740	10 200	8.240	5.460	3.920
9500-19500	23.360	10.260	6.170	4.390	3.560	3.160	4.200
4500-9500	8.820	4.010	2.280	1.710	1.380	1.160	1.460
1500-4500	5.010	2.010	1.110	0.960	0.800	0.600	0.460
500-1500	1.000	0.470	0.260	0.240	0.210	0.180	0.150
0-500	0.380	0.170	0.100	0.100	0.110	0.110	0.090
Total	100.000	100.000	100.000	100.000	100.000	100.000	100.000

TABLE C- XI. Flight distance in altitude bands.

	C	D	E	F	G	H	I	J	K	L	M	N	O	P	Q	R	S	T	U	V	W
98	PROBABILITY OF ALTITUDE FOR MEAN FLIGHT DISTANCE, 250 NM	DISTANCE IN ALTITUDE BAND (ft)	CUMULATIVE DISTANCE IN ALTITUDE BAND (ft)	PROBABILITY OF ALTITUDE FOR MEAN FLIGHT DISTANCE, 750 NM	DISTANCE IN ALTITUDE BAND (ft)	CUMULATIVE DISTSNCE IN ALTITUDE BAND (ft)	PROBABILITY OF ALTITUDE FOR MEAN FLIGHT DISTANCE, 1 250 NM	DISTANCE IN ALTITUDE BAND (ft)	CUMULATIVE DISTSNCE IN ALTITUDE BAND (ft)	PROBABILITY OF ALTITUDE FOR MEAN FLIGHT DISTANCE, 1 750 NM	DISTANCE IN ALTITUDE BAND (ft)	CUMULATIVE DISTSNCE IN ALTITUDE BAND (ft)	PROBABILITY OF ALTITUDE FOR MEAN FLIGHT DISTANCE, 2 250 NM	DISTANCE IN ALTITUDE BAND (ft)	CUMULATIVE DISTSNCE IN ALTITUDE BAND (ft)	PROBABILITY OF ALTITUDE FOR MEAN FLIGHT DISTANCE, 2 250 NM	DISTANCE IN ALTITUDE BAND (ft)	CUMULATIVE DISTSNCE IN ALTITUDE BAND (ft)	PROBABILITY OF ALTITUDE FOR MEAN FLIGHT DISTANCE, 3 250 NM	DISTANCE IN ALTITUDE BAND (ft)	CUMULATIVE DISTSNCE IN ALTITUDE BAND (ft)
99	29.23	73.075	249.98	63.42	475.65	749.93	77.34	966.75	1250.00	82.41	1442.175	1750.18	85.7	1928.25	2250.00	89.32	2456.3	2749.73	89.72	2915.9	3250.00
100	32.19	80.475	176.90	19.65	147.375	274.28	12.74	159.25	283.25	10.20	178.5	308.00	8.24	185.4	321.75	5.46	150.15	293.43	3.92	127.4	334.10
101	23.36	58.4	96.43	10.26	76.95	126.90	6.17	77.125	124.00	4.39	76.825	129.50	3.56	80.1	136.35	3.16	86.9	143.28	4.2	136.5	206.70
102	8.82	22.05	38.03	4.01	30.075	49.95	2.28	28.5	46.88	1.71	29.925	52.68	1.38	31.05	56.25	1.16	31.9	56.38	1.46	47.45	70.20
103	5.01	12.525	15.98	2.01	15.075	19.88	1.11	13.875	18.38	0.96	16.8	22.75	0.8	18	25.20	0.6	16.5	24.48	0.46	14.95	22.75
104	1.00	2.5	3.45	0.47	3.525	4.80	0.26	3.25	4.50	0.24	4.2	5.95	0.21	4.725	7.20	0.18	4.95	7.98	0.15	4.875	7.80
105	0.38	0.95	0.95	0.17	1.275	1.28	0.10	1.25	1.25	0.10	1.75	1.75	0.11	2.475	2.48	0.11	3.025	3.03	0.09	2.925	2.93
106	100.00			100	750		100.00			100.00			100			100			100		
107		249.98			749.93			1250.00			1750.18			2250.00			2749.73			3250.00	

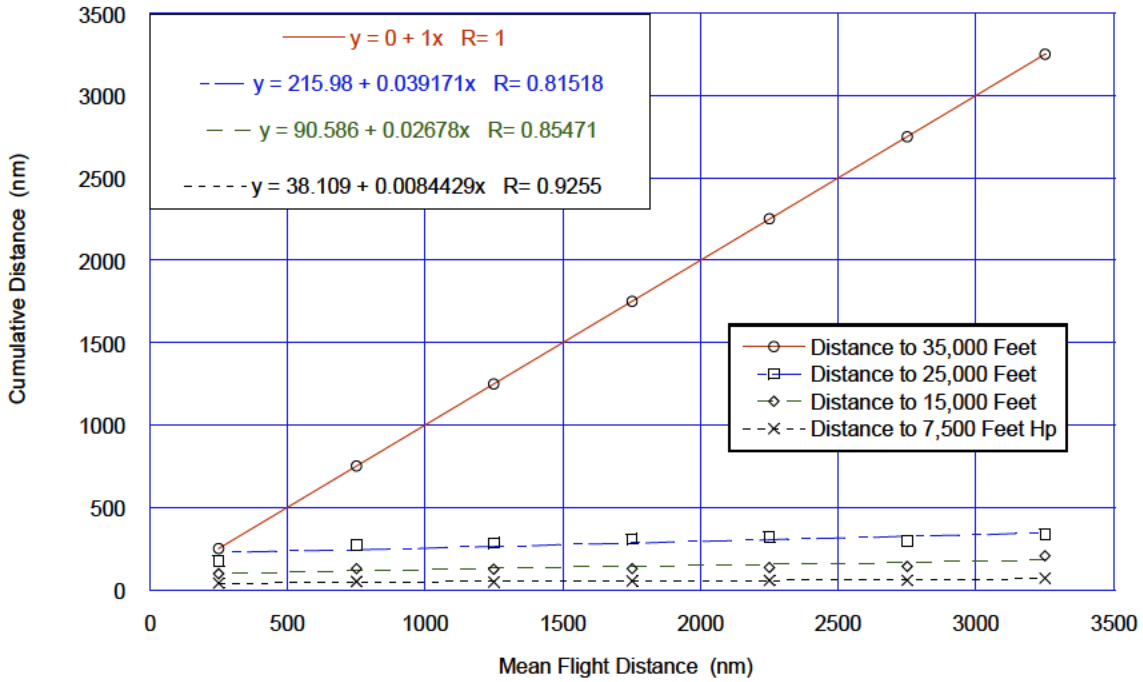

FIGURE C- 8. Cumulative distance to altitude vs mean total flight distance by altitude.

As can be seen from the slope values on Figure C-8 the flight distance for the departure and approach phases below 7,500 feet is not much influenced by the total flight distance. The climb and descent phases of flight above 7,500 feet are slightly more strongly influenced by the total flight distance. This is reasonable considering that the longer flights operate at higher gross weights and cruising altitudes. Obviously, the major flight distance occurs in the cruise phase above 30,000 feet. Sufficient information to define the average relative percentages of distances in the different flight phases is contained in the load factor cumulative occurrences plots. For instance, the total distances flown in each phase of flight are shown on Figure C-9. Table C-XI shows the distribution of flight distances by phase of flight obtained from Figure C-9 as well as the relative ratios of flight distance for the departure and approach phases and the relative ratio of the flight distance for the climb and descent phases.

These ratios in conjunction with the information on Figure C-8 can be used to obtain an estimate of the flight distance in the various phases as a function of the total flight distance.

For example let us assume a flight distance of 1,450 miles consistent with profile 3. The departure and approach phases would account for 38.109+0.0084429×1450=50.35 miles. Of this distance 0.20692×50.35=10.42 miles would be spent on departure and 0.793081×50.35=39.93 nm would be spent on approach. For the climb and descent phases, the flight distance would be a total of 215.98+0.039171×1450-50.35=222.43 nm. Of this distance, the climb phase would account for 0.542943×222.43=120.77 nm and the remainder of 101.66 nm would be assigned to the descent phase. The cruise phase would be 1450-50.35-222.43=1177.22 nm. Table C-XI shows the distance distribution by flight phase thus obtained.

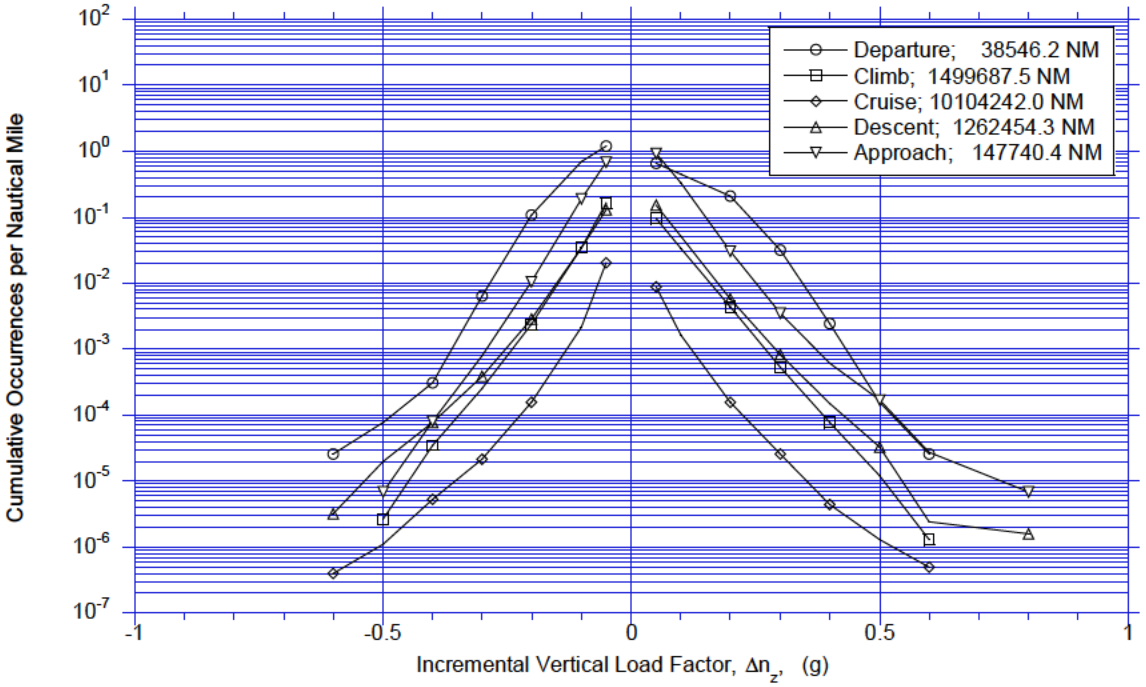

FIGURE C- 9. Cumulative occurrences of maneuver load factor by phase of flight.

TABLE C- XII. Relative flight distances in departure and approach, and climb and descent.

	A	B	C	D
116	**Phase of Flight**	**Distance (nm)**	**Ratio Departure and Approach**	**Ratio Climb and Descent**
117	Departure	38546.20	0.206918801	
118	Climb	1499687.50		0.542943704
119	Cruise	10104242.00		
120	Descent	1262454.30		0.457056296
121	Approach	147740.40	0.793081199	

TABLE C- XIII. Flight distance by phase of flight.

	A	B	C	D	E	F
112	**Flight Distance**	**Departure Distance to 7,500 feet**	**Climb Distance to 35,000 Ft**	**Distance in cruise**	**Descent Distance from 35,000 Feet**	**Approach Distance from 7,500 Feet**
113	1450	10.42	142.45	1163.06	94.14	39.93

The climb and descent phases occur over an altitude range up to the cruise altitude. This is a range where significant changes in speed occur. Thus, the climb and descent phases need to be broken down in finer detail such as 10,000 feet increments. Similar to the information presented on Figure C-9, the handbook contains indirect information on the distribution of the relative total distances

by altitude. Figure C-12 shows an example of the load factor statistics by altitude for the climb phase of flight with a legend showing the distribution of flight distances by altitude. Similar information is available for the descent phase.

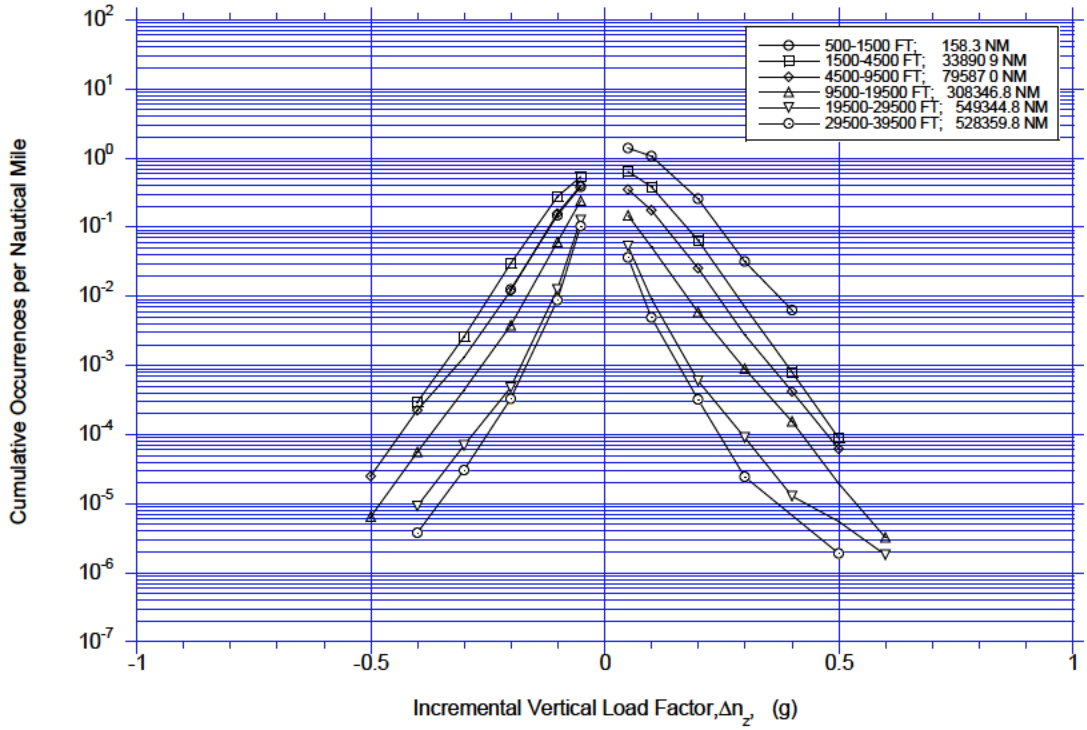

FIGURE C- 10. Cumulative occurrences of load factor during climb by altitude.

Table C-XII shows how the information contained in the legend on Figure C-10 can be used to obtain the ratio of the relative distances by altitude increment for the climb phase. These ratios can be applied to the climb and descent distances of the 1,450 nautical mile profile to obtain the distances flown as a function of the average altitudes. Because we have assumed that the departure phase covers an altitude up to 7,500 feet with a mean altitude of 3,750 feet, the initial climb segment representing a mean altitude of 7,500 feet is considered to include the sum of the distances for mean altitudes of 750, 3,000, and 7,500 feet. Since little time is spent in climb up to 7,500 feet the error in combining the 750, 3,000, and 7,500 for the mean 7,500 altitude is small.

TABLE C- XIV. Relative distances vs altitude during climb and descent.

Mean Incremental Altitude (feet)	Nautical Miles in Climb	Ratio of Total Nautical Miles in Climb	Climb Distance by Altitude for Profile #3	Nautical Miles in Descent	Ratio of Total Nautical Miles in Descent	Descent Distance by Altitude for Profile #3
750	158.3	0.000105555		236.5	0.000187334	
3000	33891	0.022598726		37577.3	0.029765278	
7500	79587	0.053069099	10.79	141008.4	0.111693874	13.33
15000	3.08E+05	0.205609667	29.29	365578	0.289577238	27.26
25000	5.49E+05	0.366303273	52.18	403528.5	0.31963813	30.09
35000	5.28E+05	0.352313681	50.19	314525.5	0.249138147	23.45
Total	1499686.3	1	142.45	1262454.2	1	94.14

C.3.5 Speed derivation.

Figure C-11 provides correlation of the maximum Mach number and coincident altitude experienced during all flight phases. This type of information as presented in the handbook can be used to define average speeds as a function of flight altitude. Figure C-12 shows the mean Mach number of Figure C-11 by altitude. Departure and approach were assumed to occur below 7,500 feet for a mean altitude of 3,750 feet. Climb and descent altitudes are defined as shown in Table C-XIV, and the cruise altitude is obtained from Figure C-7. With these altitudes the average speeds can be derived from Figure C-12. Table C-XV shows the speeds associated with the selected altitudes.

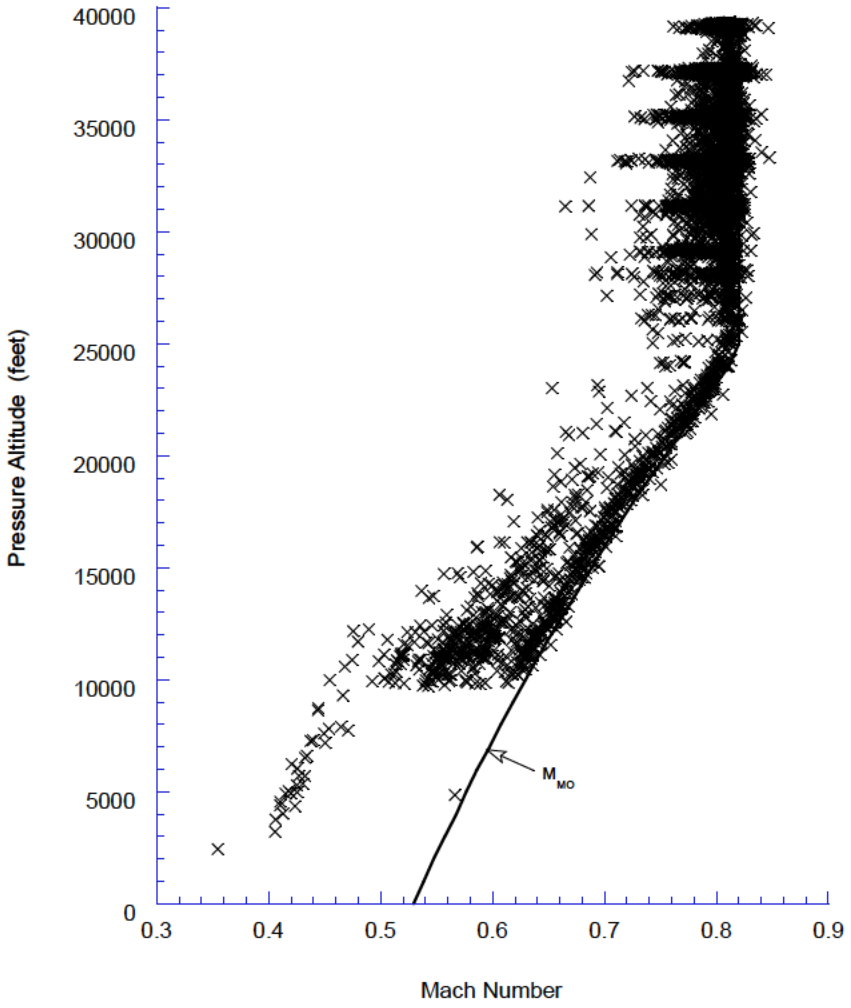

FIGURE C- 11. Maximum mach number and coincident altitude.

TABLE C- XV. Average speeds for altitude segment.

	B	C
146	**ALTITUDE (ft)**	**MACH NUMBER**
147	3250	0.43
148	7500	0.46
149	15000	0.65
150	25000	0.80
151	35000	0.80
152	35798	0.80

C.3.6 Flight profile segmentation.

The previous sections have shown how the mean gross weight, altitude, speeds, and flight distances for flight profile segments of one profile can derived from the statistical data as published in the

handbook. Knowing the Mach number and altitude equivalent speed and segment duration can be calculated.

Table C-XIV combines all previously derived profile 3 segment data into a single format showing all important segment variables throughout the entire flight. Similarly flight profile segment data can be developed for each of the profiles in a profile mix. Figure C-13 shows the information contained in Table C-XIV in graphical format.

TABLE C- XVI. Flight profile #3, 1,450 nautical mile flight profile.

	A	B	C	D	E	F	G	H	I
129	**SEGMENT**	**ALTITUDE (ft)**	**MACH NO**	**V (keas)**	**GW (lbs)**	**SEGMENT DIST. (nm)**	**TOTAL DISTANCE**	**SEGMENT TIME (min)**	**TOTAL TIME (min)**
130	Takeoff	0			151000	0			
131	Departure	3250	0.43	268	150796	10.42	10.42	2.2	2.2
132	Climb 1	7500	0.46	265	150593	10.79	21.21	2.2	4.5
133	Climb 2	15000	0.65	323	150179	29.29	50.50	4.6	9.0
134	Climb 3	25000	0.80	322	149531	52.18	102.68	7.1	16.2
135	Climb 4	35000	0.80	256	148852	50.19	152.86	7.5	23.7
136	Cruise	35798	0.80	252	132988	1163.06	1315.93	174.9	198.5
137	Descent 1	35000	0.80	256	132670	23.45	1339.38	3.5	202.1
138	Descent 2	25000	0.73	294	132260	30.09	1369.47	4.5	206.6
139	Descent 3	15000	0.65	323	131876	27.26	1396.73	4.2	210.8
140	Descent 4	7500	0.46	265	131624	13.33	1410.07	2.8	213.6
141	Approach	3250	0.43	268	130843	39.93	1450.00	8.6	222.2
142	Touchdown	0			130843	0	1450.00		222.2

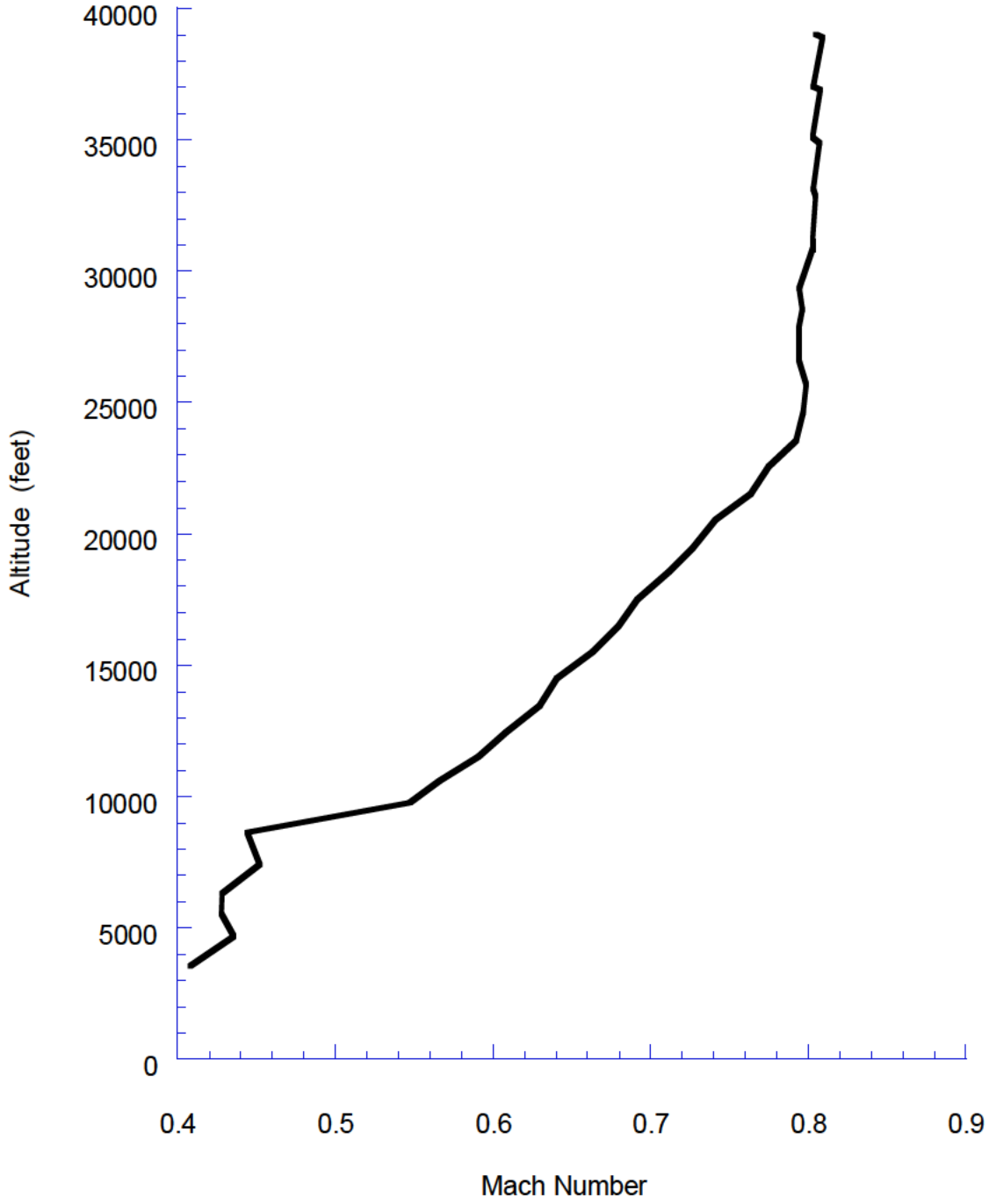

FIGURE C- 12. Mean mach number vs altitude.

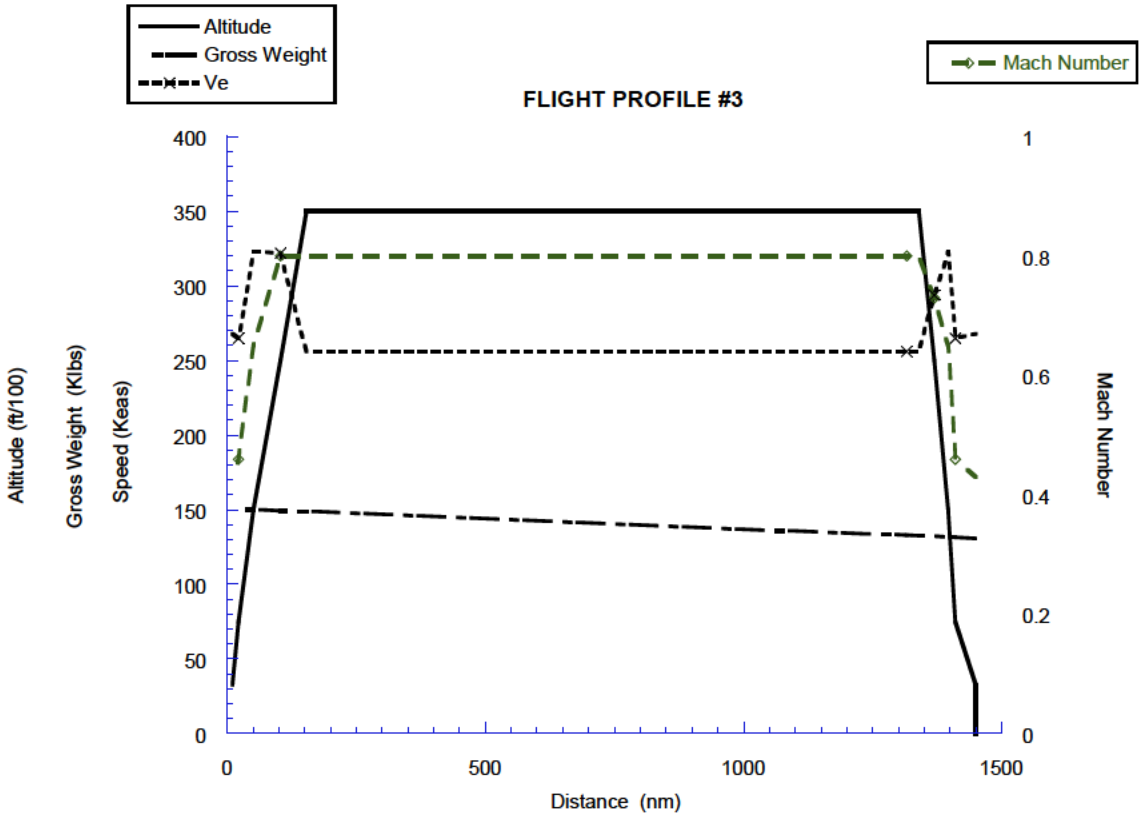

FIGURE C- 13. Flight profile #3, 1,450 nautical mile flight profile.

C.4 CONCLUSIONS

C.4.1 Conclusions.

The procedures discussed provide a means to derive profile mix and flight profile segment data from actual operational statistics. Knowing the profile mix and profile segment specifics, realistic maneuver and gust load spectra can be defined for use in subsequent durability and damage tolerance analyses.

While the procedures discussed in this appendix provide a general approach to the derivation of profile mix and segmentation, this is not to say that this is the only or best approach. Users of this handbook may prefer to find a different way to obtain certain segment information.

APPENDIX D

DEVELOPMENT OF A NORMALIZATION PROCEDURE FOR LATERAL LOAD FACTORS DUE TO GROUND TURNING

D.1 SCOPE

D.1.1 Scope.

Many variables influence the operational loads environment experienced by an aircraft. For this reason the statistical loads data for commercial aircraft have been presented by aircraft type. These data from the individual aircraft types would normally be used to predict the loading environment for aircraft judged to be similar. Applying the data to aircraft that differed greatly from the aircraft for which statistical data had been obtained always entails some degree of uncertainty. If the data could be normalized or correlated through the use of fixed parameters that account for differences in aircraft, then a single loading spectrum could be derived that would apply to any aircraft for the prediction of loading spectra. As part of the ground loads data collection effort, statistical data for lateral load factors during ground turning maneuvers are available. The lateral load factors are presented as cumulative occurrences per 1,000 flights. The data when presented in this format show differences between aircraft types. A data correlation approach has been developed that provides a means to consolidate the available ground turning data from different aircraft into a single relationship. This relationship can be used to estimate the ground turning side load spectra on any aircraft regardless of size.

D.2 DATA ANALYSIS

D.2.1 Data analysis.

Figures D-1and D-2 present the ground turning side load factor spectra for taxi-out and taxi-in for five commercial aircraft displayed by increasing gross weight. As can be seen, differences exist between the spectra for the five aircraft, as well as between the taxi-out and taxi-in operations. Acceleration data are recorded in three directions: normal (*z*), lateral (*y*), and longitudinal (x*)*. As shown on Figure D-3 the positive *y* direction is aircraft starboard. Thus, the negative load factors represent left turns and the positive load factors represent right turns. Figures D-4 to D-8 present the spectra from Figures D-1 and D-2 in terms of absolute load factor values for each of the aircrafts individually. This form of representation more clearly shows the differences in spectra due to left and right turns, and taxi-out and taxi-in operations. Review of the spectra results in two useful observations. First, the taxi-out and taxi-in spectra represent two distinct populations. Second, the spectra between left and right turns do show some asymmetry but are essentially symmetrical. Some of the asymmetry may be due to offsets in the acceleration measurements on specific aircraft. The symmetry is expected to improve as the size of the database increases from 1196 flights for the B-767, 3987 flights for the MD-82, 11723 flights for the B-737 aircraft, 6226 flights for the A-320, and 1362 flights for the B-747-400.

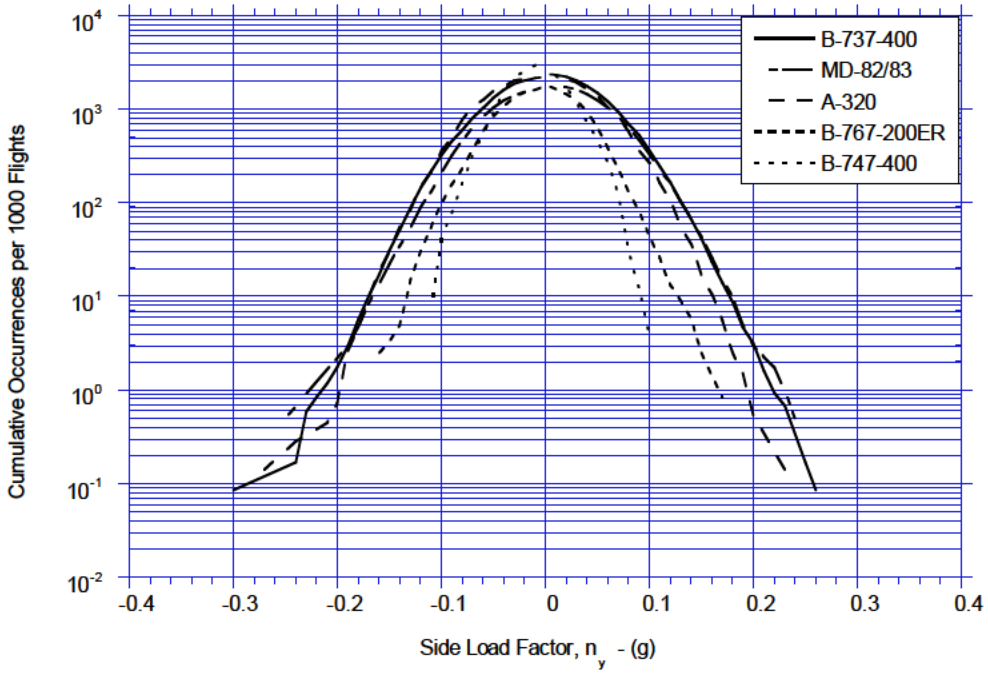

FIGURE D- 1. Cumulative frequency of lateral load factor during ground turning, taxi-out.

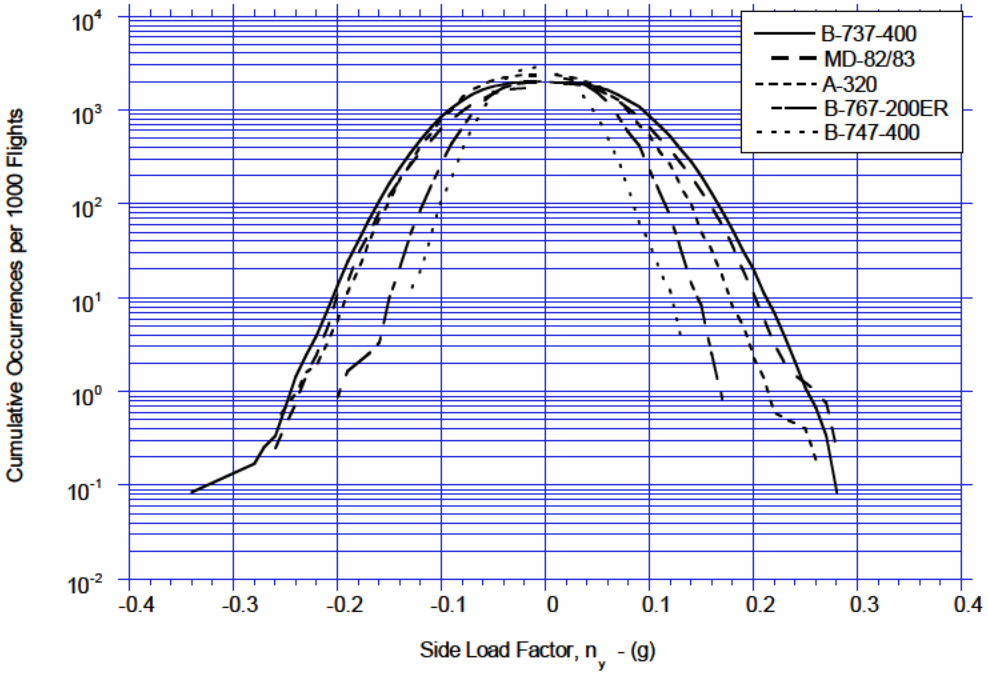

FIGURE D- 2. Cumulative frequency of lateral load factor during ground turning, taxi-in.

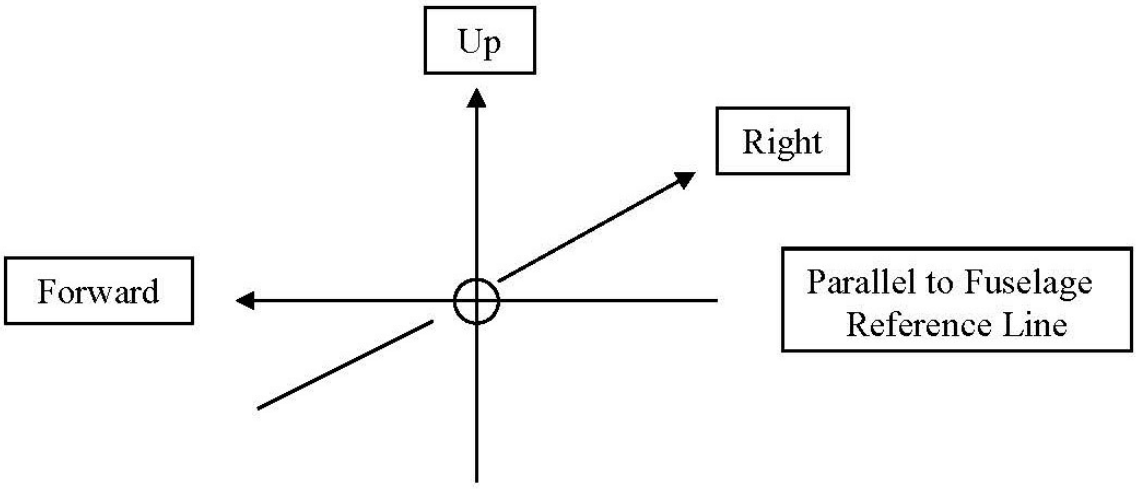

FIGURE D- 3. Sign convention.

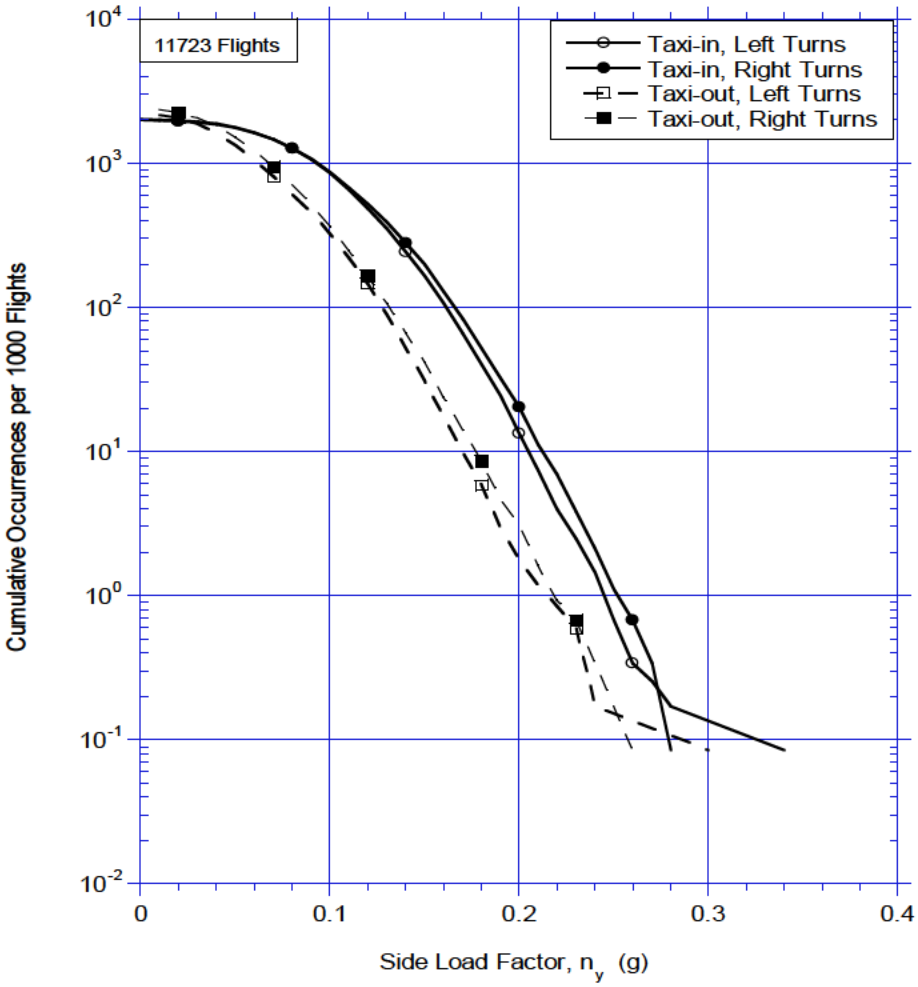

FIGURE D- 4. Cumulative frequency of lateral load factor during ground turning, B-737-400.

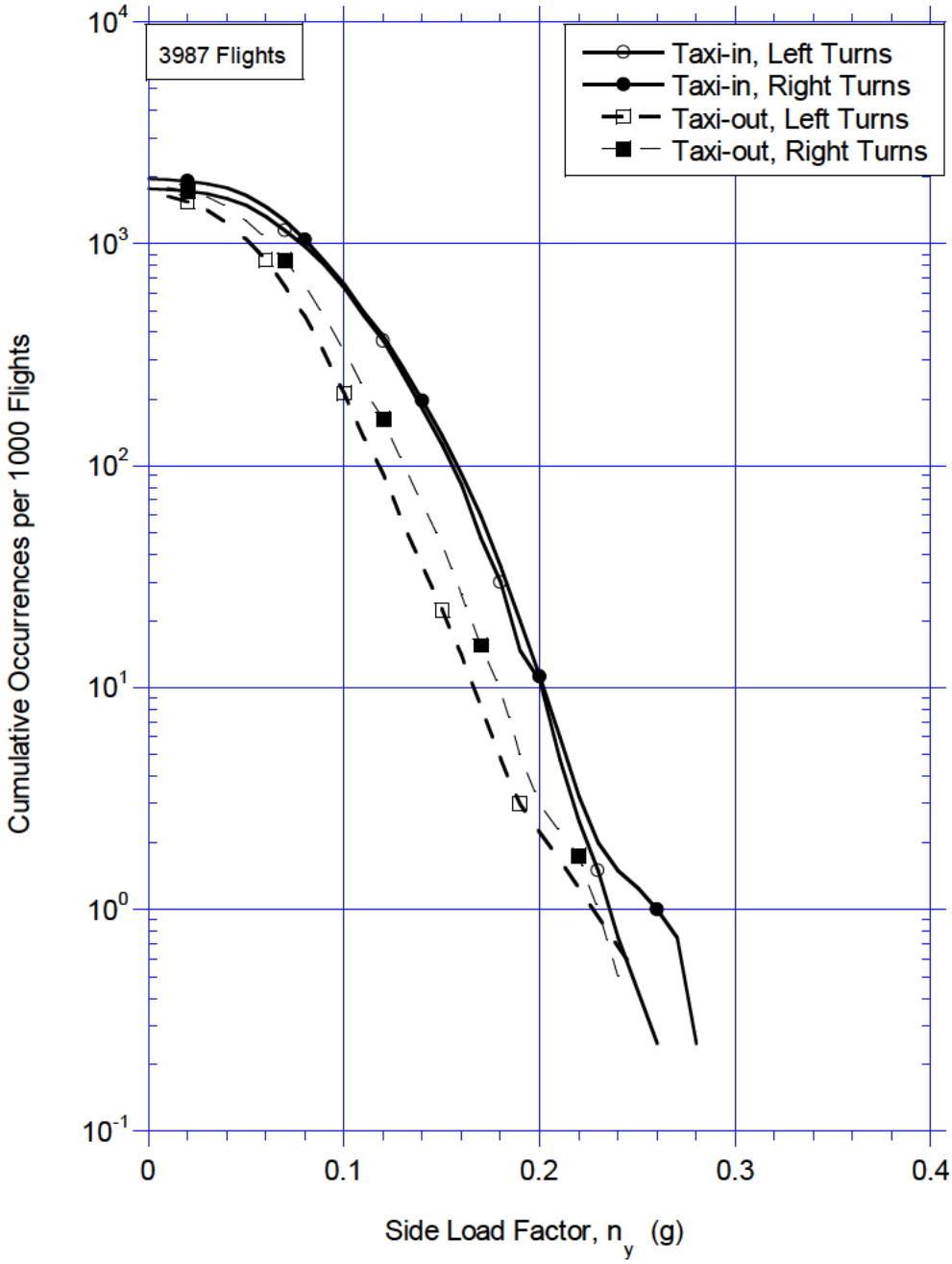

FIGURE D- 5. Cumulative frequency of lateral load factor during ground turning, MD-82/83.

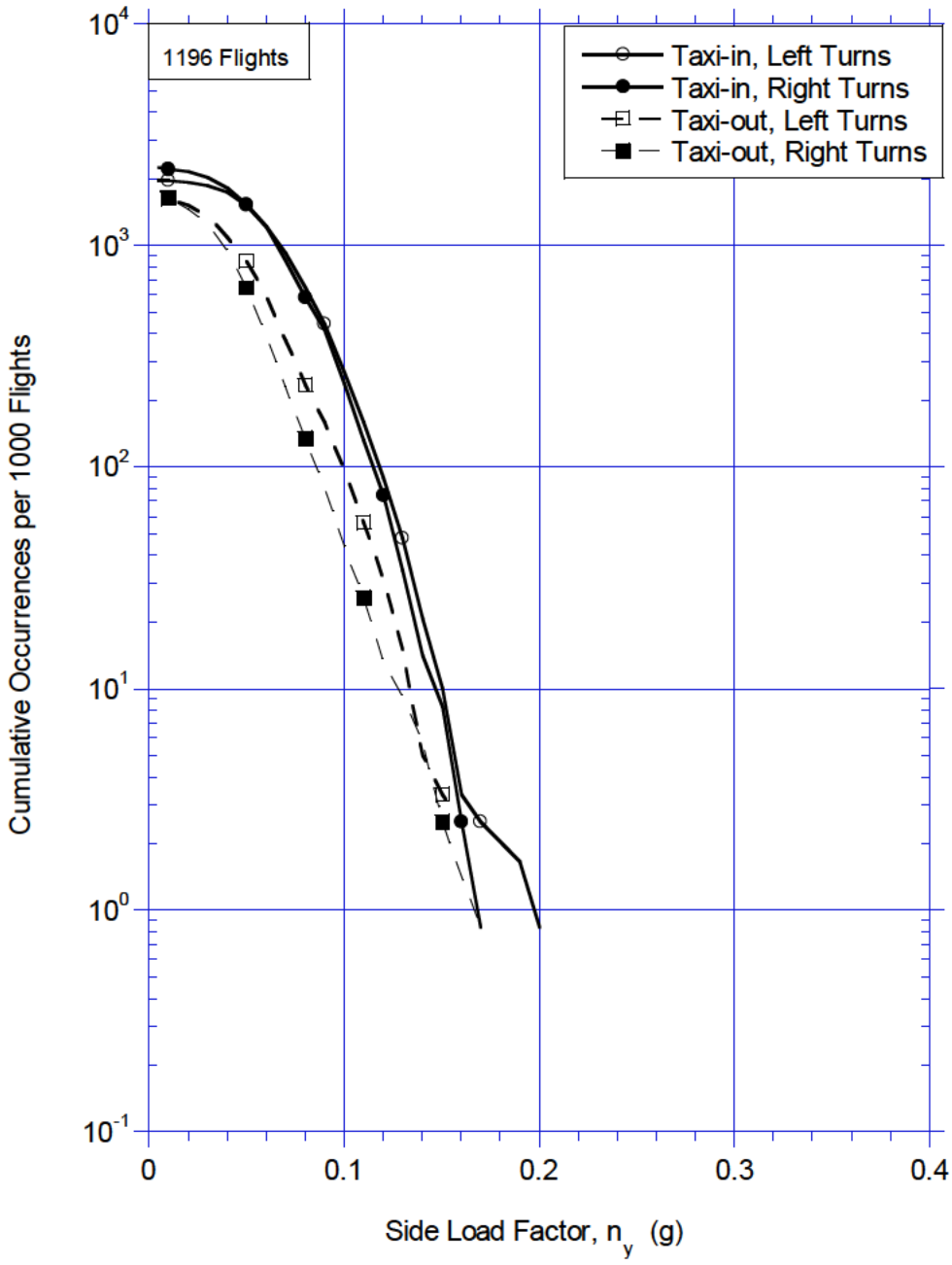

FIGURE D- 6. Cumulative frequency lateral load factor during ground turning, B-767-200ER.

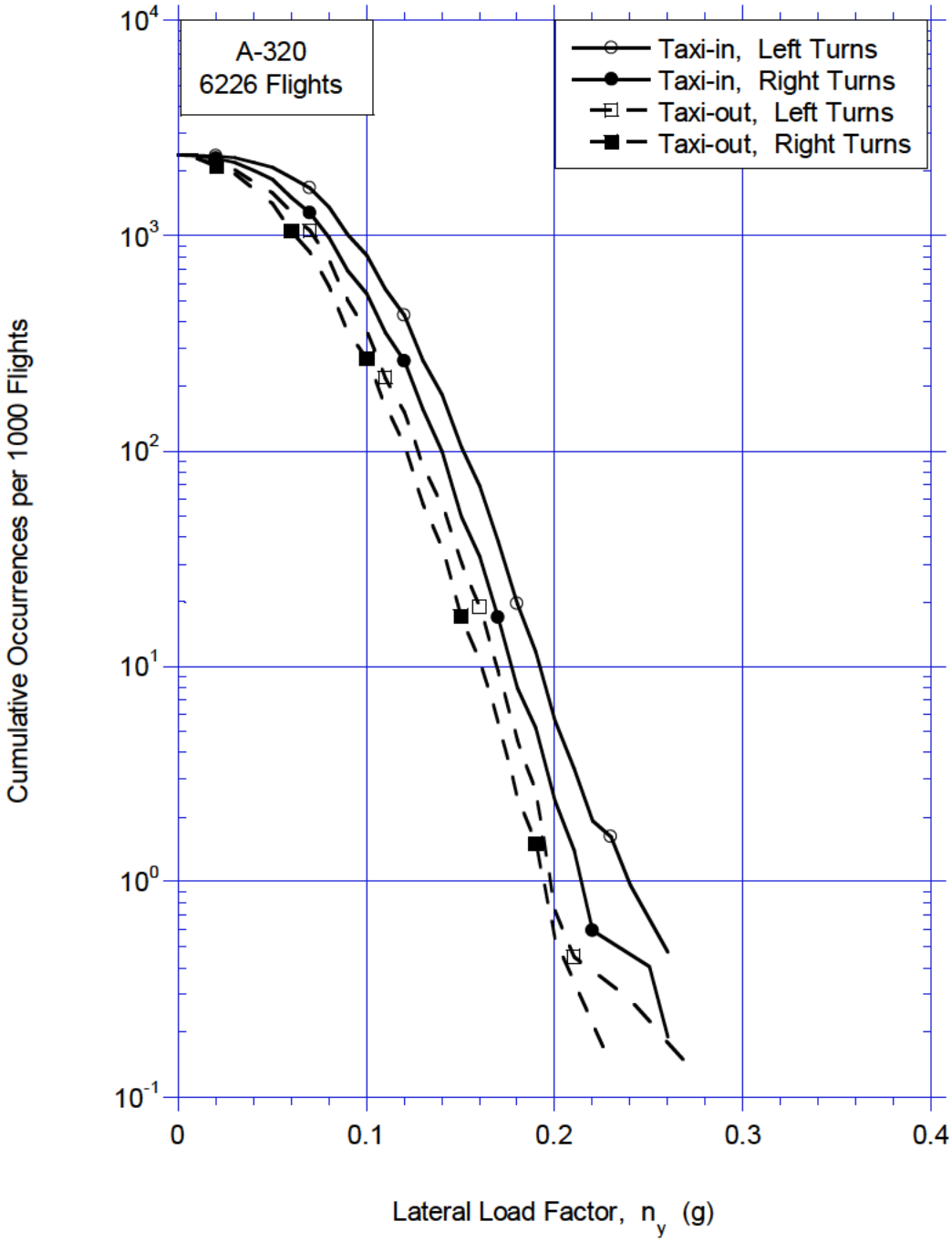

FIGURE D- 7. Cumulative frequency of lateral load factor during ground turning, A-320.

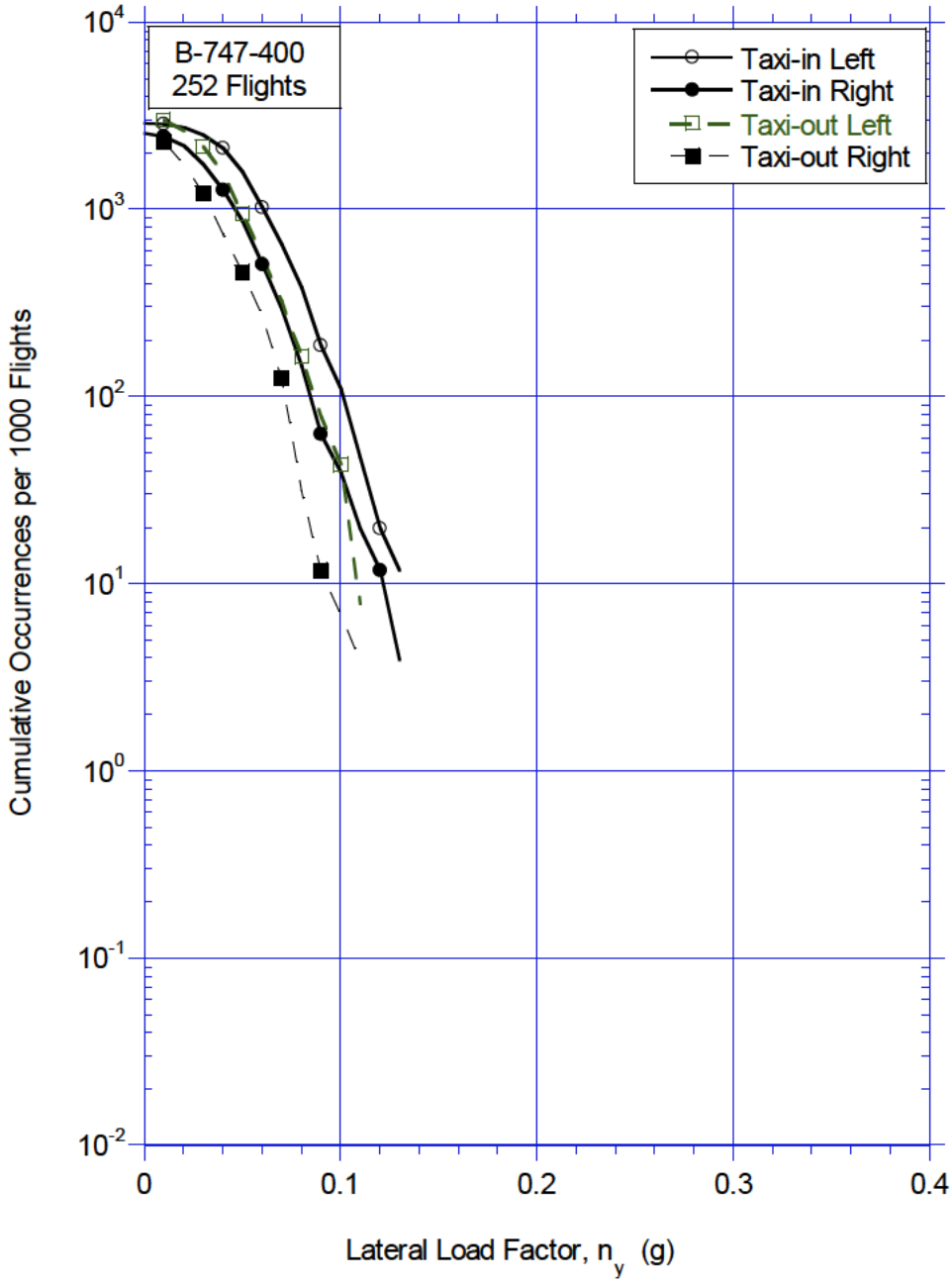

FIGURE D- 8. Cumulative frequency of lateral load factor during ground turning, B-747-400.

For the purpose of defining repeated loads spectra it is commonly assumed that there are differences between the number of occurrences for pre-flight and post-flight operations. However, for left and right turns or in-board and outboard load cycles an equal number of occurrences are normally assumed in both directions. Therefore, for this study the taxi-out and taxi-in spectra will be addressed separately, and the spectra for left and right turns will be considered symmetrical. A symmetrical spectrum of absolute load factor values representing the left and right turns can be obtained by calculating the arithmetic mean of corresponding positive and negative load factor magnitudes. However, the higher load factor levels of the left and right spectra are based on a few widely spaced load factor measurements at different magnitudes for left and right. While these are actual measurements, inclusion in the arithmetic mean calculation will require interpolation and extrapolation of sparse data that would result in questionable accuracy of the resulting spectra at the higher load factor levels. Thus, these points were eliminated from the symmetrical spectra calculations. Figures D-9 and D-10 show the resulting frequency distributions for the five aircraft for the taxi-out and taxi-in operations, respectively.

D.3 DATA CORRELATION

D.3.1 Data correlation.

Figures D-9 and D-10 clearly show the differences between the spectra for the five aircrafts. These cumulative frequency distributions can be approximated by a straight line when plotted in a semi-log form as the cumulative occurrences versus the square of the load factor. Figures D-11 and D-12 present the cumulative occurrences in this format for taxi-out and taxi-in respectively. These differences in the slopes of the spectra cannot simply be attributed to any obvious difference in commercial airline ground turning operations at civil commercial airport facilities. A number of unknown and different variables may be contributing to this difference.

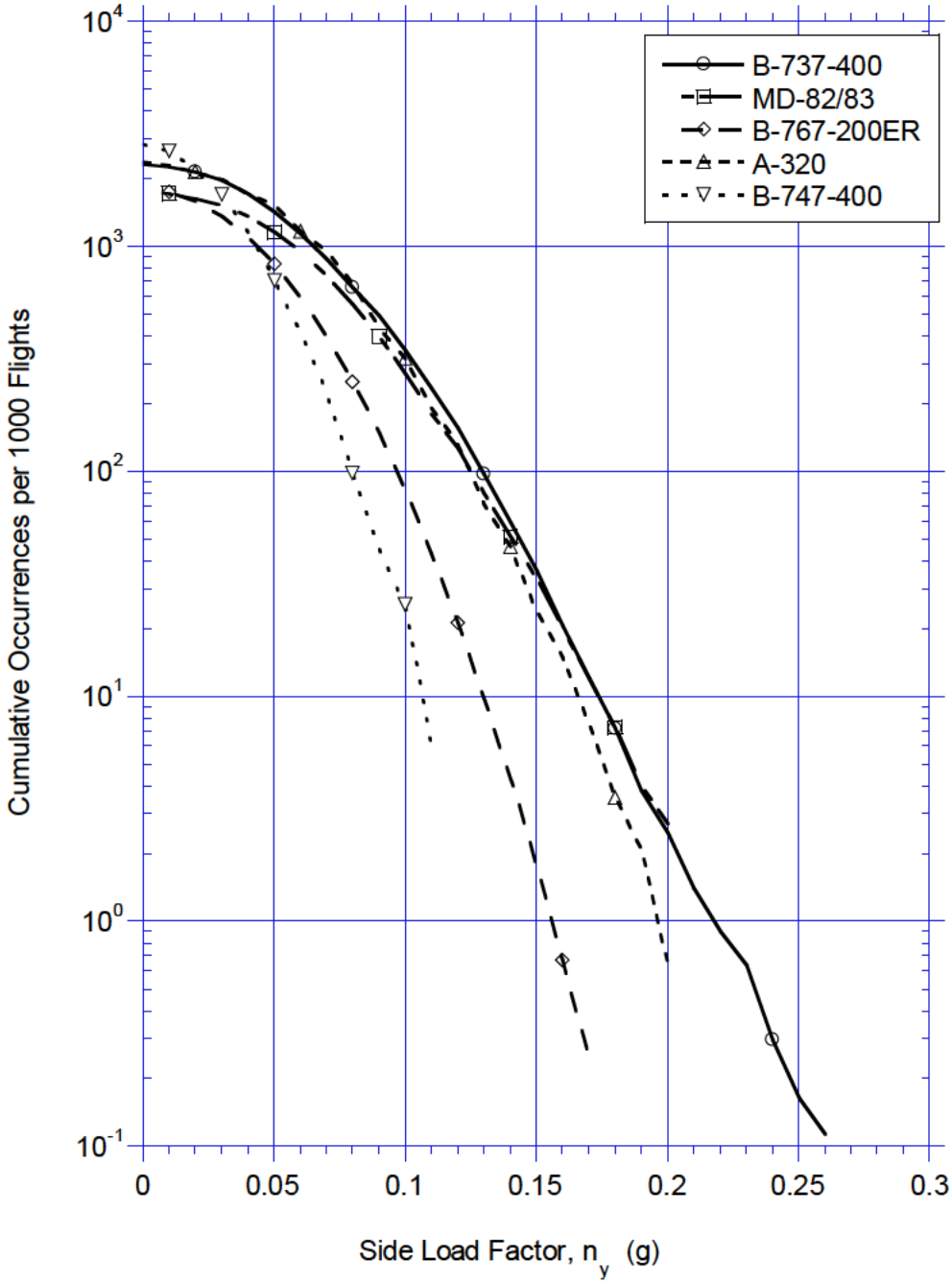

FIGURE D- 9. Cumulative frequency of lateral load factor during ground turning, taxi-out all aircraft.

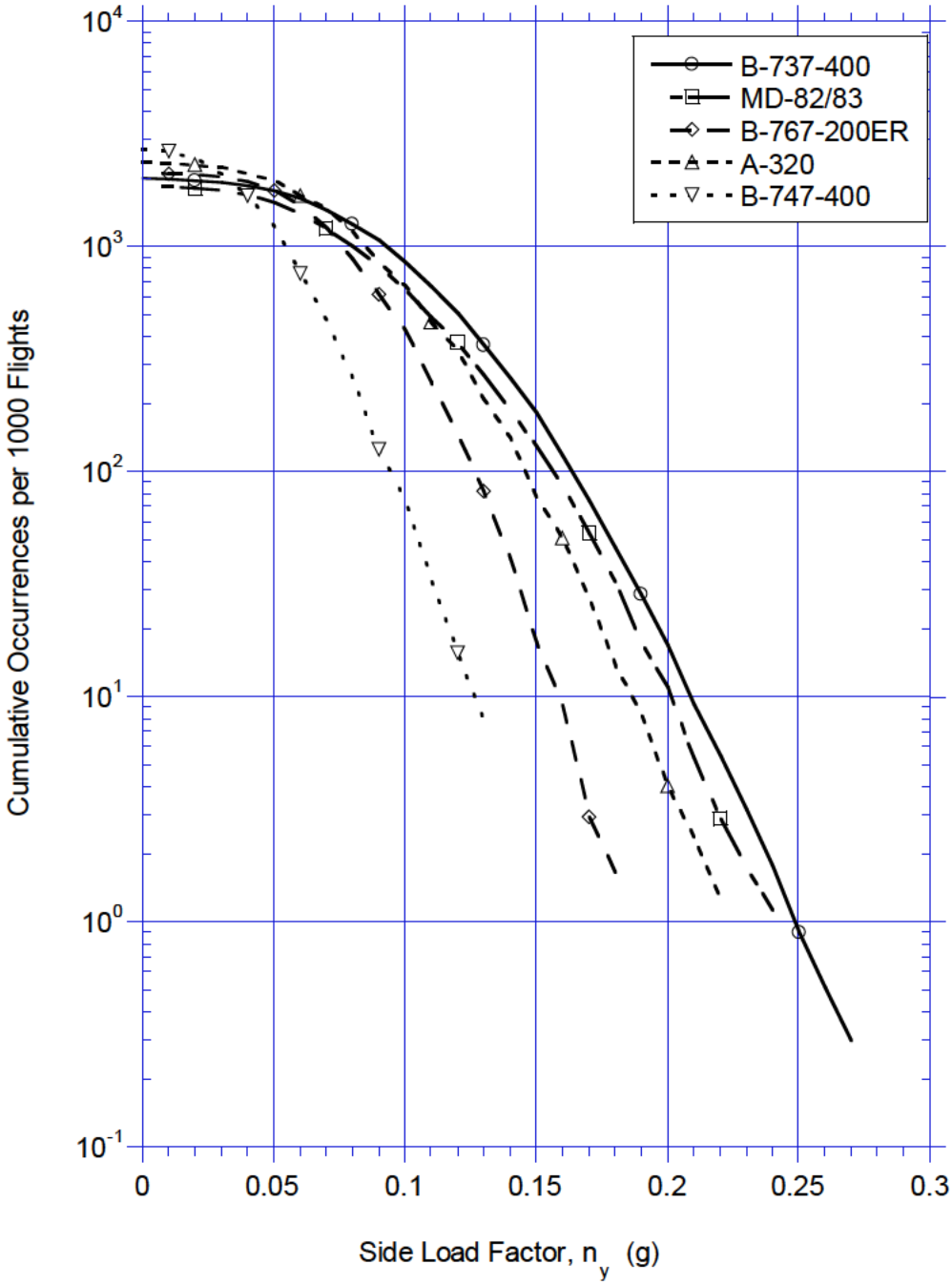

FIGURE D- 10. Cumulative frequency of lateral load factor during ground turning, taxi-in, all aircraft.

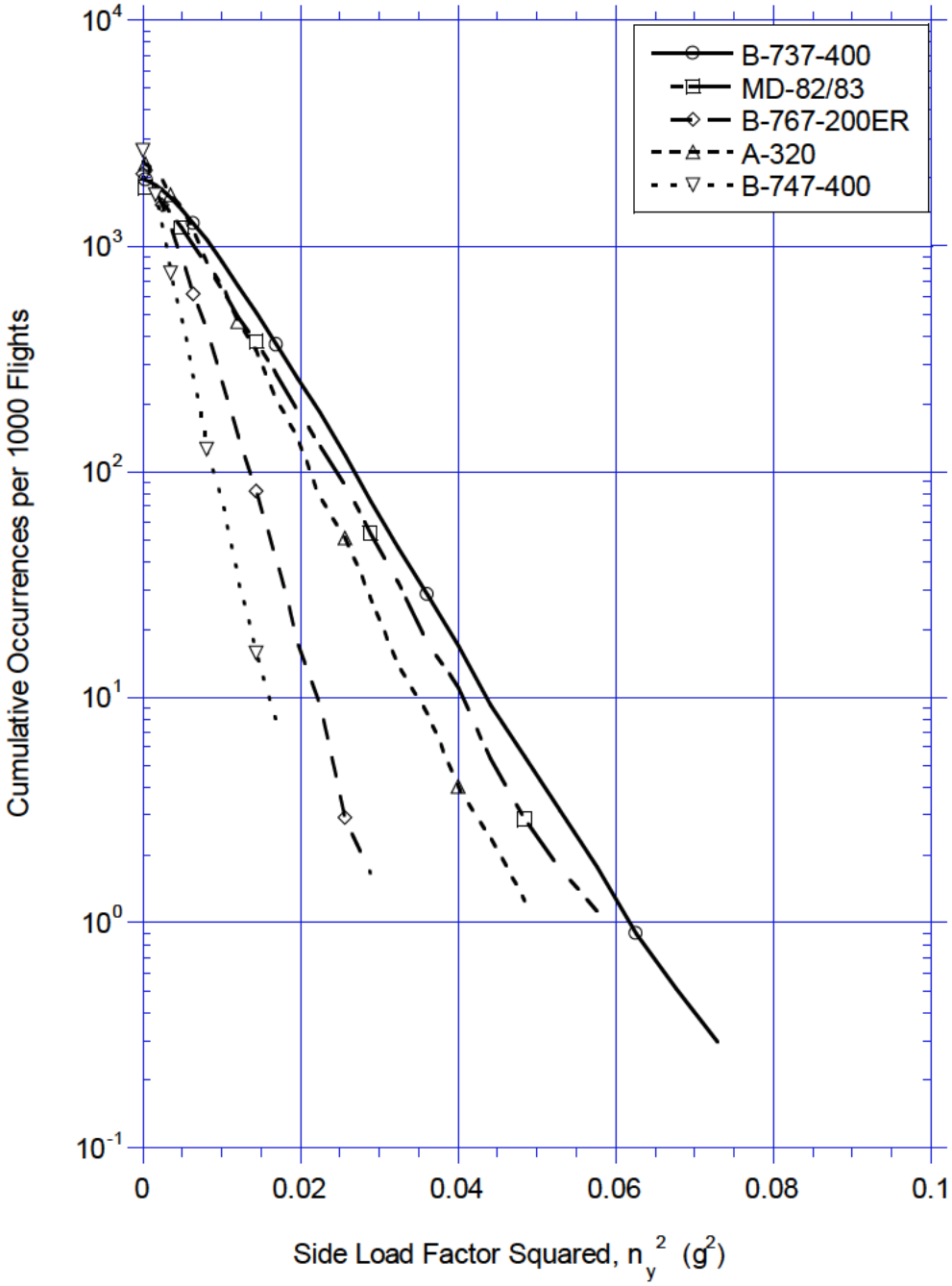

FIGURE D- 11. Cumulative occurrences of lateral load factor squared during ground turning, taxi-out, all aircraft.

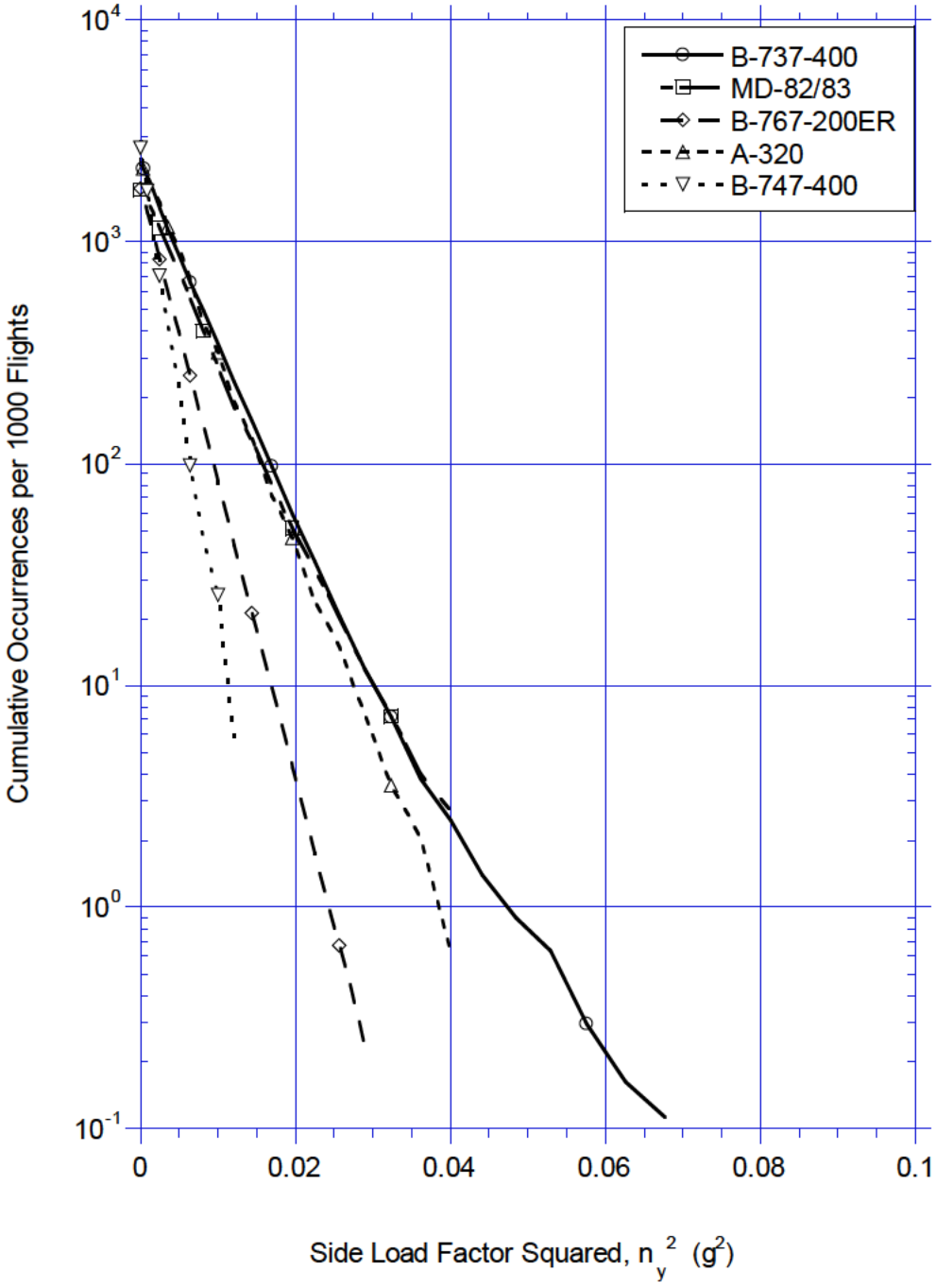

FIGURE D- 12. Cumulative occurrences of lateral load factor squared during ground turning, taxi-in, all aircraft.

It is postulated that the differences in gear geometry, such as main gear track dimension and the distance between main and nose gears, could affect the pilot's turning input options relative to the fixed widths of runways or taxiways. If this were the case it would account for the differences in the slopes of the spectra. The differences in the zero intercept of the spectra could be the result of operations into different airport types, such as international airports, large and small domestic airports, or airports with multiple or single runways. Differences in the size and the layout of these airports could account of the differences in the total number of turns in taxi-out and taxi-in operations.

Because it is not clear how the gear dimensions affect the ground turning operations no simple theoretical formulation can be derived to account for these differences. Thus, the study proceeded on the basis that it might be possible to develop some form of empirical relationship that accounts for the effect of gear geometry differences on the side load factor experience during ground turning. Such a correlation would allow consolidation of the different spectra into a single empirical relationship applicable to all aircraft. Since the spectra exhibit straight-line variations when plotted in semi-log form a general curve fit equation can be employed of the form:

$$N = N_0 e^{-\left(kn_y^2\right)} \qquad \text{(D1)}$$

Where:

N = the number of cumulative occurrences of any n_y.

N_0 = the number of cumulative occurrences at n_y=0.

n_y = the maximum lateral load factor measured in a ground turn.

k = constant reflecting the influence of the main and nose landing gear dimensional arrangement on the expected side load factor magnitude during a ground turn in comparison to other aircraft.

Correlative analyses of the measured spectrum data and various aircraft gear dimensional combinations using a curve fit equation of the form defined by Equation D1 was conducted. The purpose was to determine the combination of the landing gear geometry dimensions and the associated values of "N_0" and of "k" that would provide the best single representation of the measured values for all the aircraft when used in Equation D1. It was determined that the "k" constant that provided the best overall agreement was of the form $d^m t$, where "d" represents the landing gear base dimension and "t" represents the landing gear track dimension.

Figure D-13 shows the dimensional references of the landing gear arrangement, and Table D-I shows the dimensional values for the three aircraft of this study. Thus the optimum curve fit equation that will account for the influence of gear geometry for different aircraft thus is represented by:

$$N = N_0 e^{-\left(d^m t n_y^2\right)} \qquad \text{(D2)}$$

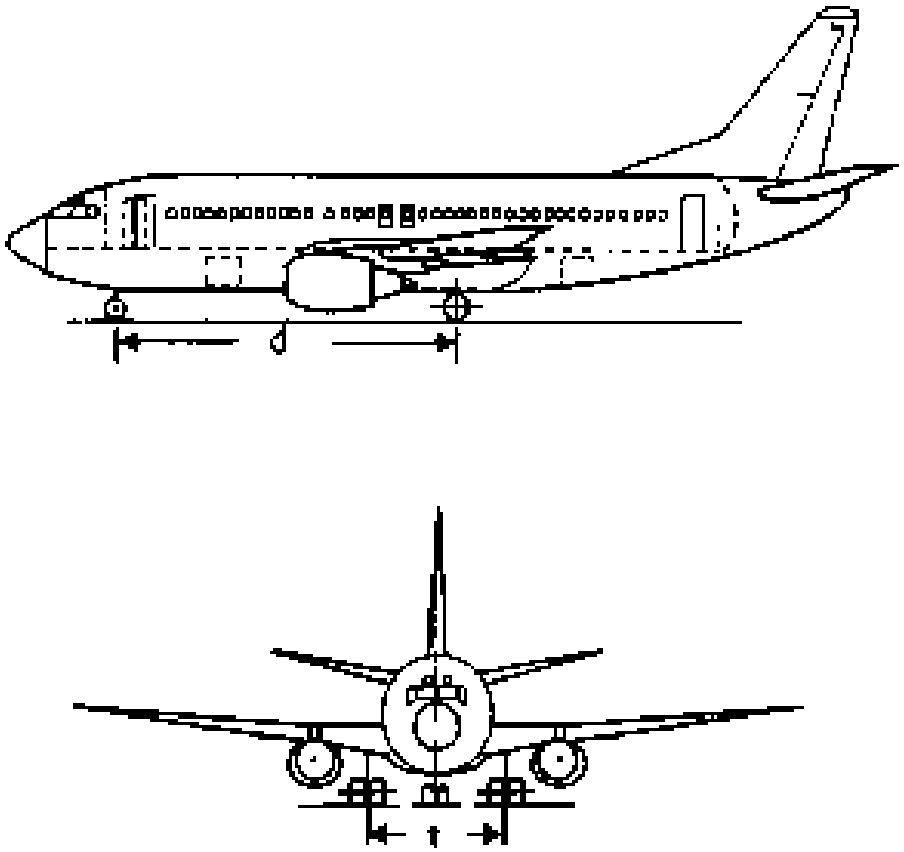

FIGURE D- 13. Gear base and track geometry.

TABLE D- I. Landing gear base and track dimensions.

AIRCRAFT	DIMENSIONS (FEET)	
	d	t
B-737-400	46.83	17.17
MD-82/83	72.40	16.70
B-767-200ER	64.58	30.50
A-320	41.47	24.92
B-747-400	84.0	36.08

A general curve fit equation of the form of Equation D2 was applied to the measured spectra to solve for the constants "N_0" and "m" using the Levenberg-Marquardt algorithm. This algorithm uses an iteration procedure to produce a curve fit until the Chi-square does not change for a specified number of iterations or the percent change in the normalized Chi-square is less than a specified allowable error. The allowable error used in the curve fit was set at 1 percent. Discussion of the procedure is beyond the scope of this report, but can be found in Numerical Recipes in C, the Art of Scientific Computing (see Reference B4). Figures D-14 to D-23 show the curve fits obtained for the taxi-out and taxi-in cases for the five aircrafts.

Table D-II presents the values for the constants derived from the curve fits to the measured spectra. Average values shown for the constants represent the arithmetic means of the constants obtained for the individual aircraft.

TABLE D- II. Equation constants.

AIRCRAFT	TAXI-OUT		TAXI-IN		FLIGHTS
	N_0	m	N_0	m	
B-737-400	2317.4	0.60407	2018.0	0.50799	11723
MD-82/83	1793	0.54300	1876.8	0.47459	3987
A-320	2378	0.56014	2378	0.49062	6226
B-767-200ER	1825	0.54920	2131.5	0.49966	1196
B-747-400	2860.2	0.59799	2724.4	0.5180	252
AVERAGE	2234.7	0.571	2225.7	0.498172	23384

$$N_{Taxi-out} = 2234.7 \times e^{-\left(d^{0.571} \times t \times n_y^2\right)}$$

$$N_{Taxi-in} = 2225.7 \times e^{-\left(d^{.498} \times t \times n_y^2\right)}$$

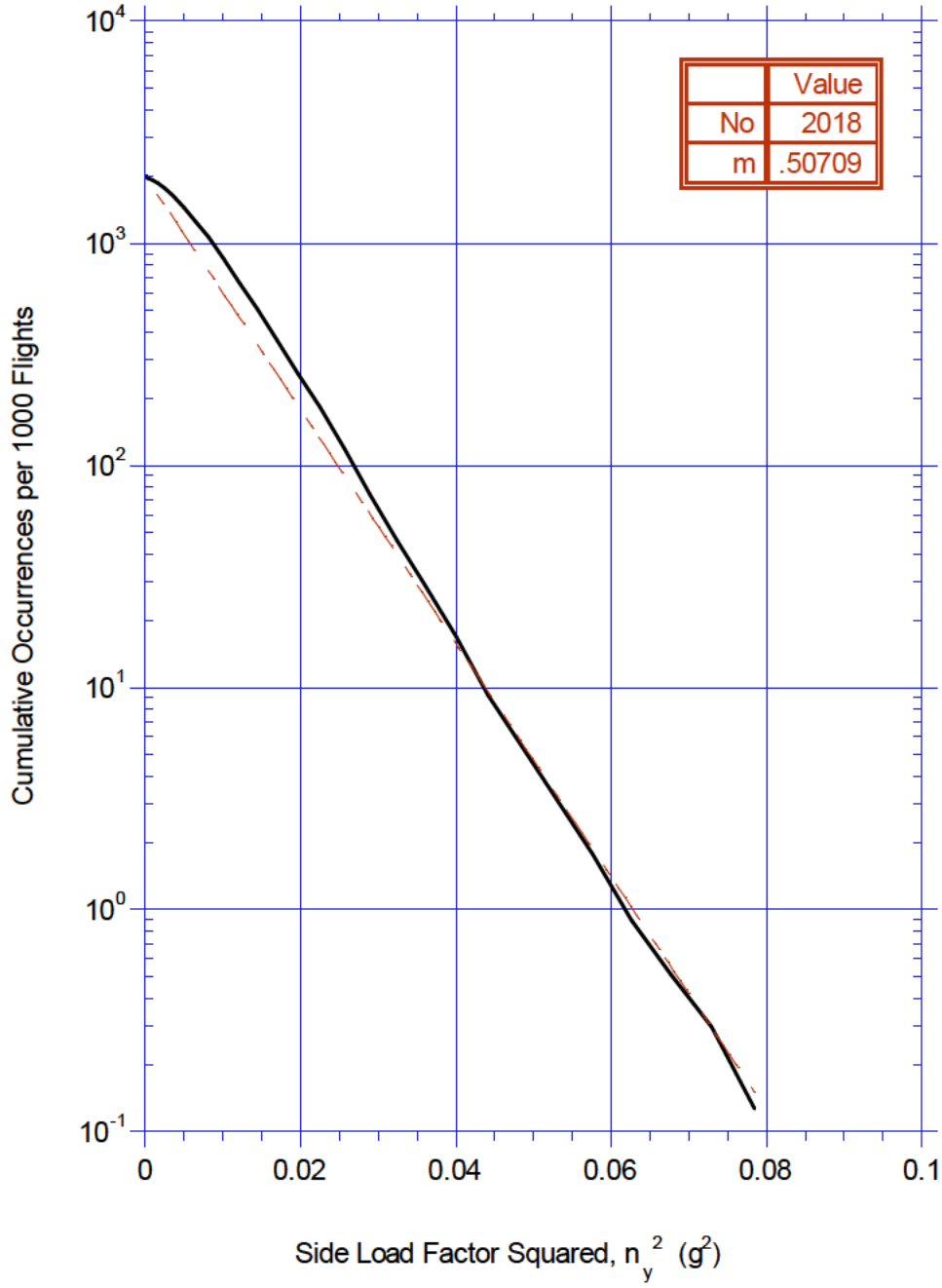

FIGURE D- 14. Curve fit of cumulative frequency of lateral load factor squared during ground turning, taxi-out, B-737-400.

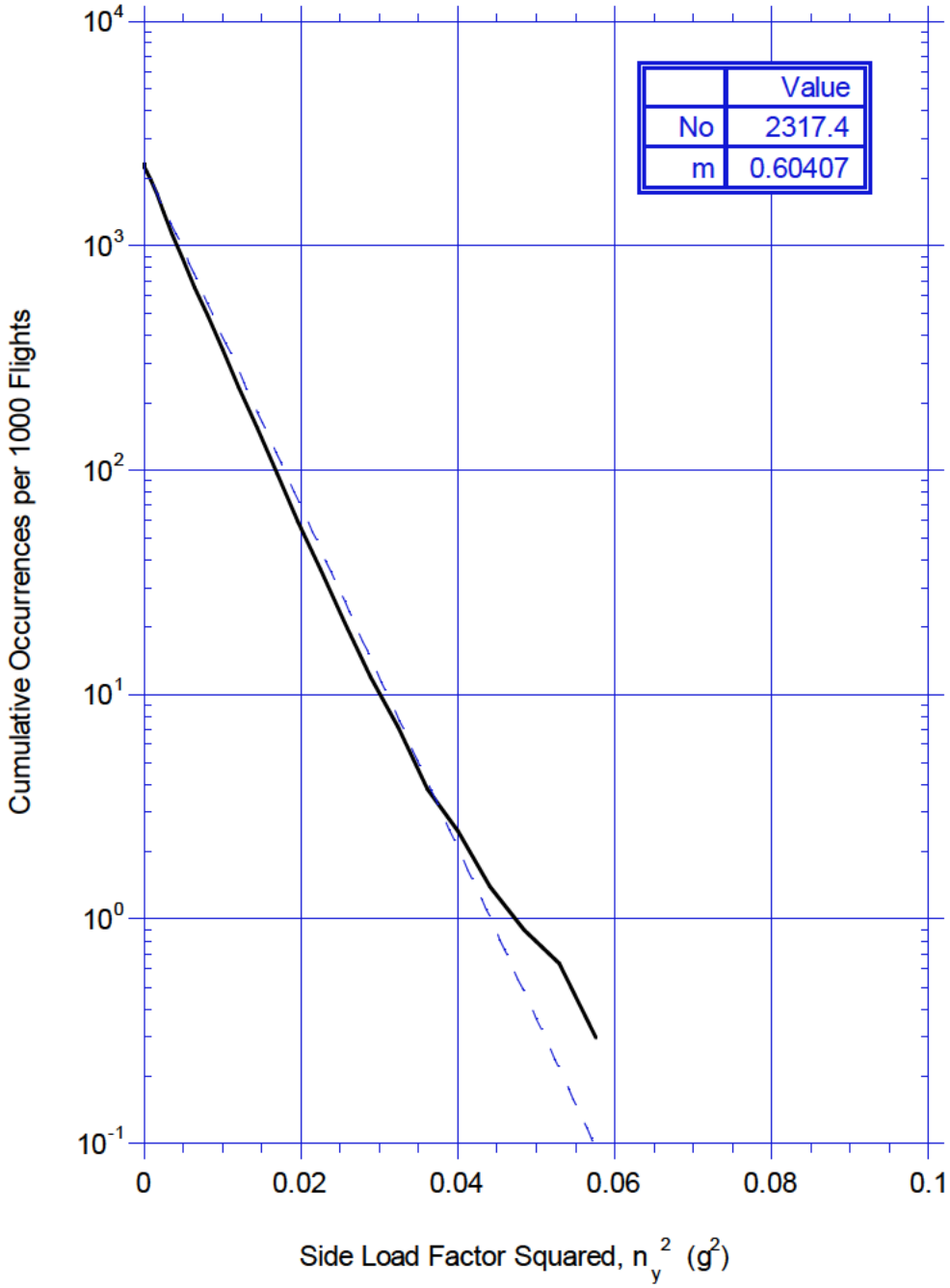

FIGURE D- 15. Curve fit of cumulative frequency of lateral load factor squared during ground turning, taxi-in, B-737-400.

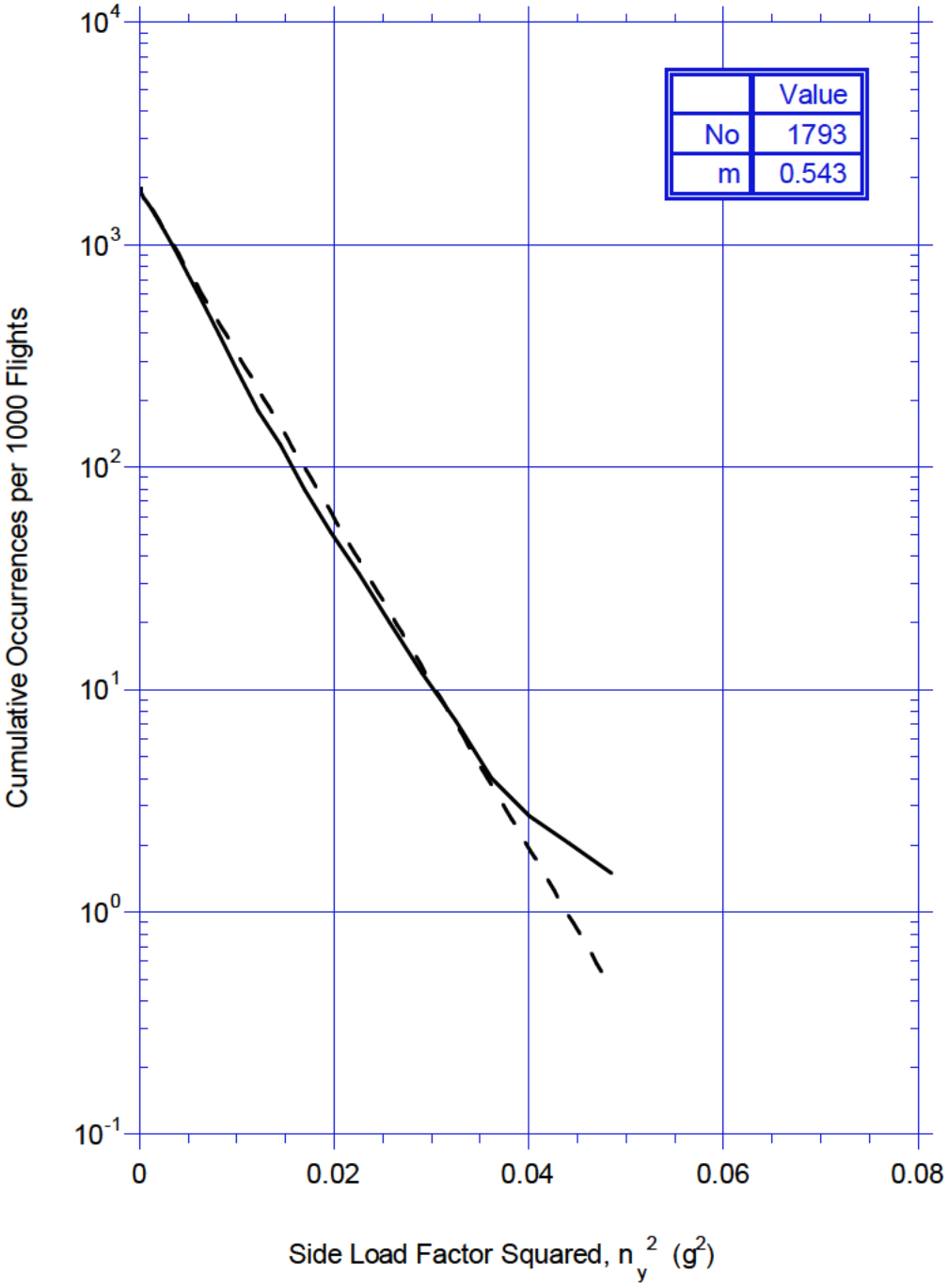

FIGURE D- 16. Curve fit of cumulative frequency of lateral load factor squared during ground turning, taxi-out, B-MD-82/83.

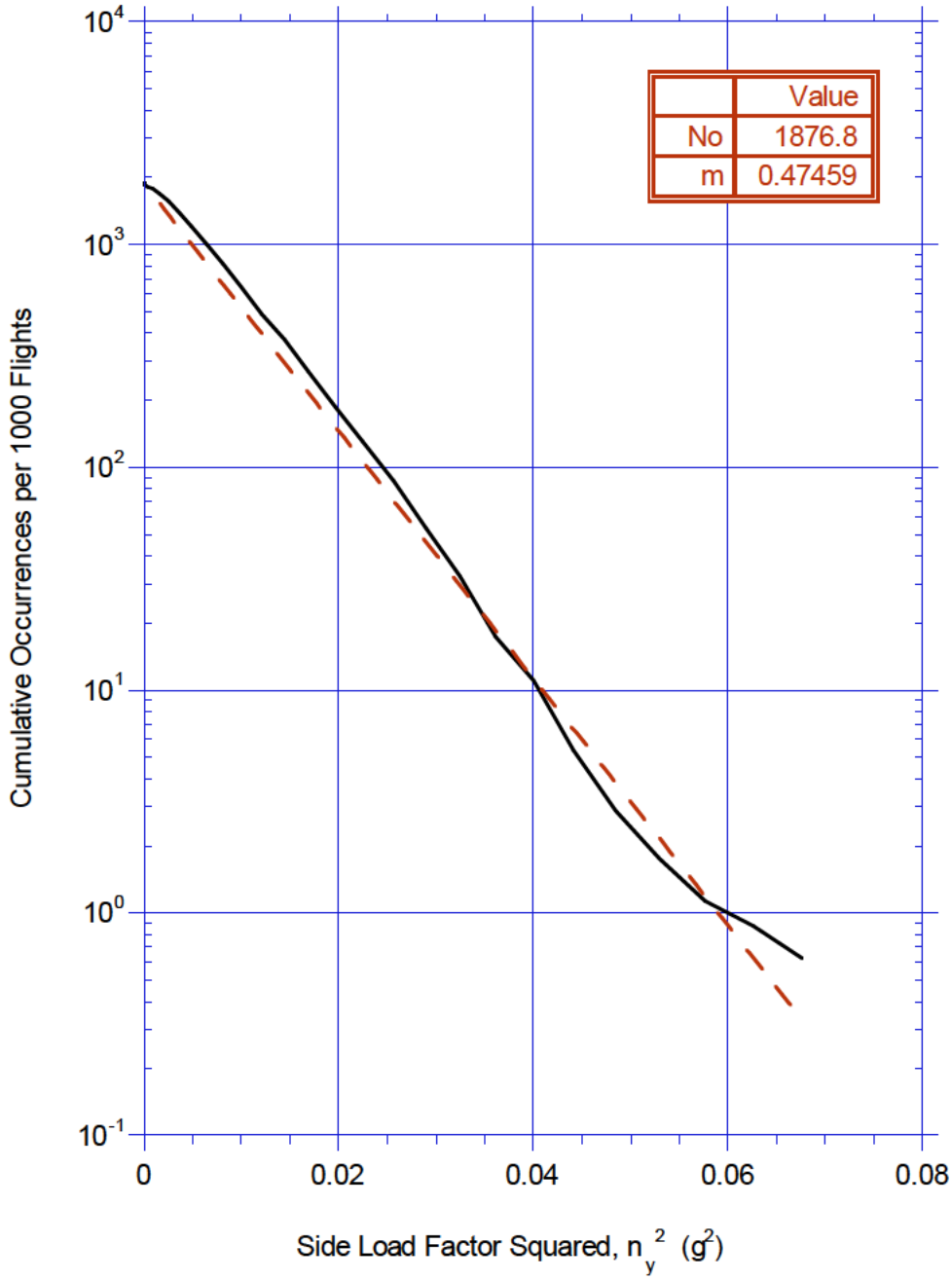

FIGURE D- 17. Curve fit of cumulative frequency of lateral load factor squared during ground turning, taxi-in, MD-82/83.

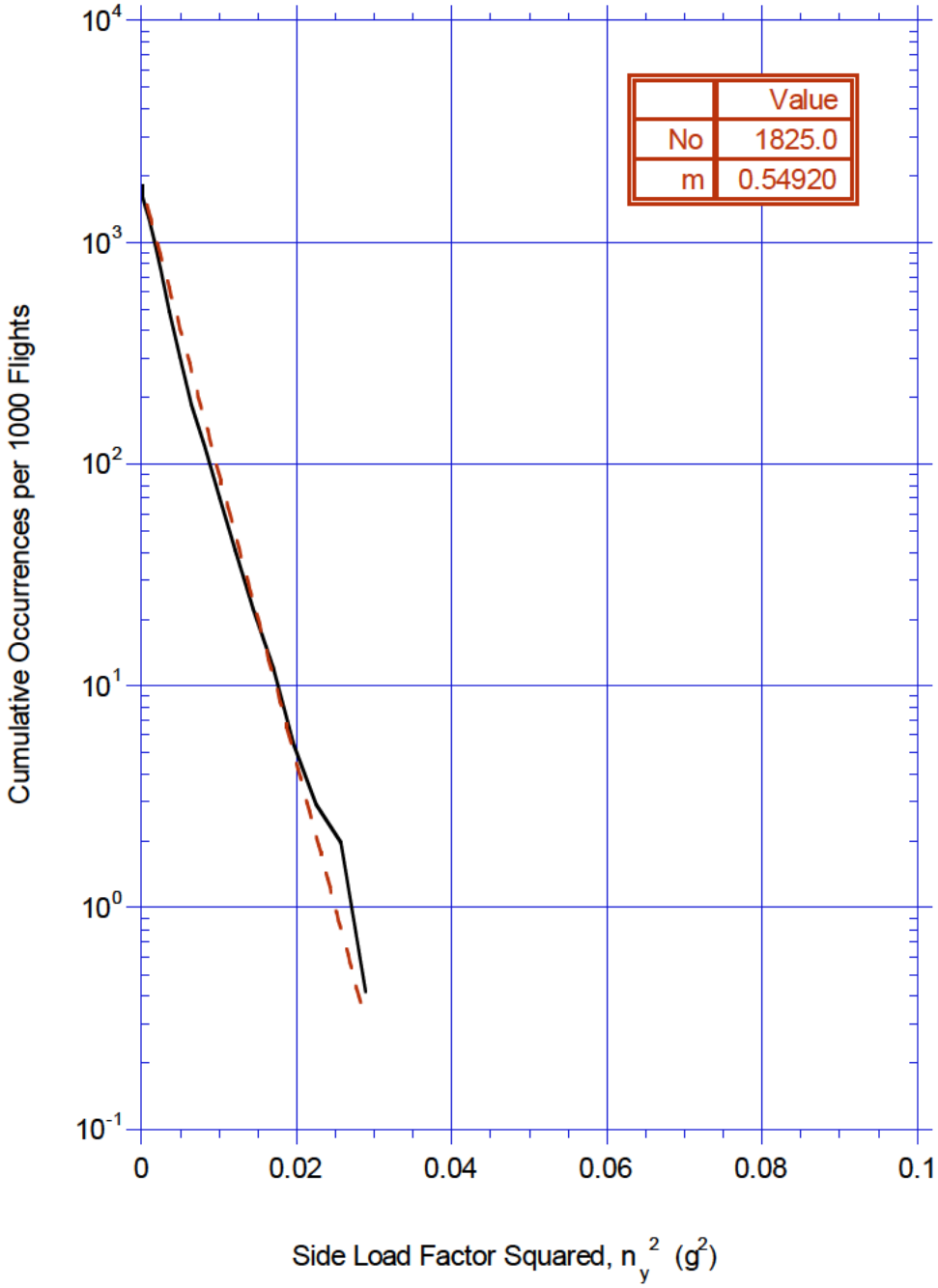

FIGURE D- 18. Curve fit of cumulative frequency of lateral load factor squared during ground turning, taxi-out, B-767-200ER.

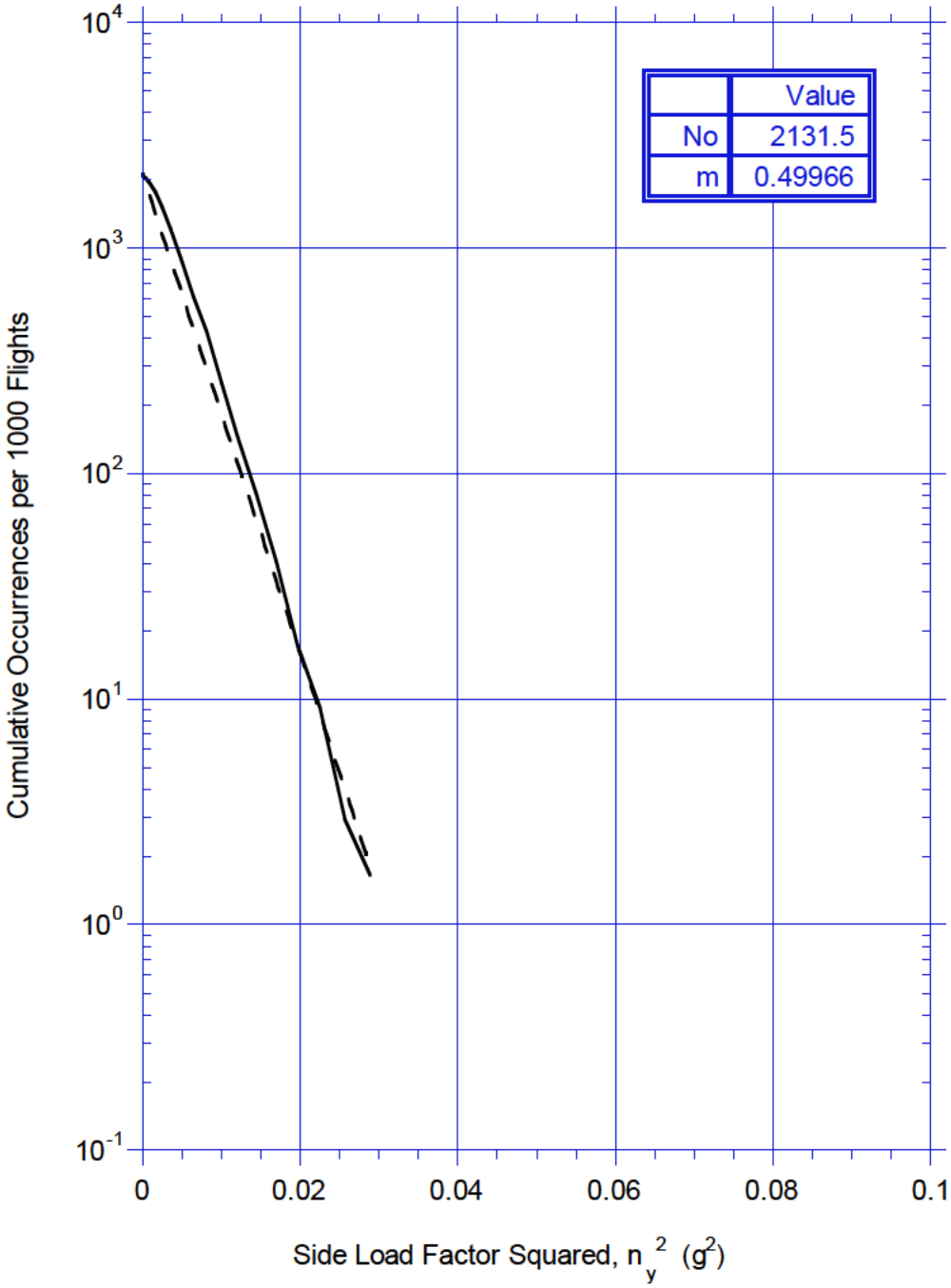

FIGURE D- 19. Curve fit of cumulative frequency of lateral load factor squared during ground turning, taxi-in, B-767-200ER.

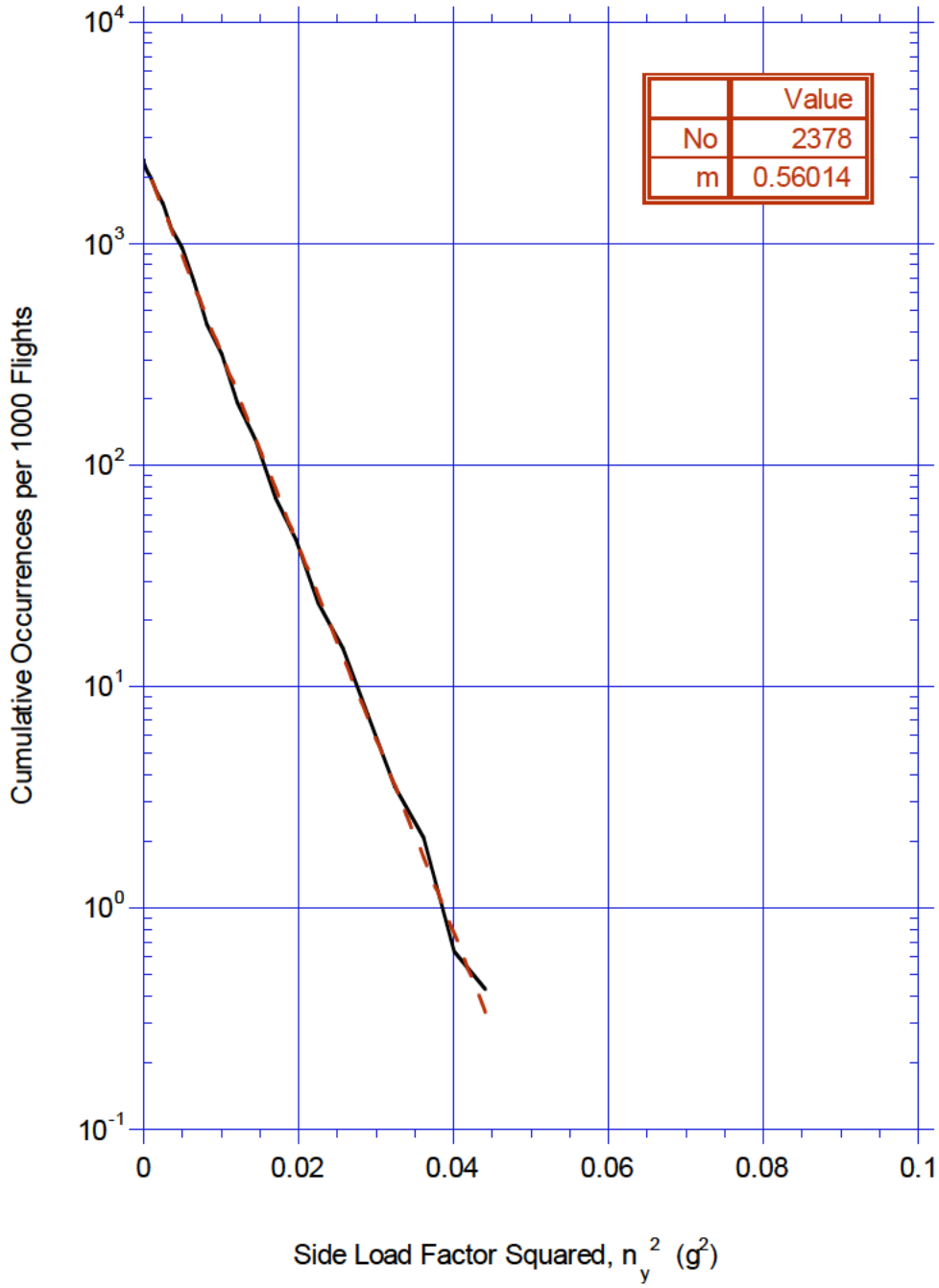

FIGURE D- 20. Curve fit of cumulative frequency of lateral load factor squared during ground turning, taxi-out, A-320.

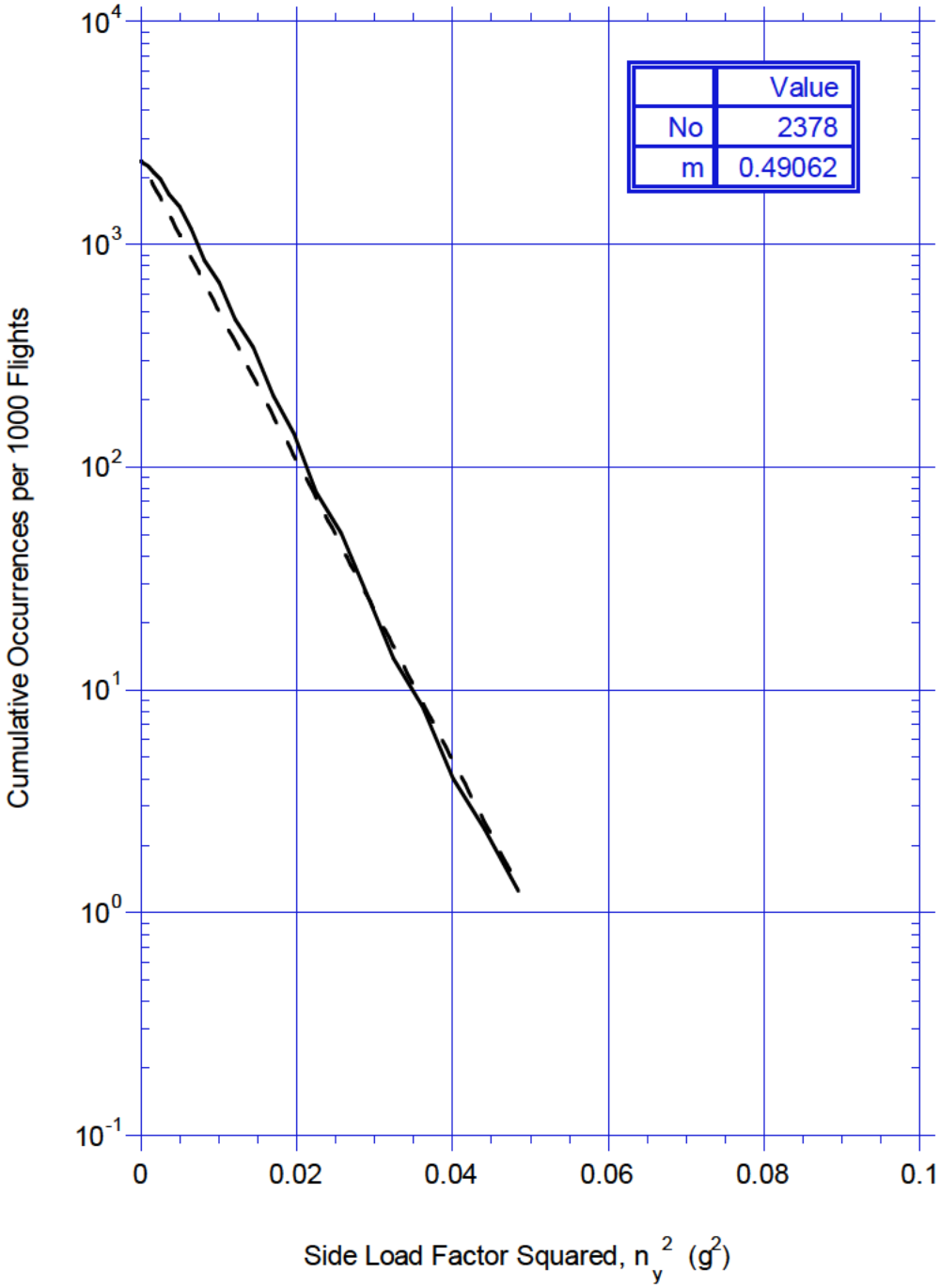

FIGURE D- 21. Curve fit of cumulative frequency of lateral load factor squared during ground turning, taxi-in, A-320.

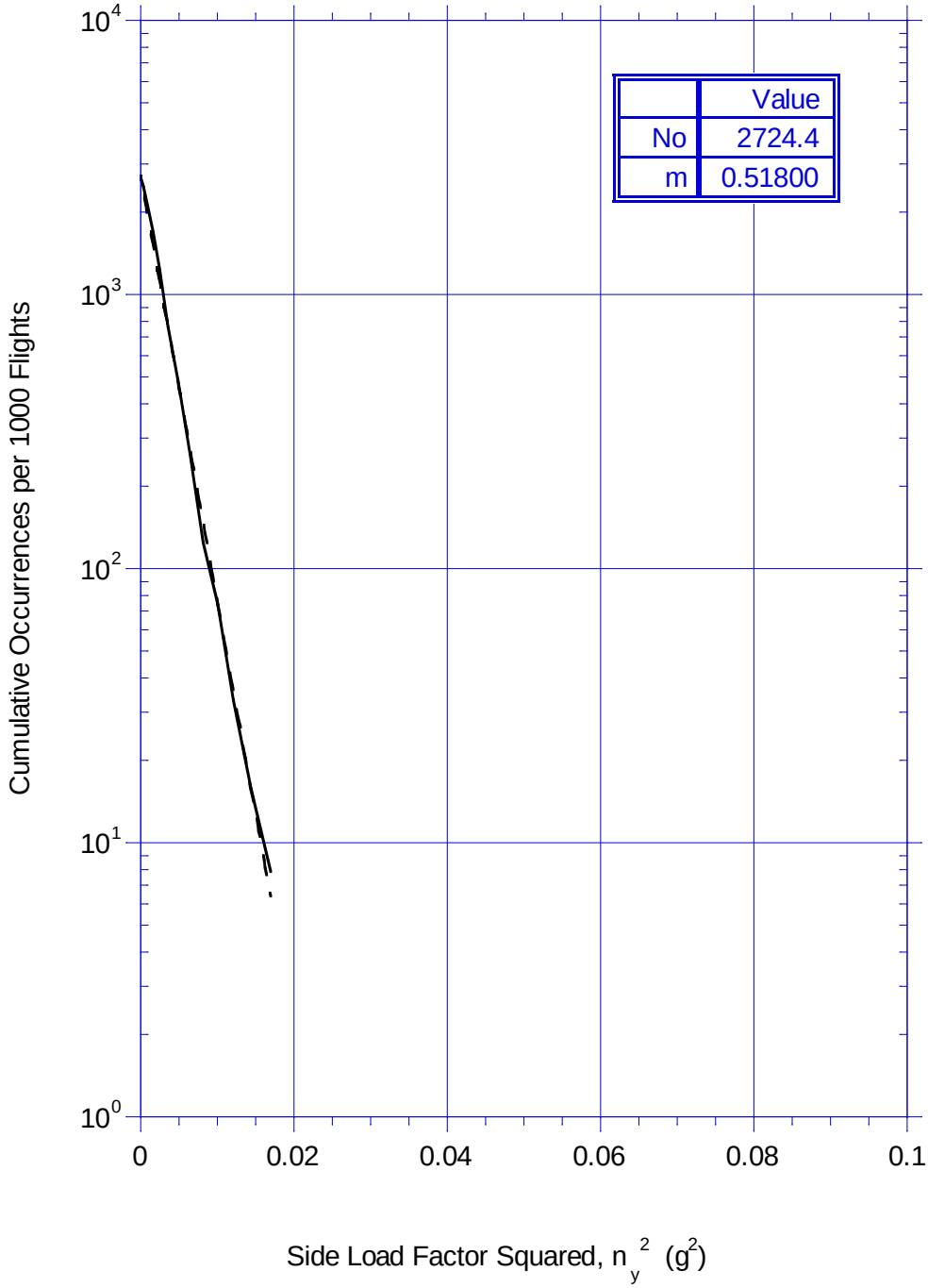

FIGURE D- 22. Curve fit of cumulative frequency of lateral load factor squared during ground turning, taxi-out, B-747-400.

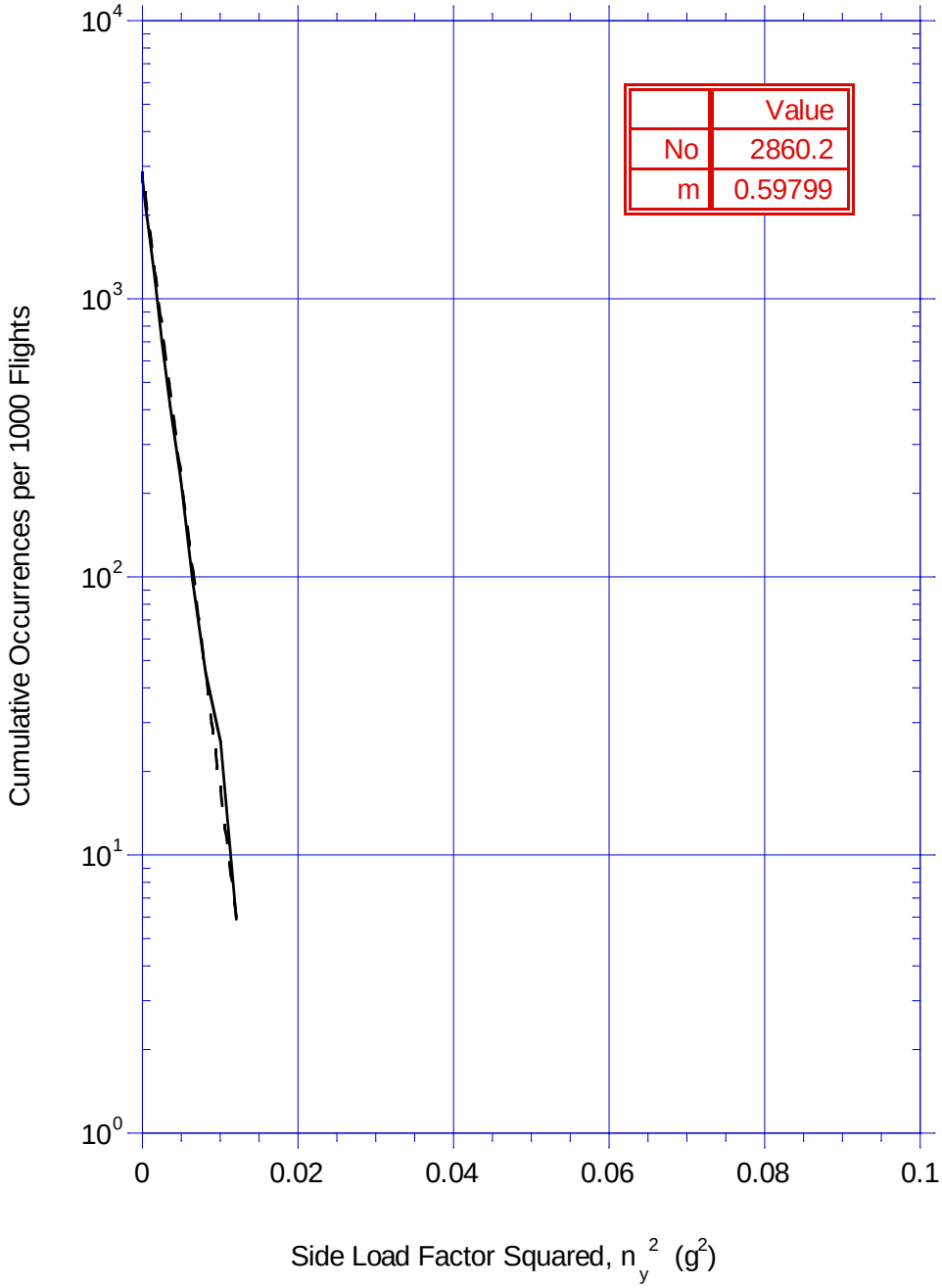

FIGURE D- 23. Curve fit of cumulative frequency of lateral load factor squared during ground turning, taxi-in, B-747-400.

The reliability of using the gear geometry dimensions in the form of $d^m t$ to account for differences in the measured spectra can now be tested by comparing the mean cumulative occurrences derived from the measured data with the cumulative occurrences calculated from the derived relationship expressed by Equation D2 using the average values shown in Table D-II. Figures D-24 to D-28

present the comparisons of taxi-out and taxi-in side load factor spectra obtained from the measured data and as calculated. In these comparisons the calculated spectra are considered quite acceptable for determining repeated loads spectra. How far these results can be extrapolated to other aircraft with widely varying landing gear dimensional arrangements cannot be known until additional data from such aircraft becomes available. However, within the variations covered by the study aircraft the present approach would be expected to provide acceptable results. Figure D-29 presents an envelope of the gear dimensions covered by the study aircraft.

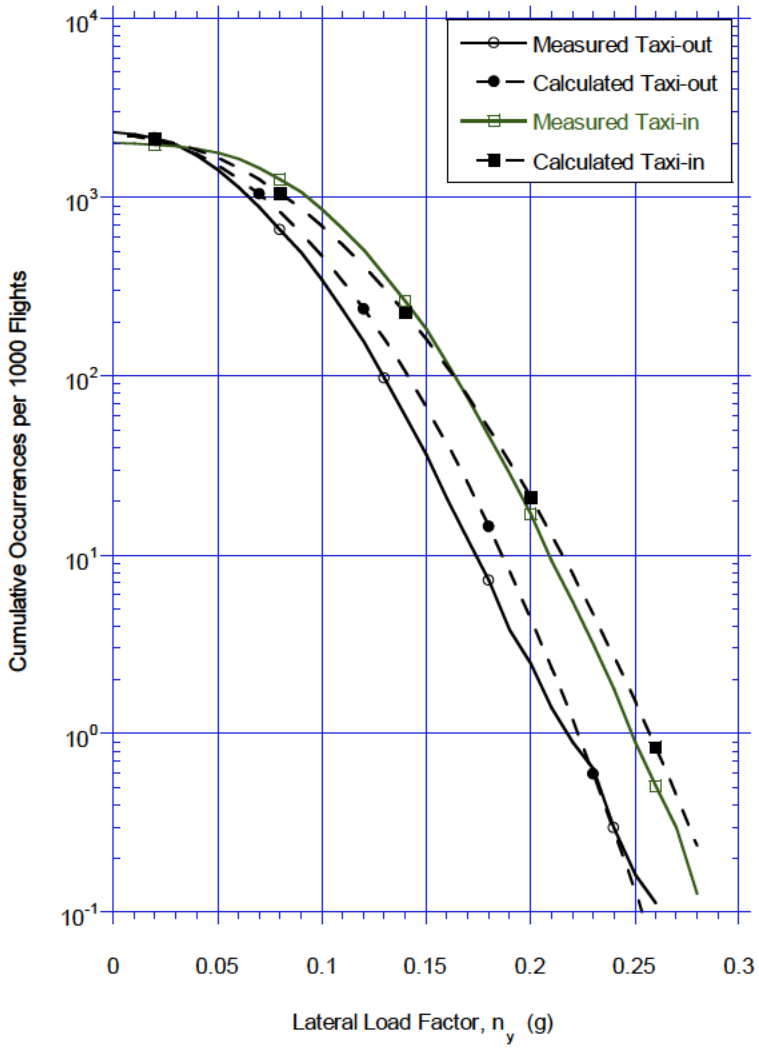

FIGURE D- 24. Comparison of measured and calculated cumulative frequency of ground turning, lateral load factor during taxi-out and taxi-in, B-737-400.

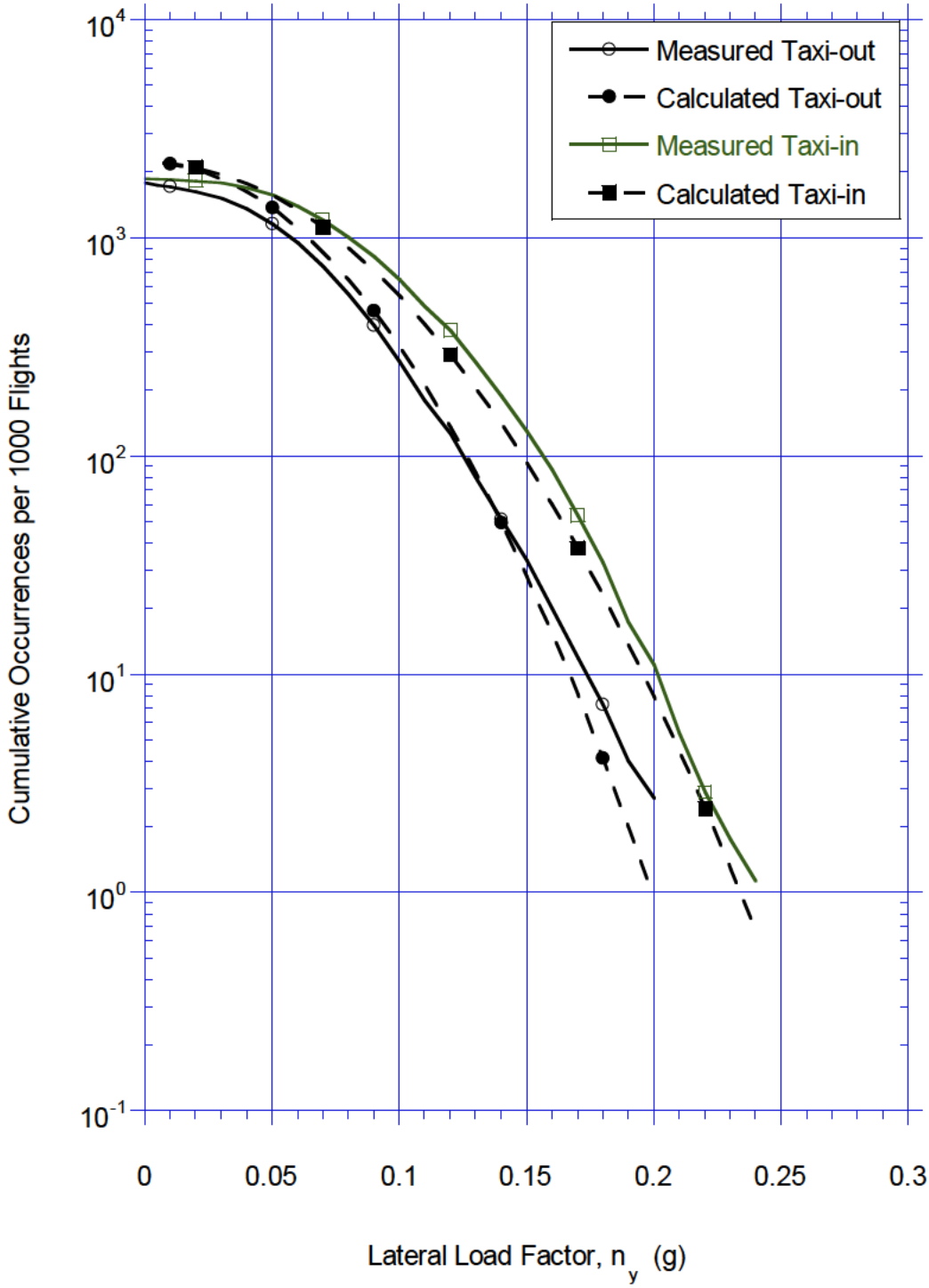

FIGURE D- 25. Comparison of measured and calculated cumulative frequency of ground turning, lateral load factor during taxi-out and taxi-in, MD-82/83.

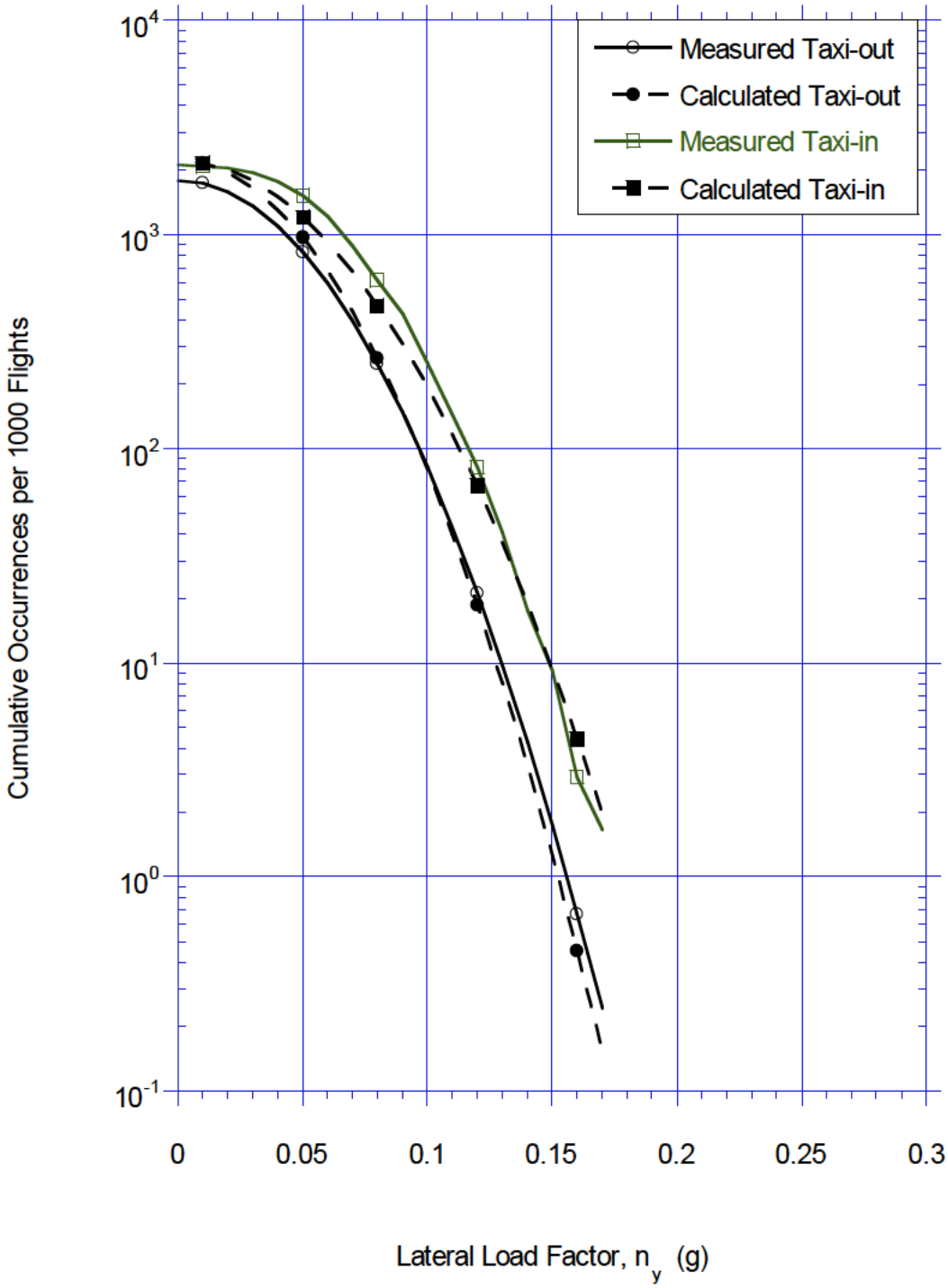

FIGURE D- 26. Comparison of measured and calculated cumulative frequency of ground turning, lateral load factor during taxi-out and taxi-in, B-767-200ER.

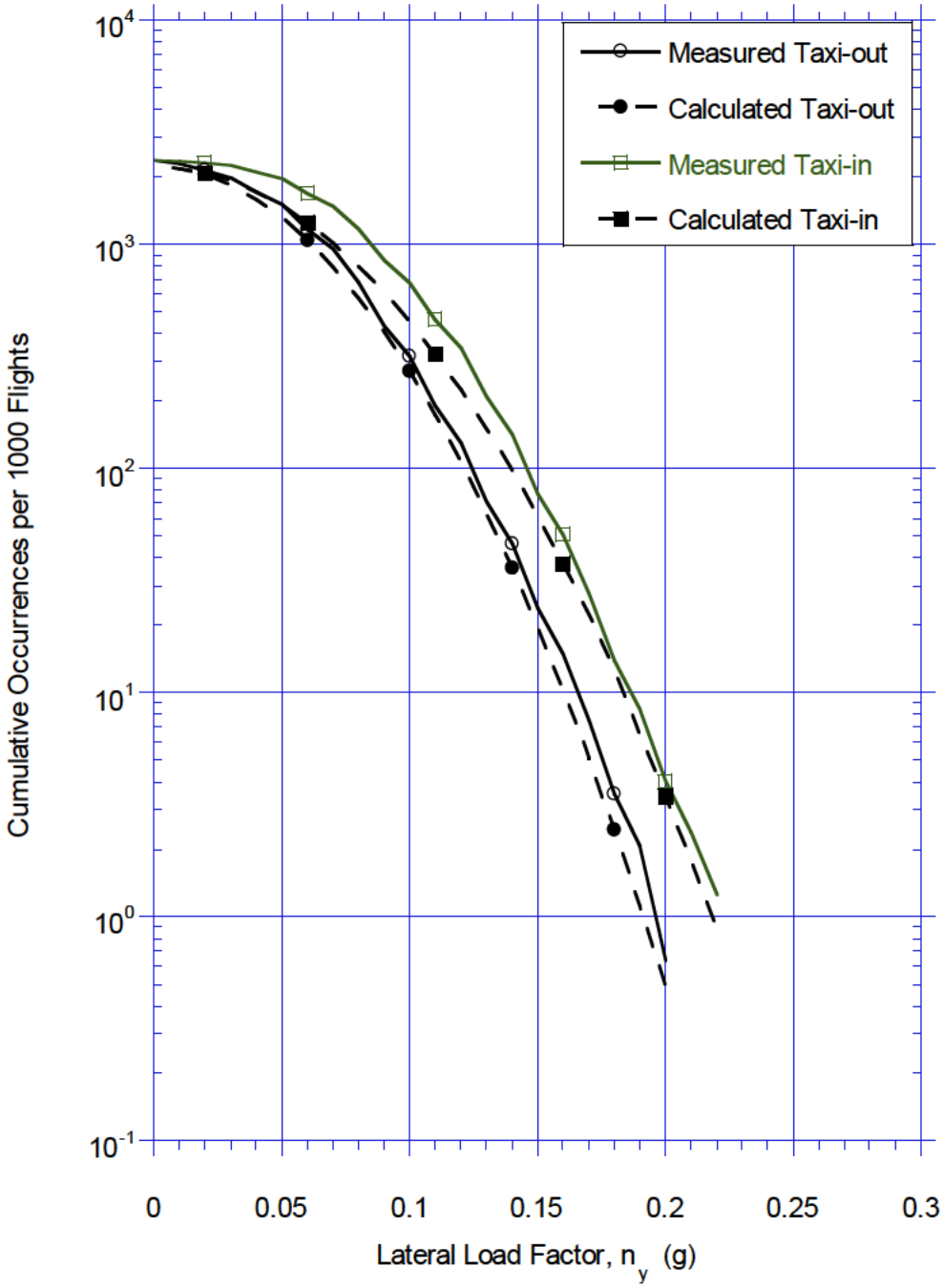

FIGURE D- 27. Comparison of measured and calculated cumulative frequency of ground turning, lateral load factor during taxi-out and taxi-in, A-320.

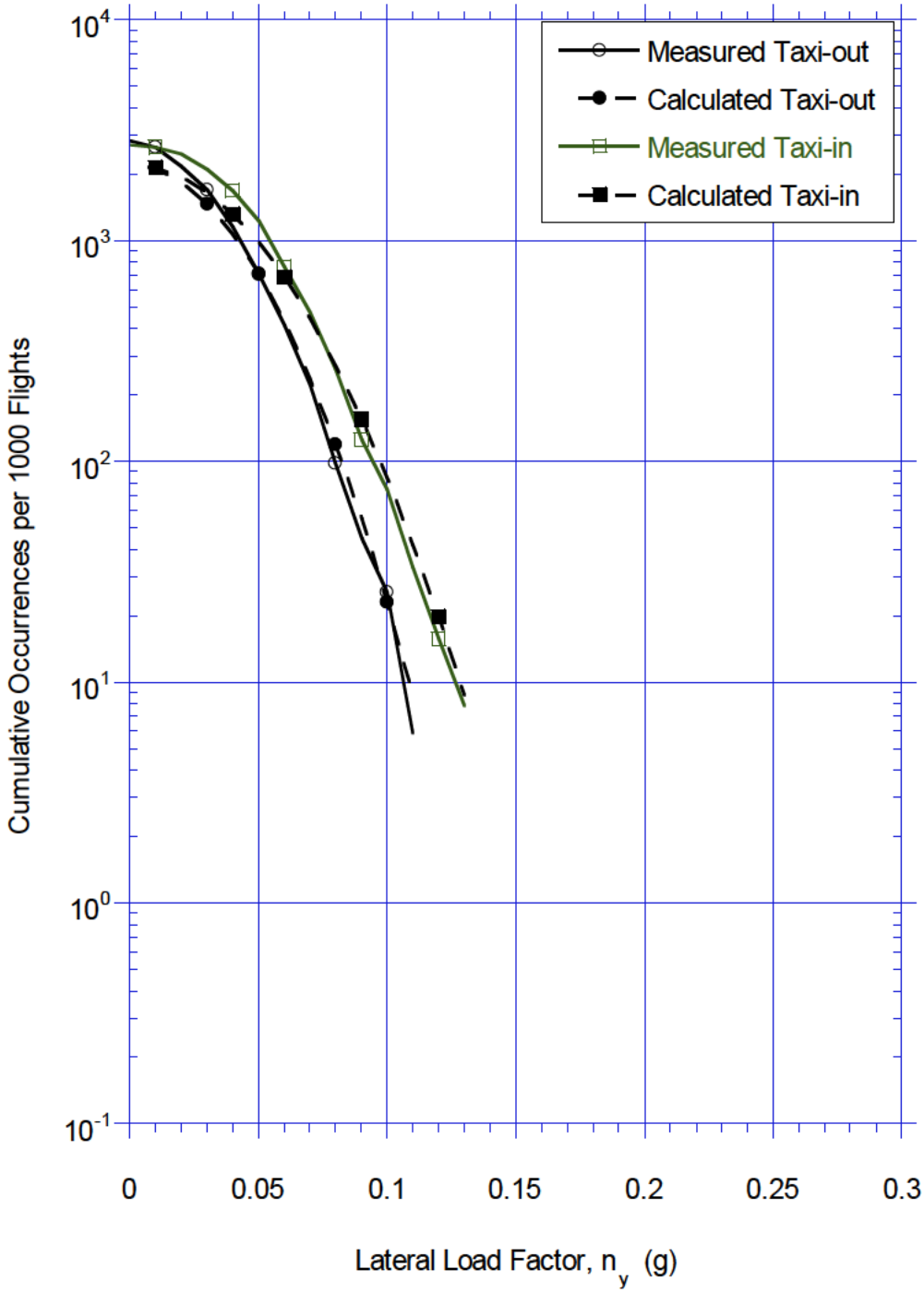

FIGURE D- 28. Comparison of measured and calculated cumulative frequency of ground turning, lateral load factor during taxi-out and taxi-in, B-747-400.

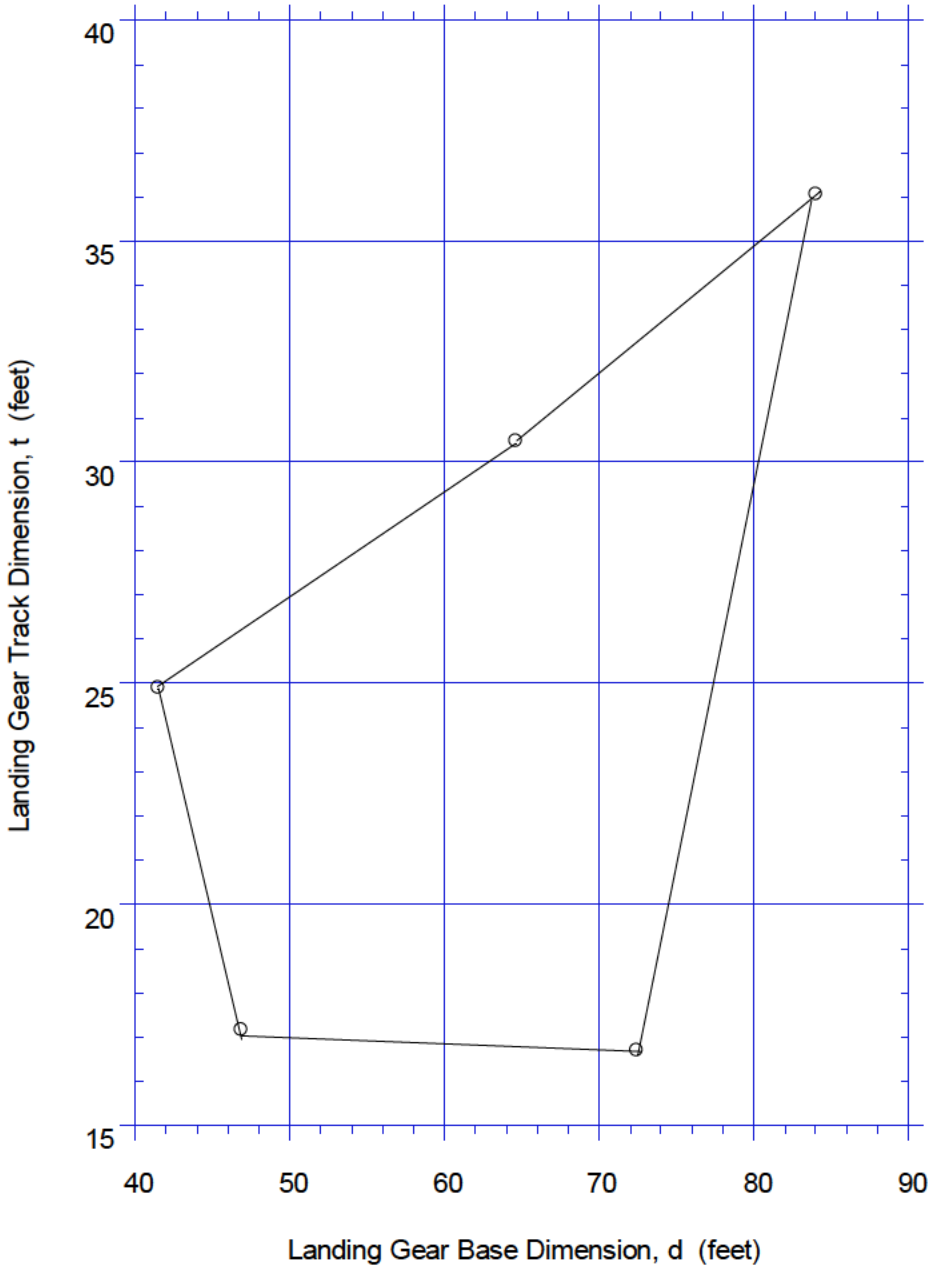

FIGURE D- 29. Landing gear dimensional envelope.

D.4 DEFINITION OF DESIGN CONDITION

D.4.1 Definition of design condition.

Not only can the approach presented be used to determine the expected ground turning acceleration spectrum for a specific aircraft; but it can also be used to define a static design condition for ground turning. At present an arbitrary value of 0.5 g is specified for the maximum required ground turning load condition. If it is agreed that an aircraft is operated in accordance with its perceived capability as determined by its landing gear dimensional arrangement then a design condition can

be specified for an aircraft based on its landing gear geometry. All that is necessary is to specify a maximum acceptable exceedance level of the design loading condition, such as once per lifetime for limit load. Equation D3 is used to determine the load factor level for a specific level of exceedances N.

$$n_y = \sqrt{\ln \frac{N}{N_0} \frac{1}{d^m t}} \qquad \text{(D3)}$$

Where:

The values of N_0, and m are as defined in Table D-II for taxi-out and taxi-in.

Establishment of an acceptable exceedance level of limit load is outside the scope of this study. Table D-III shows the respective cumulative frequency per 1000 flights of a 0.5 g lateral load factor turn for each of the aircrafts. The data show that the B-737-400 has the highest frequency of encountering a 0.5 g lateral load factor during ground turning. If this cumulative frequency is taken as establishing an acceptable design level then the lateral load factor expected for the same frequency for other aircrafts can be predicted. Figure 30 shows the lateral load factor levels for the five aircrafts in this study based on the cumulative frequency of the B-737-400 for a 0.5 g turn.

TABLE D- III. Comparison of cumulative frequencies of 0.5 g lateral load factor.

AIRCRAFT	LATERAL LOAD FACTOR	CUMULATIVE FREQUENCY, TAXI-OUT	CUMULATIVE FREQUENCY, TAXI-IN
B-737-400	0.5	4.00343E-14	4.78128E-10
MD-82/83	0.5	2.90091E-18	1.09566E-12
B-767-200ER	0.5	4.09287E-33	8.66253E-24
A-320	0.5	4.70488E-20	1.10148E-14
B-747-400	0.5	1.69683E-46	5.4205E-33

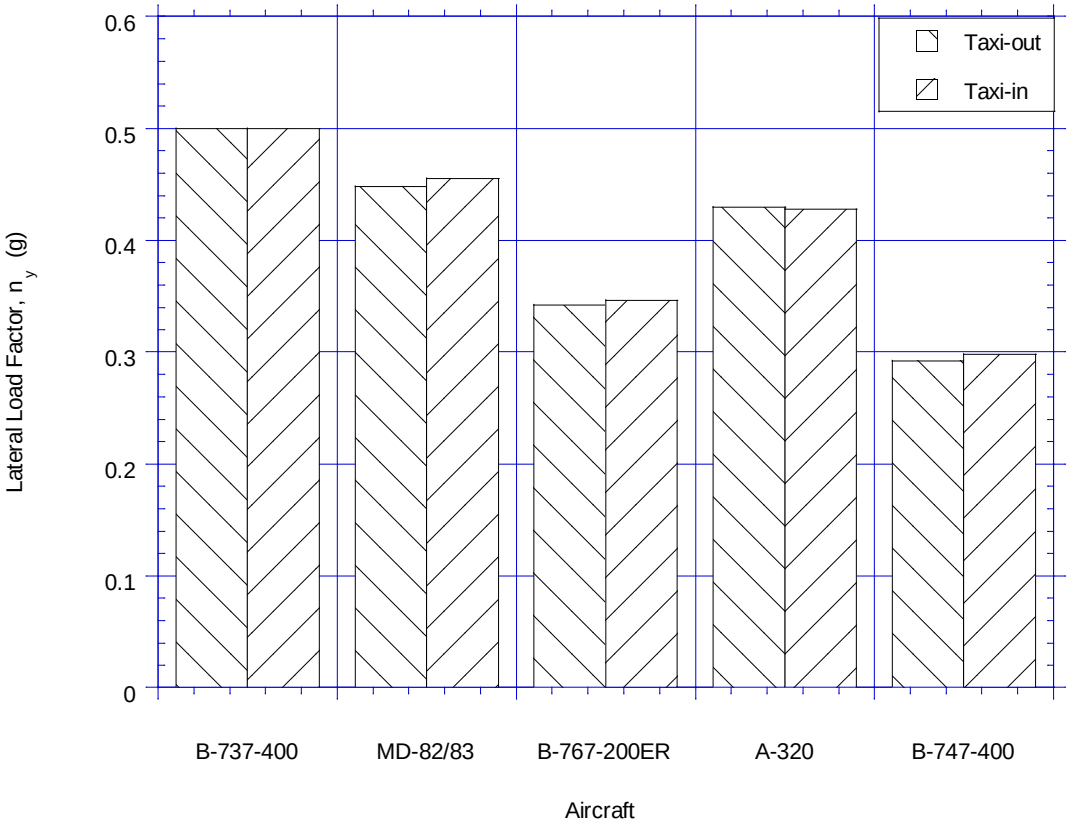

FIGURE D- 30. Comparison of equal probability lateral load factors during ground turning for five aircraft.

D.5 CONCLUSIONS

D.5.1 Conclusions.

The approach and the derived equation for mathematically predicting ground loads turning spectra are based on the average experiences of five quite different aircraft operated by different airlines at different airports. The mathematically determined ground turning load spectra will therefore never exactly duplicate the measured spectra. However, the approach presented does provide a very reasonable representation of the expected ground turning side load factors, as well as provide a better basis for predicting repeated side turning loads than has heretofore been available. It is always prudent to re-evaluate the approach as more data become available from additional aircraft and operators.

It appears that the maximum lateral load factor that can be expected during ground turning operations is influenced by the size of the aircraft in terms of the landing gear base and track dimensions. Thus, the static design requirement of a fixed lateral load factor of 0.5 g for ground turning operations regardless of aircraft size will penalize the larger aircraft. A design lateral load factor based on a fixed level of occurrences or probability would provide a more consistent strength level.

APPENDIX E

SAMPLE SIZE CONSIDERATIONS

E.1 SCOPE

E.1.1 Scope.

Aircraft usage and service loads statistics cover a large number of different parameters each of which contributes to defining external repeated loading conditions. The statistics are usually shown as a frequency or probability of exceeding predetermined levels of the parameter of interest. These statistics are derived from peak occurrence measured over a period of time or number of flights. The period of time or number of flights used in the derivation of the statistics represents a sample of the overall environment. The larger the sample, the more likely the sample will represent the true environment. The question becomes how large should the sample be. This question is particularly pertinent to parameters that are not limited in peak magnitude or are not under control of the pilot. For instance control surface deflection may include a rare maximum deflection, but we know a priory what this maximum deflection is. In case of maneuver load factors, the pilot will stay within the prescribed operational limits. However, gust load factor measurements reflect responses to a stochastic (random) input without a specific cutoff and may statistically result in rare but large excursions when considered over a long period of time. The stochastic or random variations in the gust load factor measurements involving effects due to season and geographical location exert a limitation on the detectability of a trend from a finite record.

There is no a priory or post priory knowledge as to the frequency of a rare event. If such an event were to occur in a small sample it is erroneous to take this occurrence as the sign of a long-term trend. For instance one occurrence of a specific load factor in a 1000 hours sample would be equal to 60 such occurrences in a 60,000 hour lifetime. If continued sampling to 60,000 hours resulted in no additional occurrences of the specified load factor the occurrence rate for the load factor would be once per 60,000 hour life time.

E.2 APPLICABLE DOCUMENTS

E.2.1 Other Government documents, drawings, and publications.

The following other Government documents, drawings, and publications form a part of this document to the extent specified herein.

E1. Coupry, G.,"Distribution Statistique des Turbulences Atmospheriques Extremes," Office National d'Etudes et de Recherches Aerospatiales, T.P 1987-56.

E.3 DISCUSSION

E.3.1 Discussion.

An available B-737-400 database containing a total of 62,264 flights was used to study the effects on vertical load factor statistics as a function of sample size. Figures E-1 and E-2 show the cumulative frequencies of vertical load factor by sample size based on the number of aircraft flights contained within the sample. For each figure the sample sizes contain sets of randomly selected

flight from the available B-737-400 data base. While each fixed sample size contains the same number of flights the randomly selected flights are of different flight duration. Hence, the flight times associated with the fixed number of flights are not necessarily identical for the two runs presented on Figures E-1 and E-2.

The data underlying these plots were transformed to show the cumulative frequency of fixed load factor levels as a function of sample hours. Figures E-3 and E-4 present the results for the negative and positive load factors for run number 1. A straight line indicates that the calculated cumulative frequency of a load factor level did not change as a function of sample size.

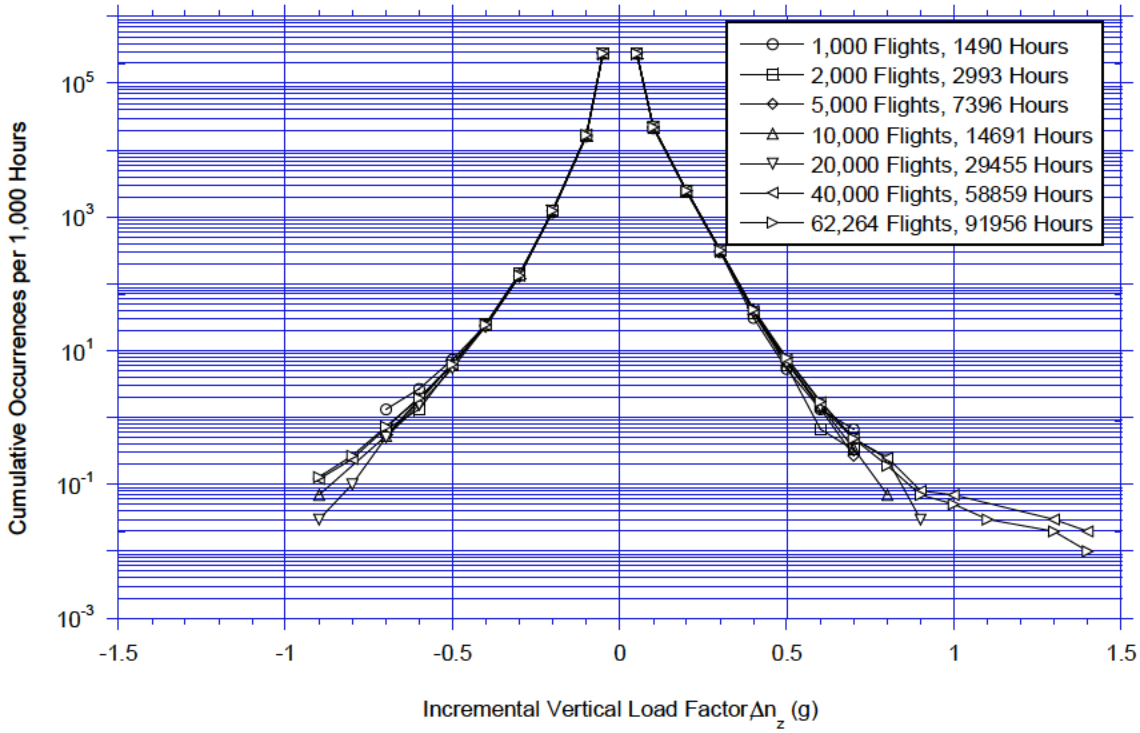

FIGURE E- 1. Cumulative frequency of incremental vertical load factor, various sample sizes, B-737-400, run 1.

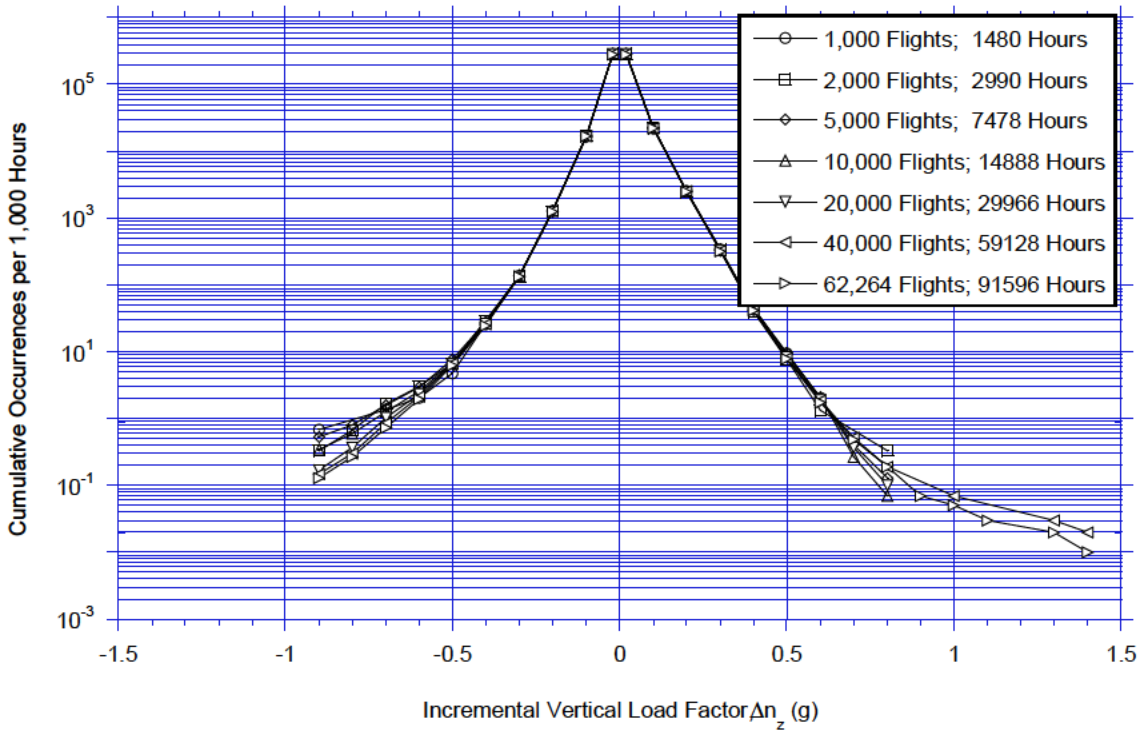

FIGURE E- 2. Cumulative frequency of incremental vertical load factor, various sample sizes, B-737-400, run 2.

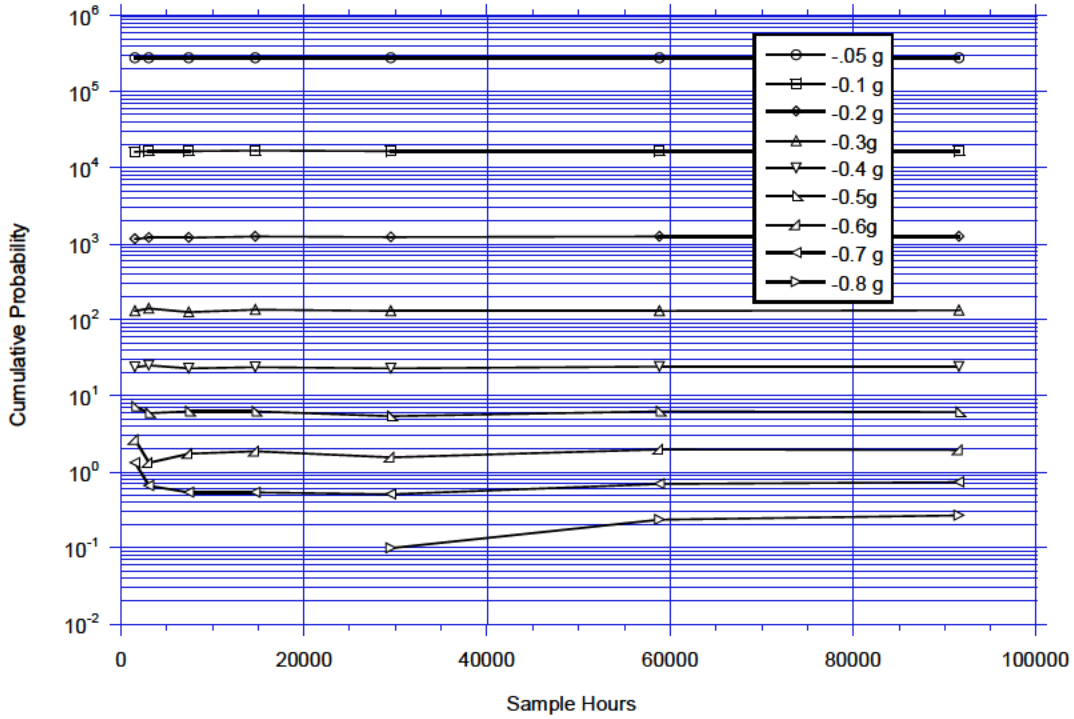

FIGURE E- 3. Cumulative probability of negative incremental load factor vs. sample hours, B-737-400, run 1.

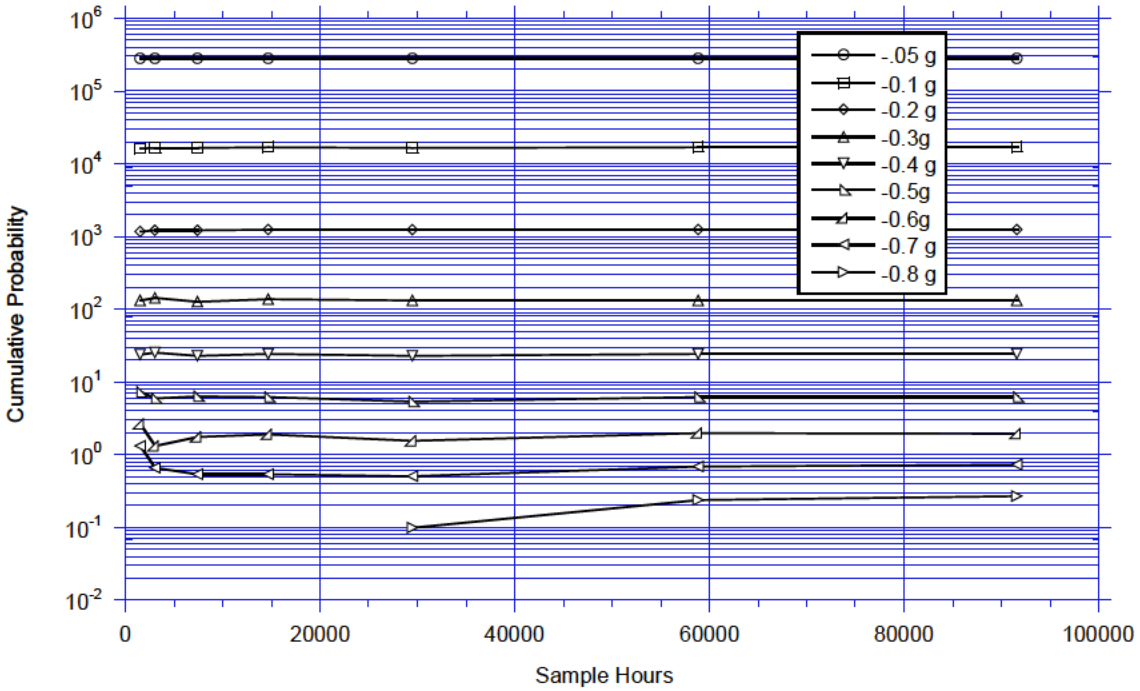

FIGURE E- 4. Cumulative probability of positive incremental load factor vs. sample hours, B-737-400, run 1.

From these figures it can be deduced that for load factor up to 0.6 g a 10,000 hour sample would be acceptable to indicate long-term trends. For load factor levels above 0.6 g the evidence is not as conclusive. In fact, the rare load factors at 1.3 g and 1.4 g would not be encountered until a sample of almost 60,000 hours was collected. Figures E-5 and E-6 show the associated cumulative frequency of fixed load factor levels as a function of sample hours for run number 2. In this case a 10,000 hour sample would again appear to be an acceptable sample to obtain repeatability for load factor levels up to 0.6 g. For levels above 0.6 g it would require a sample of approximately 60,000 hours to obtain a repeatable frequency or even to obtain a high positive load factor measurement.

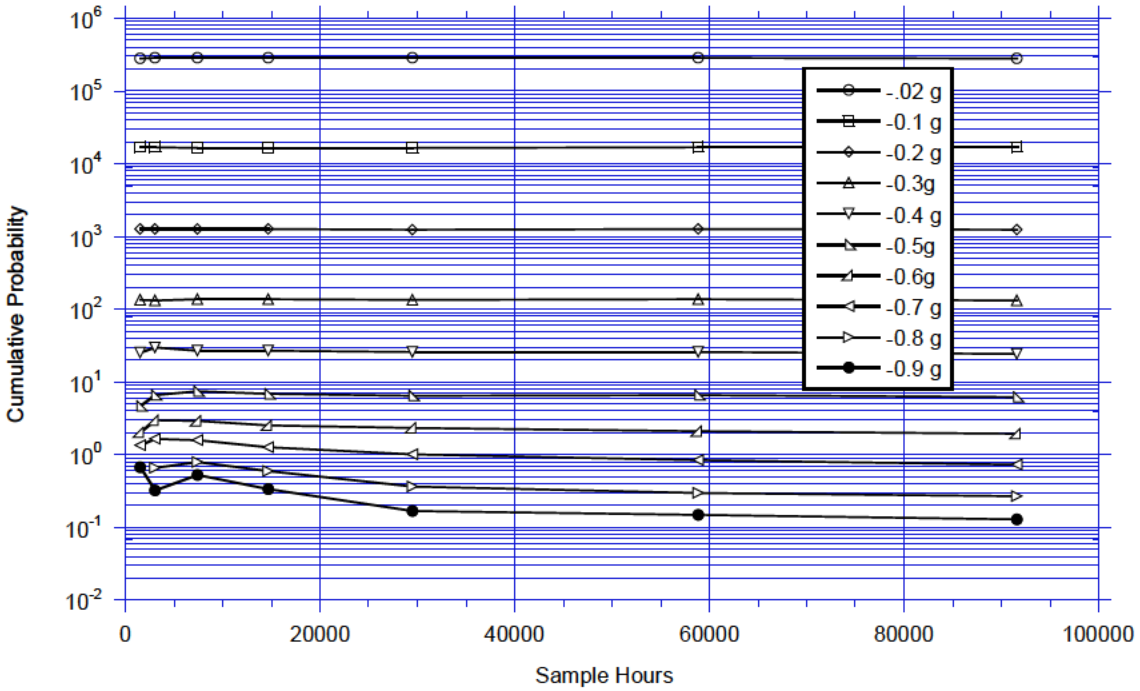

FIGURE E- 5. Cumulative probability of negative incremental load factor vs. sample hours, B-737-400, run 2.

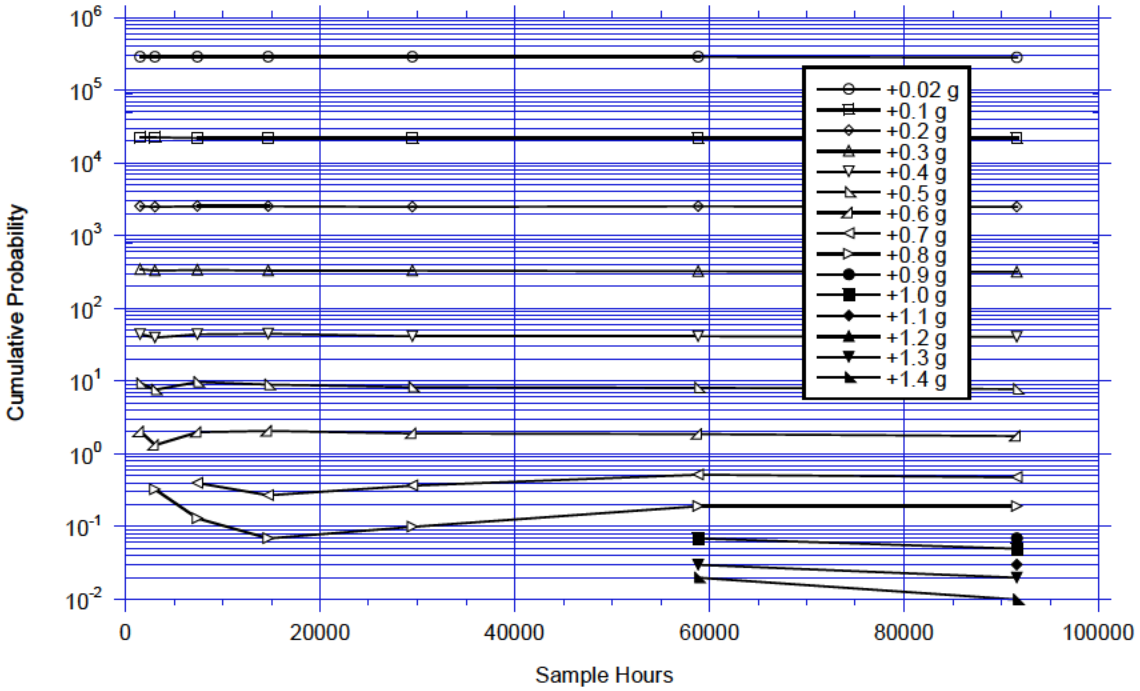

FIGURE E- 6. Cumulative probability of positive incremental load factor vs. sample hours, B-737-400, run 2.

Figure E-7 shows the maximum positive and negative load factors measured as a function of sample size for a number of different aircrafts types, from regional jet to jumbo jet. As can be seen the general trend is the measurement of higher (rarer) load factors as sampling time increases. While the trend is clear there is considerable scatter. This is likely due to differences in aircraft type that have large differences in the cruise segment duration of the flights. The result is that for the large aircrafts flying for extended durations at high altitudes with lower turbulence levels lower load factors would result. A similar plot based on load factor experience by altitude would remove this artifact.

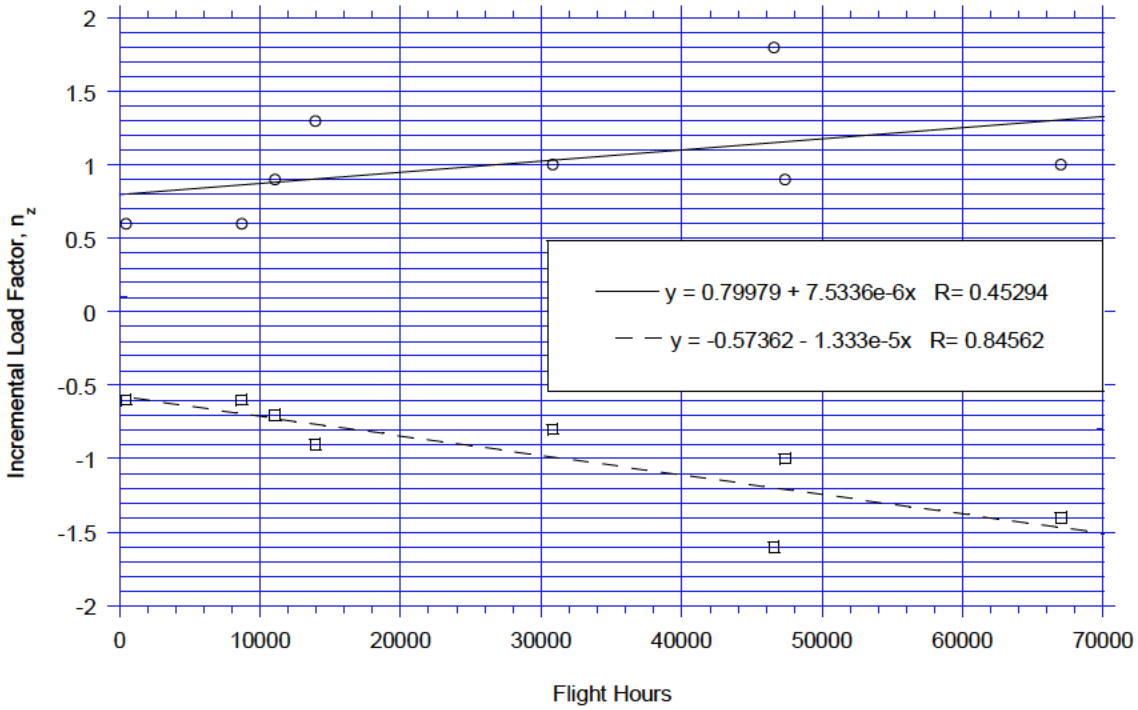

FIGURE E- 7. Maximum measured load factor vs. sample size.

From the above examples it is clear that if a small random sample of less than 10,000 hours is used, then it is likely that very few of the rare events will be included in the sample. In other words, a sample size of 10,000 hours or less decreases the probability that a rare event will even be detected for use in any trend analysis.

Sample size criteria are based on certain sample statistics such as the mean, variance, and confidence intervals. Because the true distribution of the counts at the higher load factors based on samples of less than 10,000 hours is likely to be unknown, the sample statistics of the mean, variance, and confidence limits cannot be employed to determine the desired sample size. It may be necessary to base a decision on sample size on non-statistical empirical criteria. If plausible assumptions about the unknown distribution of rare events can be made based on other sources of information outside the sample data itself then some estimate of the effect of reduced sample sizes can possibly be made.

Atmospheric turbulence as experienced over long periods is described as consisting of two general distribution types. One type consisting of light to moderate turbulence termed "non-storm"

turbulence and one consisting of more severe turbulence termed "storm" turbulence. In mathematical form this distribution in terms of cumulative probabilities is described by the following formula.

$$\frac{N_y}{N_0} = P_1 e^{\frac{y/\bar{A}}{b_1}} + P_2 e^{\frac{y/\bar{A}}{b_2}} \qquad \text{(E1)}$$

The parameters b_1 and b_2 represent the slope of the two distributions and are an indication of the turbulence severity. The distinction of non-storm and storm turbulence is misleading because the curves represent all types of turbulence from light to severe regardless of its causes. But, the "storm turbulence" distribution is reflective of the less frequent occurrences that might be encountered in larger samples but not detected in smaller samples. Equation E1 can be transformed into terms of cumulative occurrences as follows:

$$N_y = N_1 e^{\frac{x}{b_1}} + N_2 e^{\frac{x}{b_2}} \qquad \text{(E2)}$$

From Figures E-1 and E-2, it can be observed that the slope of the curves changes more rapidly above approximately 0.9 g. This acceleration level can be defined as the separation between non-storm" and "storm" turbulence distributions. Or more precisely between normal and extreme or rare gust occurrences. Distribution Statistique des Turbulences Atmospheriques Extremes (see Reference E1) presents a study of the statistical distribution of severe atmospheric turbulence. The study showed that based on measurements over nearly one million flight hours the slope of high intensity turbulence as indicated by the b_2 parameter was amazingly constant for the aircrafts in the study. This means that if plausible assumptions about the constancy of the b_2 parameter can be made based on support from sources of information outside the sample data itself then some estimate of the total distribution based on the distribution from a reduced sample size can possibly be made.

Figure E-8 shows the distribution of severe turbulence response for three aircrafts. As can be seen, the slopes for both positive and negative load factors due to severe turbulence are quite similar with an average of -2.717 for both the negative side and for the positive side. Using this value as representative value for severe turbulence intensity, a composite curve that includes both normal and severe turbulence can be estimated through Equation E1 using the normal turbulence distribution obtained from limited flight hours.

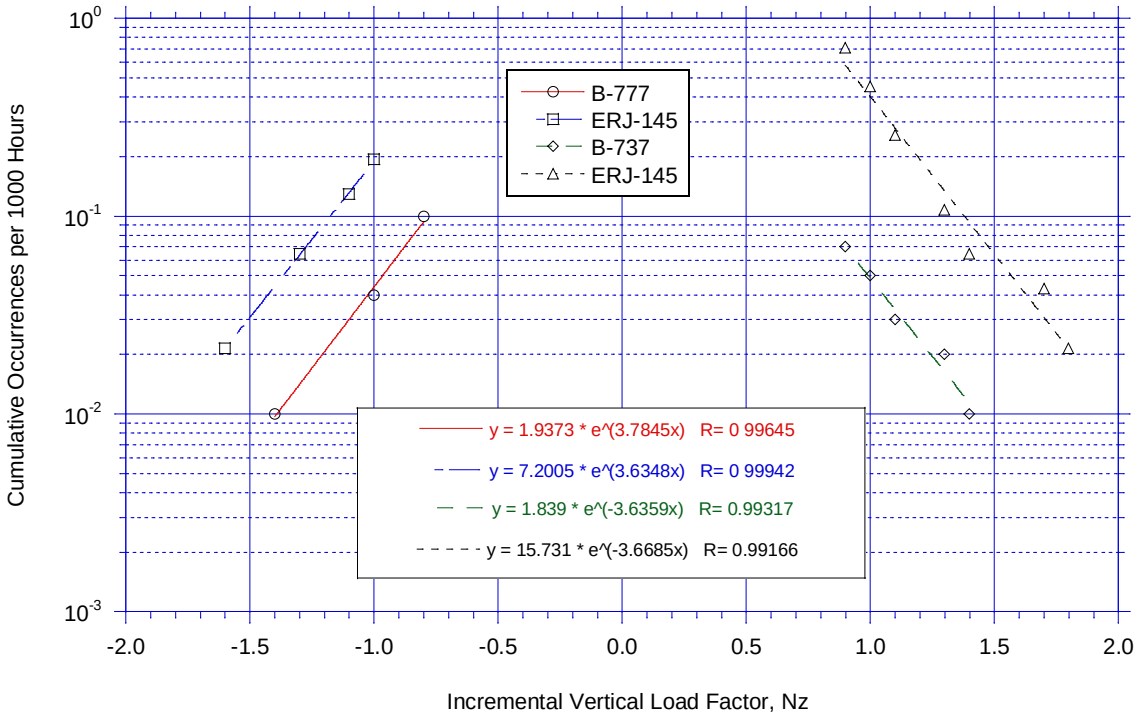

FIGURE E- 8. Severe load factor intensity slopes.

Using the 7,396 hour sample as the baseline, Figures E-9 and E-10 present the estimated total negative and positive load factor exceedance frequencies respectively. For comparison the figures also show the measured exceedance frequencies for the 91,596 hour sample. The comparison is quite acceptable and suggests that the statistics of rare load factor events in the form of the slope parameter "b" as derived from large databases of other aircraft may be used to augment the load factor statistics of other aircraft that are based on more limited flight hours.

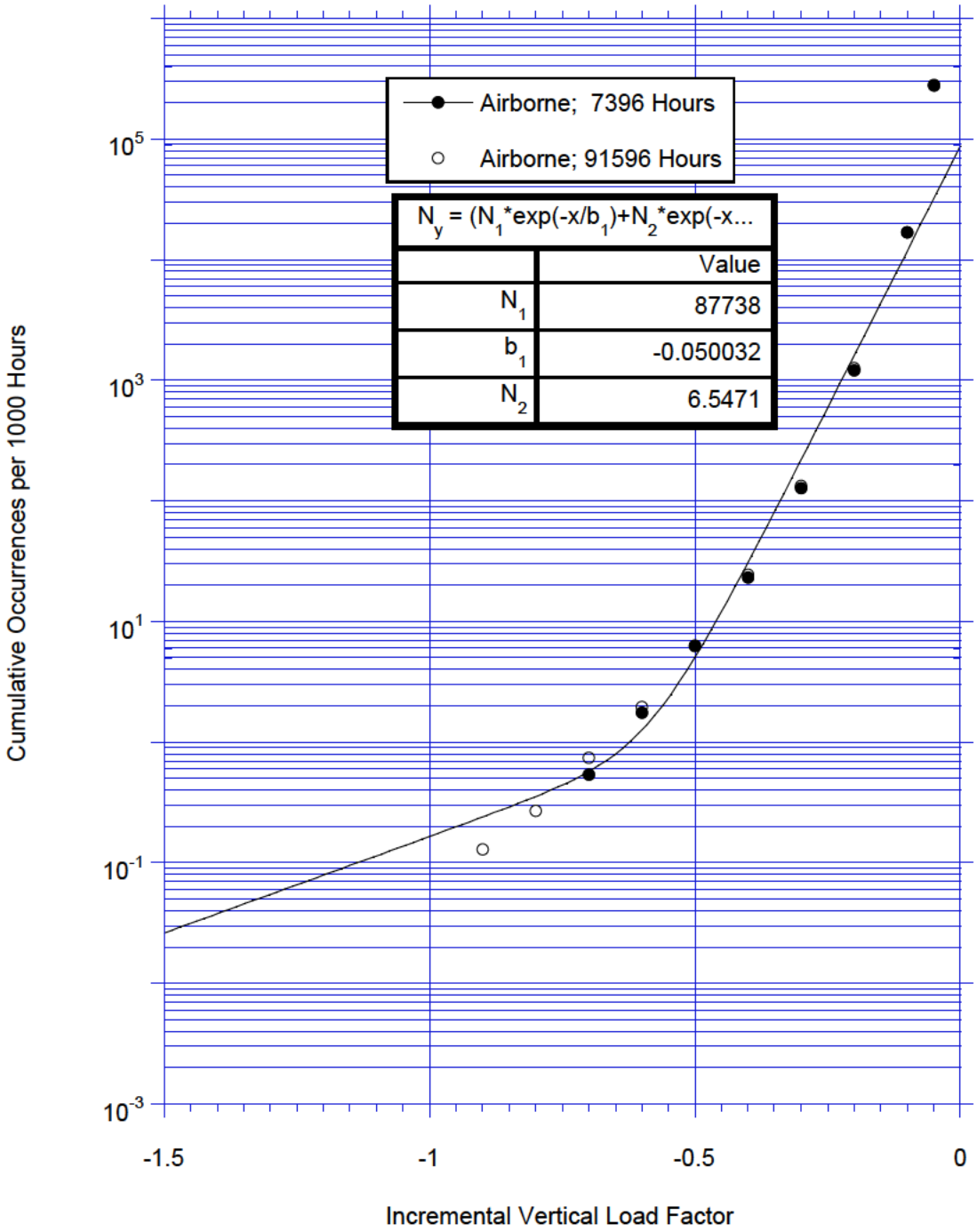

FIGURE E- 9. Cumulative frequency of incremental negative vertical load factor, B-737-400, b2 =0.2717.

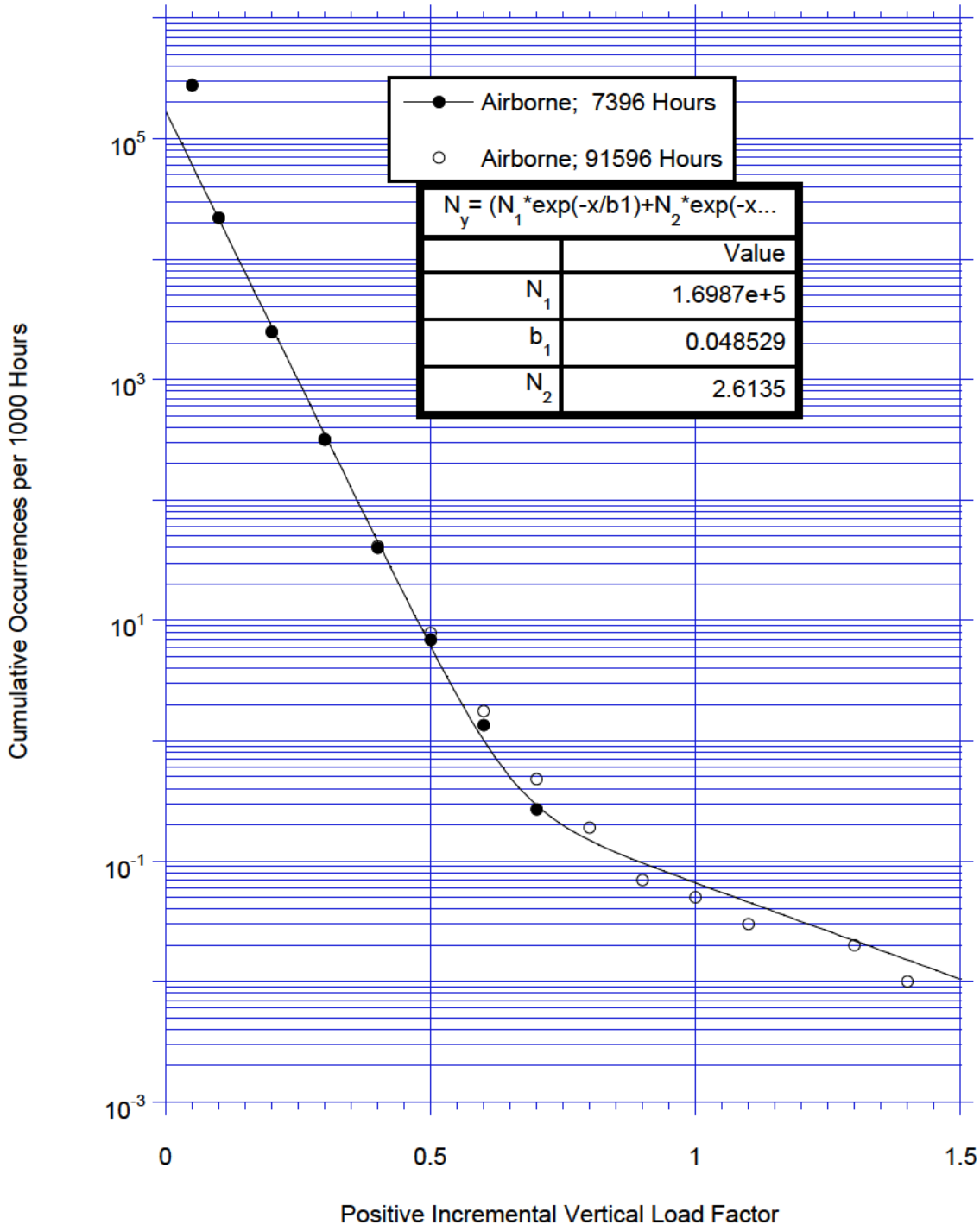

FIGURE E- 10. Cumulative frequency of incremental positive vertical load factor, B-737-400, b2 =0.2717.

E.4 CONCLUSIONS

E.4.1 Conclusions.

While the scope of this study was limited, it showed that a large database on the order of tens of thousands of flights would be needed to establish the statistics of rare load factor events with any degree of confidence. It also showed that if a rare event occurred within a small data base, the normalized occurrence statistic per unit time could be unnecessarily conservative. At the same time the comparison of the predicted rare load factor events through the use a slope parameter "b" as derived from large databases of other aircraft suggests that this parameter may be used to augment the statistics of other aircraft that are based on more limited flight hours to estimate rare load factor events.

The present study used the total (maneuvers and gusts) measured load factor occurrences. Further research should investigate the feasibility of this approach to gusts and maneuvers separately as a function of altitude or flight phase.

APPENDIX F

CALCULATION OF SPECTRUM DISPERSION

F.1 SCOPE

F.1.1 Scope.

The cumulative frequency or probability spectra presented in subsequent volumes of this handbook represent the average experience of a fleet of aircraft over a period of time, distance or number of flights. For design durability, 3.2.14.6 of the DoD Joint Service Specification Guide (JSSG) 2006, Aircraft Structures, (see Reference F1) requires definition of a severe utilization spectrum representative of 90 percent of the expected spectra.

It is assumed that aircraft load parameters, such as load factor or gust velocity represent random variable phenomena. These random values are grouped in distinct class intervals and tabulated to derive the frequency of occurrence or probability of the load parameter within the established class intervals. This provides a frequency distribution of the load parameter as obtained from recorded data. Cumulative frequencies are obtained by summing the frequencies within the class intervals starting at the highest derived load parameter interval. This provides the distribution of frequencies that a given load parameter is encountered or exceeded. Cumulative frequency percentages or probabilities are obtained by dividing the cumulative frequencies by the combined sum total frequency of all class intervals.

Statistical confidence limits can be established to describe the uncertainty associated with the sample. Thus, confidence limits indicate the reliability of the sample estimate. The likelihood that the load parameter sample will contain a specific load parameter occurrences is determined by the confidence level or confidence coefficient. For durability design purposes, the upper limit of the mean spectrum at 90 percent confidence limit could be taken as the normative spectrum for 90 percent of the fleet.

F.2 APPLICABLE DOCUMENTS

F.2.1 Other Government documents, drawings, and publications.

The following other Government documents, drawings, and publications form a part of this document to the extent specified herein.

F1. Department of Defense (DoD) Joint Service Specification Guide (JSSG)-2006, Aircraft Structures.

F2. Wilson, E. B. Probable inference, the law of succession, and statistical inference. *Journal of the American Statistical Association* 22: 209-212, 1927.

F3. Agresti, A., and Coull, B. Approximate is better than 'exact' for interval estimation of binomial proportions. *The American Statistician* 52: 119-126, 1998.

F4. Brown, L. D., Cai, T. T., and DasGupta, A. Interval Estimation for a Binomial Proportion. *Statistical Science* 16(2): 101-117, 2001.

F.3 PROPORTION CONFIDENCE LIMITS

F.3.1 Proportion confidence limits.

The cumulative probability distribution allows us to work with population probabilities rather than population means and standard deviations. If a given load parameter intensity is reached or exceeded n times in N load parameter measurements the sample probability p= n/N can be used to estimate the true probability within selected confidence limits, provided that the frequencies in the record are reasonable reliable. For longer records from similar flights, the relative number of occurrences of a specific load parameter magnitude in a series of measurements is relatively constant. Nevertheless, random differences in the frequency counts may occur if measurements were obtained over much longer durations. Figure F-1 depicts how the cumulative occurrences at a given mean occurrence level might be distributed at a given magnitude. Because the numbers of occurrences is much greater at the lower magnitudes, i.e. a larger sample size, the variation about the mean number of occurrences is narrower than at the higher magnitudes where fewer occurrences have been measured.

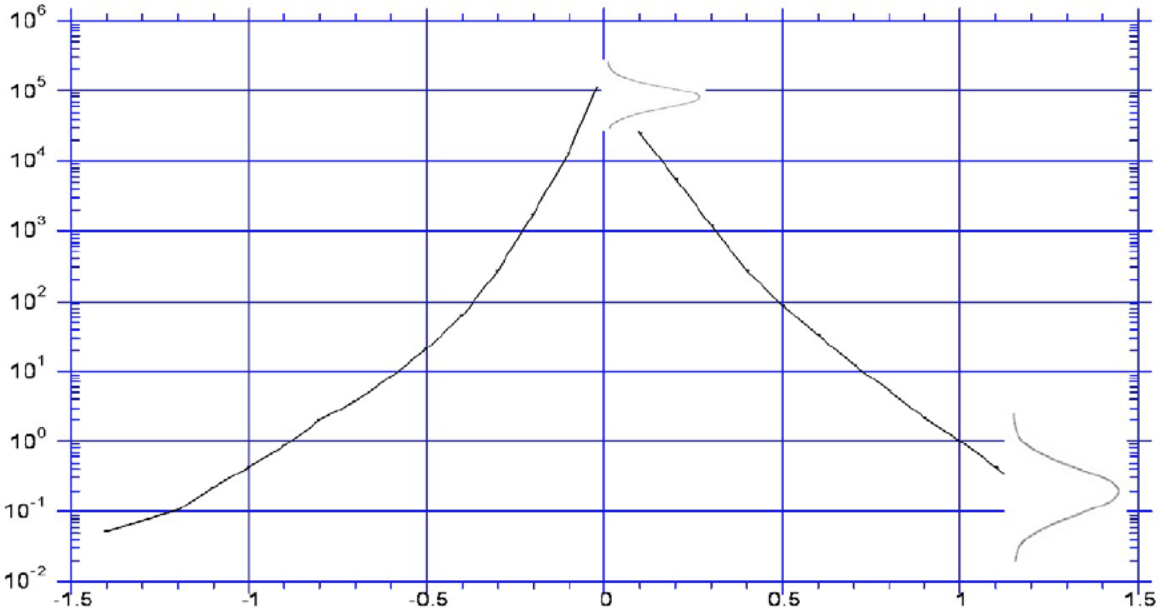

FIGURE F- 1. Depiction of cumulative occurrences distribution about the mean cumulative occurrences.

In the case of a cumulative frequency or probability there are only two possibilities; a given gust intensity is reached or exceeded or it is not. In probability parlance this equates to a number of successes (or failures) in a given number of independent trials. In that case the binomial distribution can be used whose mean and standard deviation are:

$$\mu = N\ p \tag{F1}$$

$$\sigma = \sqrt{N\ p(1-p)} \tag{F2}$$

F.3.2 Normal distribution approximation.
The simplest and most commonly used formula for a binomial confidence interval relies on approximating the binomial distribution with a normal distribution. This approximation is justified by the central limit theorem and greatly simplifies the calculation for confidence limits. The upper and lower confidence limits can then be defined as:

$$Ul = p + z_{\alpha/2}\sqrt{\frac{p(1-p)}{N}} \tag{F3}$$

$$Ll = p - z_{\alpha/2}\sqrt{\frac{p(1-p)}{N}} \tag{F4}$$

where p is the proportion estimated from the statistical sample, and $z_{\alpha/2}$ is the standard normal variable value related to the percentile of a standard normal distribution for two-sided confidence intervals, and N is the sample size.

In practice it is most common to evaluate the confidence limits at 90, 95, and 99 percent. For a two-sided 90 percent confidence interval this means that 90 percent of the population will be expected to fall between the two limits with 5 percent below the lower limit and 5 percent above the upper limit.

In the case of statistical loads parameters for design criteria and durability and damage tolerance assessment purposes, the lower confidence limit is not particularly relevant. For such purposes it is more important to estimate the higher load statistics than the low ones. Thus, for our purposes it is more relevant to determine the upper limit. In that case a 90 percent confidence limit would indicate that 90 percent of the population is less than the upper limit with 10 percent above the upper limit and the normal variable value would be indicated by z_α. The one-sided upper confidence limit would be defined as:

$$Ul = p + z_{\alpha}\sqrt{\frac{p(1-p)}{N}} \tag{F5}$$

Table F-I shows the $z_{\alpha/2}$ and z_α variate values for two-sided and one-sided confidence intervals.

TABLE F- I. Normal distribution variate values.

Confidence Limit (%)	$Z_{\alpha/2}$	z_α
70	0.85	0.53
80	1.28	0.85
90	1.65	1.28
95	1.96	1.65
99	2.57	2.33

The normal curve approximation for the binomial distribution starts to fail when the sample probabilities approach 1 or 0. Thus as the probability approaches 1 or 0 at the beginning or end of the cumulative probability curve the calculated confidence limits become less reliable. A general rule of thumb is that the normal distribution approximation works well for cases where Np representative of the tail end and N(1-p) representative of the top end of the probability curve are both greater than 5. It is of course precisely at the tail end of the gust probability curve where we encounter frequencies less than 5 that the normal distribution approximation for the binomial distribution breaks down. Fortunately, a method developed by Wilson, Probable inference, the law of succession, and statistical inference (see Reference F2) and recommended by Agresti and Coulli, Approximate is better than 'exact' for interval estimation of binomial proportions (see Reference F3) and also by Brown, Cai, and DasGupta, Interval Estimation for a Binomial Proportion, (see Reference F4) provides a procedure that does not strongly depend on the value of N or p. The upper and lower limits using this procedure are shown below.

$$p_{i-twosided} = \frac{p_i + \frac{z^2_{\alpha/2}}{2N_T} \pm z_{\alpha/2}\sqrt{\frac{p_i(1-p_i)}{N_T} + \frac{z^2_{\alpha/2}}{4N_T^2}}}{1 + \frac{z^2_{\alpha/2}}{N_T}} \quad \text{(F6)}$$

For a one sided limit probability replace the normal distribution value $z_{\alpha/2}$ by z_{α}.

$$p_{i-onesided} = \frac{p_i + \frac{z^2_{\alpha}}{2N_T} + z_{\alpha}\sqrt{\frac{p_i(1-p_i)}{N_T} + \frac{z^2_{\alpha}}{4N_T^2}}}{1 + \frac{z^2_{\alpha}}{N_T}} \quad \text{(F7)}$$

The value of p_i at any load parameter level is derived by dividing the cumulative occurrences at i^{th} load parameter level by the load cumulative occurrences at the zero load parameter level.

$$p_i = \frac{N_i}{N_0} \quad \text{(F8)}$$

The probabilities p_i for the specific tolerance level can be reverted back to the cumulative occurrences by multiplication of p_i by the cumulative occurrences at the zero parameter level.

$$N_i = p_i \, x \, N_0 \quad \text{(F9)}$$

The value of N_T represents the total number of measured occurrences in the sample. This value can be derived from the sample size information presented on the plots.

Let N_0 equal the cumulative frequency at the lowest n_z level (usually 0.02g). This frequency is normally defined as the cumulative occurrences per 1,000 hours, per 1,000 flights, etc.

Calculate the N_0 for a single hour or flight by dividing cumulative occurrences at the lowest n_z level by the normalizing factor such as per 1,000 hours, per 1,000 flights.

Multiply the resulting cumulative occurrences per single hour, single nautical mile, or single flight, by the number of total hours, flights, or nautical miles in the sample. Add 1 occurrence to obtain the total number N_T of measured occurrences.

To obtain a one-sided cumulative frequency N_i where the frequency is defined in terms of cumulative occurrences per x number of hours, nautical miles, or flights can also be obtained as follows.

$$N_{i-onesided} = \frac{N_i + \frac{z_\alpha^2 N_0}{2N_T} + z_\alpha \sqrt{\frac{N_0 N_i - N_i^2}{N_T} + \frac{N_0^2 z_\alpha^2}{4N_T^2}}}{1 + \frac{z_\alpha^2}{N_T}} \qquad \text{(F10)}$$

F.4 EXAMPLE PROBLEM

F.4.1 Example problem.

Figure F-2 and Table F-II show the cumulative occurrences per 1,000 hours for load factor measured during flight.

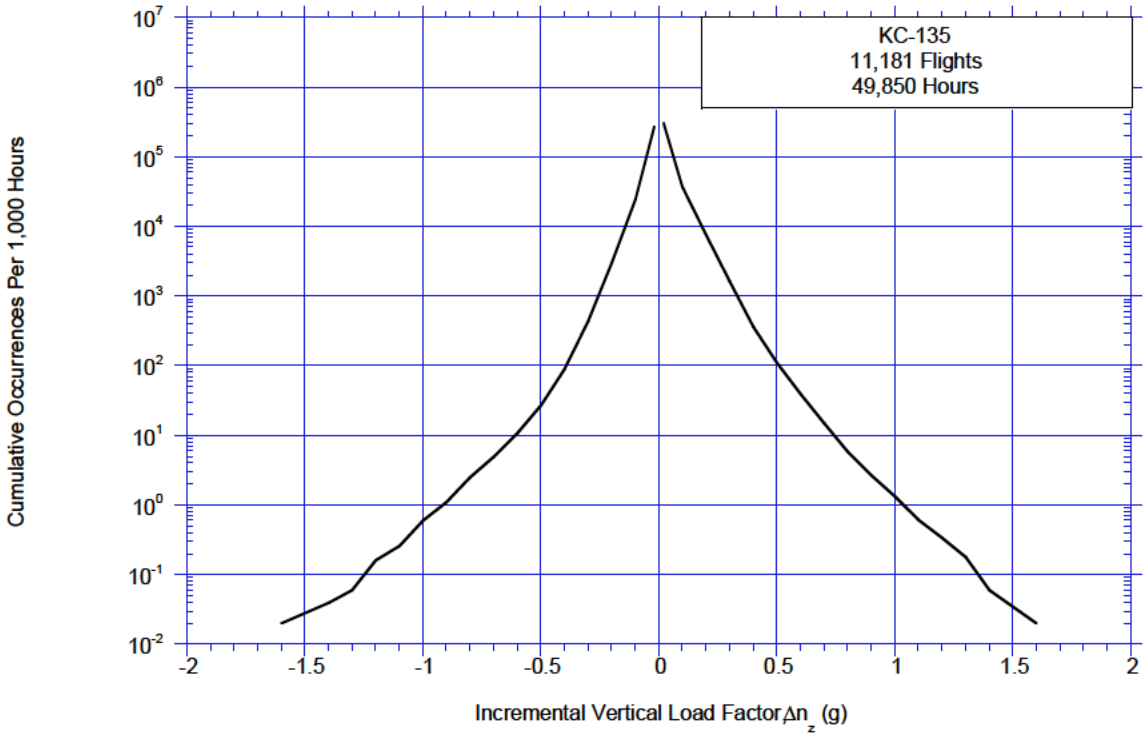

FIGURE F- 2. Cumulative occurrences per 1,000 hours of incremental vertical load factor.

TABLE F- II. Cumulative occurrences per 1,000 hours of incremental vertical load factor.

$-\Delta n_z$	Cumulative Occurrences per 1,000 Hours	$+\Delta n_z$	Cumulative Occurrences per 1,000 Hours
-0.02	2.7337e+05	0.02	3.0460e+05
-0.10	25106	0.10	37532
-0.20	3009.0	0.20	7702.1
-0.30	433.40	0.30	1636.4
-0.40	89.248	0.40	359.02
-0.50	27.202	0.50	108.27
-0.60	10.853	0.60	39.198
-0.70	4.9348	0.70	14.965
-0.80	2.5276	0.80	5.7774
-0.90	1.1033	0.90	2.6680
-1.00	0.60180	1.00	1.3240
-1.10	0.26080	1.10	0.62190
-1.20	0.16050	1.20	0.34100
-1.30	0.060180	1.30	0.18050
-1.40	0.040120	1.40	0.060180
-1.50		1.50	
-1.60	0.020060	1.60	0.020060

The total number of cumulative occurrences per 1,000 hours is N_0.

N_0 =304600 cumulative occurrences per 1,000 hours

The total number of counts in the database is N_T.

$$N_T = \frac{304600}{1000}49850 + 1 = 15{,}184{,}311\ occurrences$$

At Δn_z = 1.0 the cumulative frequency is 1.324 occurrences per 1,000 hours

For a one-sided limit at 90 percent, z_α = 1.28

Using Equation 10 the 90 percent one-sided cumulative occurrences are

$$N_{one-sided} = \frac{1.324 + \frac{1.28^2 x 304{,}600}{2x15{,}184{,}311} + 1.28\sqrt{\frac{304{,}600x1.324 - 1.324^2}{15{,}184{,}311} + \frac{304{,}600^2 x 1.28^2}{4x15{,}184{,}311^2}}}{1 + \frac{1.28^2}{15{,}184{,}311}} = 1.55$$

Thus the 90 percent cumulative occurrences at Δn_z =1.0 are 1.55 cumulative occurrences per 1,000 hours. Figure F-3 and Table F-III show the mean (50 percent) and 90 percent cumulative frequency data.

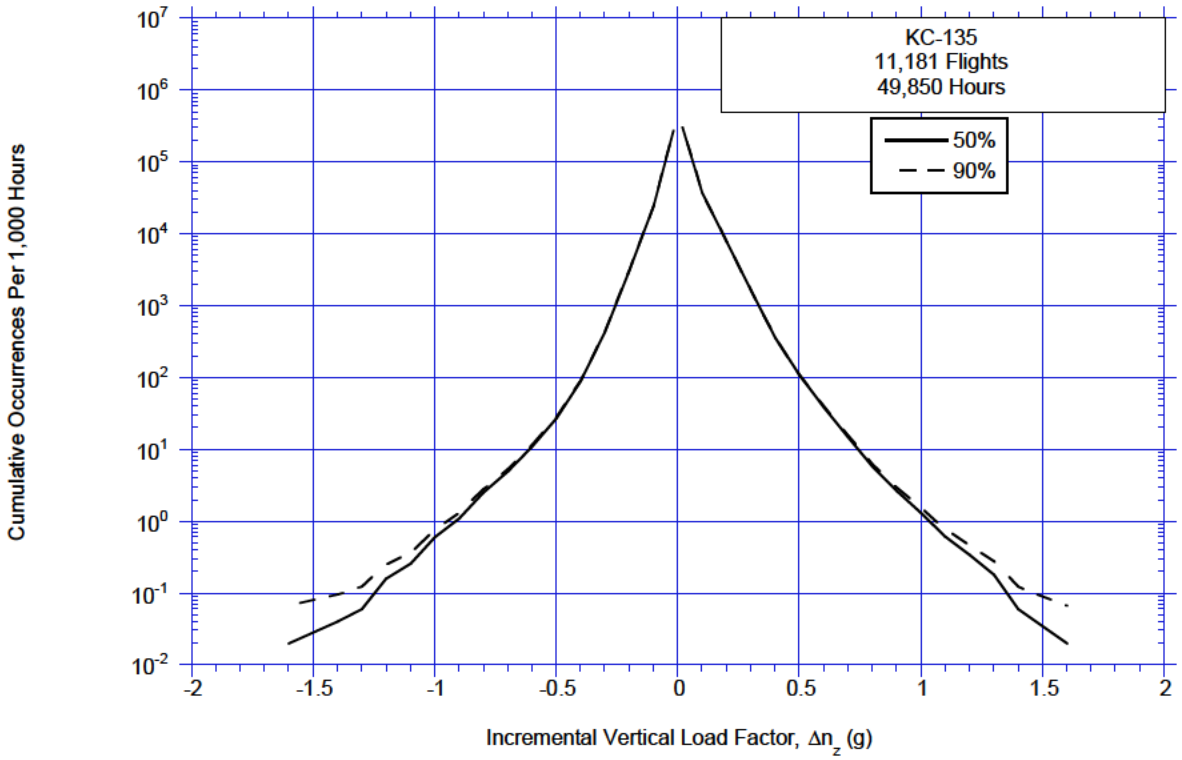

FIGURE F- 3. Cumulative occurrences per 1,000 hours of incremental vertical load factor, mean and 90 percent disposal.

TABLE F- III. Cumulative occurrences per 1,000 hours of incremental vertical load factor, mean and 90 percent dispersal.

$-\Delta n_z$	Mean (50%) Cumulative Occurrences per 1,000 Hours	One-sided 90% Cumulative Occurrences per 1,000 Hours	$+\Delta n_z$	Mean (50%) Cumulative Occurrences per 1,000 Hours	One-sided 90% Cumulative Occurrences per 1,000 Hours
-0.02	273375	273000	0.02	304600	305000
-0.10	25106.0	25100.0	0.10	37532.2	37600.0
-0.20	3008.99	3020.00	0.20	7702.10	7720.00
-0.30	433.403	437.188	0.30	1636.40	1640.00
-0.40	89.2483	90.9770	0.40	359 019	362.469
-0.50	27.2018	28.1640	0.50	108 266	110.173
-0.60	10.8526	11.4670	0.60	39.1978	40.3500
-0.70	4.93480	5.35400	0.70	14.9650	15.6830
-0.80	2.52760	2.83300	0.80	5.77740	6.23000
-0.90	1.10330	1.31100	0.90	2.66800	2.98100
-1.00	0.601800	0.760000	1.00	1.32400	1.55000
-1.10	0.260800	0.371000	1.10	0.621900	0.782000
-1.20	0.160500	0.251000	1.20	0.341000	0.465000
-1.30	0.0601800	0.124000	1.30	0.180500	0.276000
-1.40	0.0401200	0.0960000	1.40	0.0601800	0.124000
-1.50			1.50		
-1.60	0.0200600	0.0670000	1.60	0.0200600	0.0670000

CONCLUDING MATERIAL

Custodians:	Preparing activity:
Army - AV	Air Force - 11
Navy - AS	
Air Force - 11	(Project 15GP-2019-004)

NOTE: The activities above were interested in this document as of the date of this document. Since organizations and responsibilities can change, you should verify the currency of the information above using the ASSIST Online database at https://assist.dla.mil.